

12-1-2014

Simulation, and Overload and Stability Analysis of Continuous Time Sigma Delta Modulator

Kyung Kang
University of Nevada, Las Vegas

Follow this and additional works at: <https://digitalscholarship.unlv.edu/thesesdissertations>



Part of the [Computer Sciences Commons](#), [Digital Communications and Networking Commons](#), and the [Electrical and Computer Engineering Commons](#)

Repository Citation

Kang, Kyung, "Simulation, and Overload and Stability Analysis of Continuous Time Sigma Delta Modulator" (2014). *UNLV Theses, Dissertations, Professional Papers, and Capstones*. 2274.
<http://dx.doi.org/10.34917/7048593>

This Dissertation is protected by copyright and/or related rights. It has been brought to you by Digital Scholarship@UNLV with permission from the rights-holder(s). You are free to use this Dissertation in any way that is permitted by the copyright and related rights legislation that applies to your use. For other uses you need to obtain permission from the rights-holder(s) directly, unless additional rights are indicated by a Creative Commons license in the record and/or on the work itself.

This Dissertation has been accepted for inclusion in UNLV Theses, Dissertations, Professional Papers, and Capstones by an authorized administrator of Digital Scholarship@UNLV. For more information, please contact digitalscholarship@unlv.edu.

SIMULATION, AND OVERLOAD AND STABILITY ANALYSIS
OF CONTINUOUS TIME SIGMA DELTA MODULATOR

By

Kyung Kang

Bachelor of Engineering in Electrical Engineering

Korea University, South Korea

2001

Master of Engineering in Electrical Engineering

Korea University, South Korea

2003

A dissertation submitted in partial fulfillment of the requirements for the

Doctor of Philosophy - Electrical Engineering

Department of Electrical and Computer Engineering

Howard R. Hughes College of Engineering

The Graduate College

University of Nevada, Las Vegas

December 2014

We recommend the dissertation prepared under our supervision by

Kyung Kang

entitled

Simulation, and Overload and Stability Analysis of Continuous Time Sigma Delta Modulator

is approved in partial fulfillment of the requirements for the degree of

Doctor of Philosophy in Engineering - Electrical Engineering

Department of Electrical Engineering

Peter Stubberud, Ph.D., Committee Chair

Sahjendra Singh, Ph.D., Committee Member

Ebrahim Saberinia, Ph.D., Committee Member

R. Jacob Baker, Ph.D., Committee Member

Laxmi Gewali, Ph.D., Graduate College Representative

Kathryn Hausbeck Korgan, Ph.D., Interim Dean of the Graduate College

December 2014

ABSTRACT

By

Kyung Kang

Dr. Peter Stubberud, Examination Committee Chair
Professor of Electrical and Computer Engineering
University of Nevada, Las Vegas

The ever increasing demand for faster and more powerful digital applications requires high speed, high resolution ADCs. Currently, sigma delta modulators ($\Sigma\Delta$) ADCs are extensively used in broadband telecommunication systems because they are an effective solution for high data-rate wireless communication systems that require low power consumption, high speed, high resolution, and large signal bandwidths.

Because mixed-signal integrated circuits such as Continuous Time sigma delta modulators (CT $\Sigma\Delta$ s) contain both analog and digital circuits, mixed signal circuits are not as simple to model and simulate as all discrete or all analog systems. In this dissertation, the delta transform is used to simulate CT $\Sigma\Delta$ s, and its speed and accuracy are compared to the other methods. The delta transform method is shown to be a very simple and effective method to get accurate results at reasonable speeds when compared with several existing simulation methods.

When a CT $\Sigma\Delta$ is overloaded, the $\Sigma\Delta$'s output signal to quantization noise ratio (SQNR) decreases when the $\Sigma\Delta$'s input is increased over a certain value. In this dissertation, the range of quantizer gains that cause overload are determined and the values were used to determine the input signal power that prevents overload and the CT $\Sigma\Delta$'s maximum SQNR. The CT $\Sigma\Delta$ s from 2nd to 5th order are simulated to validate the predicted maximum input power that prevents overload and the maximum SQNR.

Determining the stability criteria for CT $\Sigma\Delta$ s is more difficult than it is for Discrete time sigma delta

modulators (DT $\Sigma\Delta$ M) because CT $\Sigma\Delta$ M include delays which are modeled mathematically by exponential functions for CT systems. In this dissertation an analytical root locus method is used to determine the stability criteria for CT $\Sigma\Delta$ M. This root locus method determines the range of quantizer gains for which a CT $\Sigma\Delta$ M is stable. These values can then be used to determine input signal and internal signal powers that prevent $\Sigma\Delta$ M from becoming unstable. Also, the maximum input power that keeps the CT $\Sigma\Delta$ M stable for CT $\Sigma\Delta$ M operating in overload can be determined. The CT $\Sigma\Delta$ M from 2nd to 5th order are simulated to validate the predicted maximum input power that keeps the CT $\Sigma\Delta$ M stable.

TABLE OF CONTENTS

ABSTRACT.....	iii
TABLE OF CONTENTS.....	v
LIST OF TABLES.....	vii
LIST OF FIGURES.....	ix
CHAPTER 1 INTRODUCTION.....	1
CHAPTER 2 FUNDAMENTALS OF CT $\Sigma\Delta$	6
2.1 Performance of Analog to Digital Converters.....	6
2.1.1 Mathematical models of sampling and quantization.....	6
2.1.2 Oversampling.....	9
2.1.3 Overload.....	11
2.1.4 Dynamic Range (DR).....	12
2.1.5 Signal to Quantization Noise Ratio (SQNR).....	12
2.2 The Operation Principles of Sigma Delta Modulators.....	14
2.3 Classification of Sigma Delta Modulators.....	19
2.3.1 Single-bit $\Sigma\Delta$ s versus Multi-bit $\Sigma\Delta$ s.....	19
2.3.2 Single-loop $\Sigma\Delta$ s versus Cascaded $\Sigma\Delta$ s.....	20
2.3.3 2nd order $\Sigma\Delta$ s versus Higher order $\Sigma\Delta$ s.....	20
2.3.4 Lowpass $\Sigma\Delta$ s versus Bandpass $\Sigma\Delta$ s.....	20
2.3.5 Discrete Time $\Sigma\Delta$ s versus Continuous Time $\Sigma\Delta$ s.....	20
2.3.6 $\Sigma\Delta$ s in this dissertation.....	21
2.4 Topology Selection of the CT $\Sigma\Delta$ for simulations.....	21
2.5 Conclusion.....	25
CHAPTER 3 A COMPARISON OF CT $\Sigma\Delta$ SIMULATION METHODS.....	30
3.1 The Conventional Approaches to Simulating CT $\Sigma\Delta$ s.....	30
3.1.1 Macromodel in SPICE.....	30
3.1.2 Solving differential equations.....	32
3.1.3 Implementing difference equation (CT/DT equivalence).....	33
3.1.4 MATLAB/Simulink.....	35
3.2 Simulating CT $\Sigma\Delta$ s Using the Delta Operator.....	36
3.2.1 Definition of Delta Transform.....	36

3.2.2 Application of Delta Transform for CT $\Sigma\Delta$ M simulation.....	39
3.3 Simulation Comparison.....	42
CHAPTER 4 OVERLOAD ANALYSIS OF CT $\Sigma\Delta$ MS.....	53
4.1 Definition of Overload for a Single-bit Quantizer	53
4.2 Overload Analysis.....	55
4.3 Example	59
4.4 Other Simulation Results	61
4.5 Predicting the SQNR of a $\Sigma\Delta$ M	65
4.5.1 Derivation of SQNR Approximation when operating in no-overload range....	66
4.5.2 Prediction of the SQNR of a $\Sigma\Delta$ M in overload.....	68
4.5.3 Simulation results.....	70
CHAPTER 5 STABILITY ANALYSIS OF CT $\Sigma\Delta$ MS.....	76
5.1 Analytical Root Locus.....	77
5.1.1 Root locus equation and Gain equation.....	77
5.1.2 Illustrative example of analytical root locus.....	79
5.2 Stability Analysis for CT $\Sigma\Delta$ Ms that are not overloaded.....	89
5.3 Stability Analysis Example of $\Sigma\Delta$ Ms that are not overloaded.....	92
5.4 Other Stability Simulation Results of CT $\Sigma\Delta$ Ms that are not overloaded.....	97
5.5 Stability Analysis for overloaded CT $\Sigma\Delta$ Ms.....	99
5.6 Stability Analysis Example of an overloaded $\Sigma\Delta$ M	101
5.7 Other Simulation Results of overloaded $\Sigma\Delta$ Ms	106
5.8 Conclusion	108
CHAPTER 6 CONCLUSIONS.....	110
REFERENCES.....	112
CURRICULUM VITAE.....	115

LIST OF TABLES

Table 2.1	Classification of $\Sigma\Delta$ s.....	19
Table 2.2	CT $\Sigma\Delta$ STF and NTF coefficients for <i>RC</i> implementations.....	28
Table 2.3	CT $\Sigma\Delta$ STF and NTF coefficients for <i>G_mC</i> implementations.....	29
Table 3.1	Simulation Condition.....	43
Table 3.2	The SQNR comparison of simulation methods for the 4th order CT $\Sigma\Delta$ s.....	46
	(a) Simulated SQNR	
	(b) The SQNR difference from the SQNR of SPICE	
	(c) The percentage of SQNR difference	
Table 3.3	The SQNR comparison of simulation methods for the 5th order CT $\Sigma\Delta$ s.....	47
	(a) Simulated SQNR	
	(b) The SQNR difference from the SQNR of SPICE	
	(c) The percentage of SQNR difference	
Table 3.4	The SQNRs comparison between <i>RC</i> implementation and <i>G_mC</i> implementation for each of simulation methods.....	49
Table 3.5	The elapsed time comparison between <i>RC</i> implementation and <i>G_mC</i> implementation for each of simulation methods.....	50
Table 3.6	Performance comparison of simulation methods.....	51
Table 4.1	Specification for each CT $\Sigma\Delta$	62
	(a) Common specification	
	(b) NTF attenuation for each CT $\Sigma\Delta$	
Table 4.2	Comparison of the theoretical minimum quantizer gains and the simulated minimum quantizer gains at predicted $x_{\max O}$	65
Table 4.3	Comparison of the predicted maximum sinusoidal input amplitude with the simulated maximum sinusoidal input amplitude that prevents overloading for the $\Sigma\Delta$ s in Table 4.1.....	65
Table 5.1	<i>F(s)</i> , <i>G(s)</i> and <i>H(s)</i> for <i>RC</i> implementations.....	83
Table 5.2	<i>F(s)</i> , <i>G(s)</i> and <i>H(s)</i> for <i>G_mC</i> implementations.....	84
Table 5.3	Re{ <i>D(s)</i> }, Im{ <i>D(s)</i> }, Re{ <i>N(s)</i> } and Im{ <i>N(s)</i> } for <i>RC</i> implementations.....	85
Table 5.4	Re{ <i>D(s)</i> }, Im{ <i>D(s)</i> }, Re{ <i>N(s)</i> } and Im{ <i>N(s)</i> } for <i>G_mC</i> implementations.....	87
Table 5.5	Specification for each CT $\Sigma\Delta$	97
	(a) Common specification	
	(b) NTF attenuation for each CT $\Sigma\Delta$	
Table 5.6	Comparison of the theoretical minimum quantizer gains and the simulated minimum quantizer gains at predicted $x_{\max S}$	98
Table 5.7	Comparison of the predicted maximum sinusoidal input amplitude with the simulated maximum sinusoidal input amplitude that keeps the $\Sigma\Delta$ stable..	98
Table 5.8	Comparison of the prediction and the simulation.....	107
	(a) Predicted minimum stable quantizer gain and simulated quantizer gain for sinusoidal input with predicted maximum amplitude	
	(b) Predicted maximum input amplitude and simulated input amplitude at predicted $K_{\min S}$	

(c) Predicted maximum input amplitude and simulated maximum input amplitude

Table 5.9	Summary of the stability analysis for both overloaded CT $\Sigma\Delta$ M and CT $\Sigma\Delta$ M that are not overloaded.....	109
	(a) Predicted minimum stable quantizer gain and simulated quantizer gain for sinusoidal input with predicted maximum amplitude,	
	(b) Predicted maximum input amplitude and simulated input amplitude at predicted K_{\min} ,	
	(c) Predicted maximum input amplitude and simulated maximum input amplitude,	
	(d) The difference between predicted maximum input amplitude and simulated maximum input amplitude	

LIST OF FIGURES

Figure 2.1	Operation principles of an ADC.....7 (a) Block diagram of a classical analog to digital converter (b) Time domain example (c) Frequency domain example	7
Figure 2.2	(a) B -bit quantizer block.....8 (b) Equivalent linear model of quantizer (c) Probability density function of $e(n)$ (d) Power spectral density of $e(n)$	8
Figure 2.3	Power spectral density of the total quantization noise for.....10 (a) a Nyquist rate ADC (b) an oversampling ADC with $OSR=2$ (c) power spectral density of the quantization noise power within signal bandwidth for an oversampling ADC with $OSR=2$	10
Figure 2.4	Transfer characteristic for a typical B -bit quantizer.....11	11
Figure 2.5	(a) Block diagram of a CT $\Sigma\Delta$15 (b) A linear model for the CT $\Sigma\Delta$'s STF (c) A linear model for the CT $\Sigma\Delta$'s NTF	15
Figure 2.6	STF/NTF magnitude response designed with the Chebyshev2 filter.....17	17
Figure 2.7	The spectra of the input signal and the quantization noise.....18 (a) before the noise shaping, (b) after the noise shaping	18
Figure 2.8	2nd order lowpass CT $\Sigma\Delta$ block diagram.....22 (a) RC implementation, (b) G_mC implementation	22
Figure 2.9	3rd order lowpass CT $\Sigma\Delta$ block diagram.....25 (a) RC implementation, (b) G_mC implementation	25
Figure 2.10	4th order lowpass CT $\Sigma\Delta$ block diagram.....26 (a) RC implementation, (b) G_mC implementation	26
Figure 2.11	5th order lowpass CT $\Sigma\Delta$ block diagram.....27 (a) RC implementation, (b) G_mC implementation	27
Figure 3.1	Macromodel of a 2nd order CT $\Delta\Sigma$31 (a) Functional blocks of a 2nd order CT $\Sigma\Delta$ (b) RC integrators implementation for a loop filter (c) G_mC integrators implementation for a loop filter	31
Figure 3.2	Circuit model of a 2nd order CT $\Sigma\Delta$32	32
Figure 3.3	Equivalence between a CT $\Sigma\Delta$ and a DT $\Sigma\Delta$34	34
Figure 3.4	Simulink model for a 2nd order CT $\Sigma\Delta$35	35
Figure 3.5	Delta operator block diagram.....38	38
Figure 3.6	Stability regions for the continuous Laplace plane, and the discrete z -plane, delta-plane.....39	39
Figure 3.7	The 2nd order CT $\Sigma\Delta$ block diagram.....39	39
Figure 3.8	2nd order DT model $\Sigma\Delta$ using delta transform.....41	41
Figure 3.9	The output power spectra comparison for the simulation methodologies for 2nd order CT $\Sigma\Delta$ s with an excess loop delay of (a) zero, (b) $0.5T$, (c) T , (d) $1.5T$, (e) $2T$, (f) $2.5T$44	44

Figure 3.10	Simulation comparison of the maximum SQNR for (a) 2nd order CT $\Sigma\Delta$ Ms, (b) 3rd order CT $\Sigma\Delta$ Ms, (c) 4th order CT $\Sigma\Delta$ Ms, (d) 5th order CT $\Sigma\Delta$ Ms.....	45
Figure 3.11	The output power spectra for the G_mC implementation for the 2nd order CT $\Sigma\Delta$ Ms with an excess loop delay of zero.....	48
Figure 3.12	Simulation comparison of the elapsed time to complete the simulation for (a) 2nd order CT $\Sigma\Delta$ Ms, (b) 3rd order CT $\Sigma\Delta$ Ms, (c) 4th order CT $\Sigma\Delta$ Ms, (d) 5th order CT $\Sigma\Delta$ Ms.....	49
Figure 4.1	(a) The transfer characteristic for a single-bit quantizer (b) quantization error, e of a single-bit quantizer (c) quantizer gain, K of a single-bit quantizer.....	54
Figure 4.2	(a) Block diagram of a CT $\Sigma\Delta$ M's STF (b) Block diagram of a CT $\Sigma\Delta$ M's NTF.....	56
Figure 4.3	Bell curve of the standard normal distribution.....	57
Figure 4.4	The root locus of a 2nd order CT $\Sigma\Delta$ M with a sampling frequency, f_s , where $f_s=1/T$, of 1GHz and Chebyshev Type 2 NTF for (a) $D = 0$, (b) $D = 0.5T$, (c) $D = T$	59
Figure 4.5	Simulated SQNR and the minimum quantizer gain (K_{\min}) using a sinusoidal input for the 2nd order CT $\Sigma\Delta$ M in example.....	61
Figure 4.6	Simulated SQNR and the minimum quantizer gain (K_{\min}) using a sinusoidal input (a) for the 2nd order CT $\Sigma\Delta$ M, (b) for the 3rd order CT $\Sigma\Delta$ M, (c) for the 4th order CT $\Sigma\Delta$ M, (d) for a 5th order CT $\Sigma\Delta$ M with $D = 0$	63
Figure 4.7	Simulated SQNR and the minimum quantizer gain (K_{\min}) using a sinusoidal input (a) for the 2nd order CT $\Sigma\Delta$ M, (b) for the 3rd order CT $\Sigma\Delta$ M, (c) for the 4th order CT $\Sigma\Delta$ M, (d) for a 5th order CT $\Sigma\Delta$ M with $D = T$	64
Figure 4.8	(a) A linear model for the CT $\Sigma\Delta$ M's STF in overload (b) A linear model for the CT $\Sigma\Delta$ M's NTF in overload.....	68
Figure 4.9	Simulated SQNR and estimated SQNR for the 2nd order CT $\Sigma\Delta$ M with (a) $D = 0$, (b) $D = 0.5T$, (c) $D = T$, (d) $D = 1.5T$, (e) $D = 2T$, (f) $D = 2.5T$	71
Figure 4.10	Simulated SQNR and estimated SQNR for the 3rd order CT $\Sigma\Delta$ M with (a) $D = 0$, (b) $D = 0.5T$, (c) $D = T$, (d) $D = 1.5T$, (e) $D = 2T$, (f) $D = 2.5T$	73
Figure 4.11	Simulated SQNR and estimated SQNR for the 4th order CT $\Sigma\Delta$ M with (a) $D = 0$, (b) $D = 0.5T$, (c) $D = T$, (d) $D = 1.5T$	75
Figure 5.1	The root locus of six lowpass 3rd order CT $\Sigma\Delta$ Ms that have Chebyshev Type 2 NTFs with 30dB attenuation in stopband, a sampling frequency of 1GHz, for and excess loop delays of (a) $D = 0$, (b) $D = 0.5T$, (c) $D = T$, (d) $D = 1.5T$, (e) $D = 2T$, (f) $D = 2.5T$	81
Figure 5.2	Bode plot for the 3rd order CT $\Sigma\Delta$ M shown in Fig 5.1 (a).....	89
Figure 5.3	(a) Block diagram of a CT $\Sigma\Delta$ M's STF (b) Block diagram of a CT $\Sigma\Delta$ M's NTF.....	90
Figure 5.4	Bell curve of the standard normal distribution.....	91
Figure 5.5	The root locus of 4th order CT $\Sigma\Delta$ Ms that uses Chebyshev Type 2 NTFs with a sampling frequency of 1GHz for (a) $D = 2T$, (b) $D = 2.5T$	93
Figure 5.6	Simulated SQNR and the minimum quantizer gain (K_{\min}) using a sinusoidal input for the 4th order CT $\Sigma\Delta$ M with (a) $D = 2T$, (b) $D = 2.5T$	96
Figure 5.7	(a) A linear model for the CT $\Sigma\Delta$ M's STF in overload (b) A linear model for the CT $\Sigma\Delta$ M's NTF in overload.....	99
Figure 5.8	The root locus of 3rd order CT $\Sigma\Delta$ Ms that uses Chebyshev Type 2 NTFs with a sampling frequency of 1GHz for (a) $D = 0$, (b) $D = 0.5T$, (c) $D = T$	102
Figure 5.9	Simulated SQNR and the minimum quantizer gain (K_{\min}) using a sinusoidal input for the 3rd order CT $\Sigma\Delta$ M with $D = T$ in example.....	104

Figure 5.10 Simulated SQNR and the minimum quantizer gain (K_{\min}) using a sinusoidal input for the 3rd order CT $\Sigma\Delta$ M for (a) $D = 0$, (b) $D = 0.5T$105

CHAPTER 1

INTRODUCTION

Most modern digital systems including communication systems, flight controllers and data acquisition systems are actually mixed signal systems that possess both analog and digital electronics. In mixed signal systems, analog to digital converters (ADCs) convert analog signals into digital signals, and digital to analog converters (DACs) convert digital signals into analog signals. Because the performance of digital systems can typically be improved by simple hardware and software changes, the performance of mixed signal systems is typically limited by the performance of the system's ADCs and DACs and not the system's digital circuitry.

The ever increasing demand for faster and more powerful digital applications requires high speed, high resolution ADCs. Many portable electronic devices not only require high resolution, high speed ADCs, but also have low power requirements. Portable wireless communication systems not only require low power, high speed, high resolution ADCs, but are also requiring increasingly wide bandwidth data conversion. Currently, sigma delta modulator ($\Sigma\Delta$ M) ADCs are extensively used in broadband telecommunication systems because they are an effective solution for high data-rate wireless communication systems that require low power consumption, high speed, high resolution, and moderate signal bandwidths.

ADCs can be classified into two categories, Nyquist-rate converters and oversampling converters [1]. Nyquist-rate converters operate near the Nyquist rate, or the signal's minimum sampling frequency, which is twice the signal's bandwidth. Sampling at or above the Nyquist rate prevents signal loss due to aliasing. Oversampling converters operate at rates much greater than the signal's Nyquist rate.

Nyquist-rate converters can be implemented by employing a variety of architectures including flash ADCs, pipeline ADCs, and successive approximation register (SAR) ADCs. Flash ADCs

typically consist of a resistive voltage divider network and 2^B parallel high speed comparators where B is the number of bits of the ADC's resolution. Flash ADCs are appropriate for applications requiring high speed data conversion of signals with large bandwidths; however, flash ADCs dissipate more power and have relatively lower resolution than other ADC architectures. Pipeline ADCs feature multiple low resolution flash conversion stages cascaded in series to form a pipeline. Repeating the quantization through a series of the stages in the pipeline allows high resolution data conversion; however, pipeline ADCs have greater data latency than other ADC architectures because in a pipeline ADC, each sample must propagate through the entire pipeline. SAR ADCs convert signals using a single comparator to implement a binary search algorithm. SAR ADC architectures convert signals using less power and smaller foot prints than other architectures; however, SAR ADCs have lower sampling rates compared to other architectures.

Oversampling converters are so named because their sampling rate is much greater than the Nyquist rate of the signal. Whereas Nyquist-rate converters are suitable for applications requiring moderate resolution conversion of wide bandwidth signals, oversampling converters typically provide high resolution conversion of signals with moderate bandwidths. The most popular oversampling ADC is the Sigma Delta Modulator ($\Sigma\Delta$ M). The $\Sigma\Delta$ M's loop filter attenuates the noise of a low resolution quantizer in the frequency band of interest while passing the input signal to the $\Sigma\Delta$ M's output. Because $\Sigma\Delta$ Ms use relatively few, simple, low power analog circuit components, $\Sigma\Delta$ M ADCs can provide high resolution and lower power signal conversion of moderate bandwidth signals and are commonly used in mobile wireless communications applications.

$\Sigma\Delta$ M ADCs can be classified as either discrete time (DT) $\Sigma\Delta$ M ADCs or continuous time (CT) $\Sigma\Delta$ M ADCs. $\Sigma\Delta$ M ADCs with loop filters consisting of the discrete-time circuits such as switched-capacitor or switched-current circuits are classified as DT $\Sigma\Delta$ Ms. Similarly, $\Sigma\Delta$ M ADCs

with the loop filters consisting of continuous-time circuits such as transconductors and integrators are classified as CT $\Sigma\Delta$ s. Some of the advantages that CT $\Sigma\Delta$ s have over DT $\Sigma\Delta$ s are that CT $\Sigma\Delta$ s have inherent antialiasing filtering in the $\Sigma\Delta$'s signal transfer function (STF) and they can operate at higher frequencies because they don't have settling time requirements in their loop filters [2]. Because DT $\Sigma\Delta$ s are simply made up of delays and gains, they can be accurately modeled using simple difference equations whereas CT $\Sigma\Delta$ s can be more difficult to simulate due to the mixed signal nature of the feedback loop.

Because mixed-signal integrated circuits such as CT $\Sigma\Delta$ s contain both analog and digital circuits, mixed signal circuits are not as simple to model and simulate as all discrete or all analog systems. Several common approaches for simulating CT $\Sigma\Delta$ s include SPICE modeling, solving differential equations analytically and numerically, implementing difference equations based on the impulse invariance transformation and using Simulink. Each simulation method has a tradeoff between speed, simplicity and accuracy. In this dissertation, the delta transform is used to simulate CT $\Sigma\Delta$ s, and its speed and accuracy are compared to the other methods.

This delta transform method simulates CT $\Sigma\Delta$ s by determining difference equations that model CT $\Sigma\Delta$ s. The difference equations use the $\Sigma\Delta$'s input signal and the quantizer's feedback signal to determine the input at the quantizer's next sample time. However, unlike the other difference equation methods, the delta transform can be used to determine all loop filter signal values at times other than the sampling time. The delta transform has the particular property that as the delta transform sample time approaches zero, the delta transform variable converges toward its continuous time counterpart, the Laplace transform variable [3].

Because a $\Sigma\Delta$'s output is typically the $\Sigma\Delta$'s quantizer output which has a minimum and maximum output, it is possible for the $\Sigma\Delta$'s input to overload the $\Sigma\Delta$'s quantizer. The $\Sigma\Delta$'s quantizer is said to be overloaded when the quantization error exceeds the quantizer's minimum and maximum values by more than half of one quantized level. When overloaded, a $\Sigma\Delta$'s output signal to quantization noise ratio (SQNR) decreases when the $\Sigma\Delta$'s input is increased

over a certain value; however, in these cases, the $\Sigma\Delta$'s output SQNR can be restored to its previous values when the $\Sigma\Delta$'s input is decreased to its previous amplitudes. In this dissertation, the range of quantizer gains that cause overload are determined, and these values are used to determine the input signal power that prevents overload.

Because a $\Sigma\Delta$'s output is typically the $\Sigma\Delta$'s quantizer output which has a minimum and maximum output, $\Sigma\Delta$ s cannot be unstable in the bounded input bounded output (BIBO) sense. Instead, a $\Sigma\Delta$ is considered to have become unstable when the amplitude of a $\Sigma\Delta$'s input is increased so as to cause the $\Sigma\Delta$'s output SQNR to decrease dramatically and to create the condition that the $\Sigma\Delta$'s output SQNR cannot be restored to its previous values even when the $\Sigma\Delta$'s input is decreased to its previous amplitudes. DT root locus methods have been successfully used to determine the stability of DT $\Sigma\Delta$ s; however, determining the stability criteria for CT $\Sigma\Delta$ s is more difficult than it is for DT $\Sigma\Delta$ s because CT $\Sigma\Delta$ s include delays which are modeled mathematically by exponential functions for CT systems. Because both the STF and noise transfer function (NTF) of CT $\Sigma\Delta$ s contain exponential functions, traditional root locus methods cannot be used for determining the root locus of CT $\Sigma\Delta$ s. Instead, in this dissertation, an analytical root locus method is used to determine the stability criteria for CT $\Sigma\Delta$ s. This root locus method determines the range of quantizer gains for which a CT $\Sigma\Delta$ is stable. These values can then be used to determine input signal and internal signal powers that prevent $\Sigma\Delta$ s from becoming unstable.

Using the analytical root locus stability analysis and the overload analysis, the SQNR of a CT $\Sigma\Delta$ can be predicted. The quantization noise power is determined from the range of quantizer gains that prevent $\Sigma\Delta$ s from becoming unstable or overloaded. The maximum input amplitude to prevent $\Sigma\Delta$ s from becoming unstable or overloaded can be predicted using the range of quantizer gains.

Chapter 2 in this dissertation reviews basic ADC and $\Sigma\Delta$ metrics and operation principles. Also, the $\Sigma\Delta$ topologies that are used throughout this dissertation are developed using block

diagrams. In Chapter 3, a delta transform method for simulating CT $\Sigma\Delta$ Ms is developed. This simulation method is compared with several existing CT $\Sigma\Delta$ Ms simulation methods with respect to accuracy, speed and modeling simplicity. Chapter 4 states the necessary conditions that prevent quantizers in CT $\Sigma\Delta$ Ms from overloading. Using these conditions, the maximum input signal power that prevents a CT $\Sigma\Delta$ M from overloading is determined. Also, a method is developed that predicts a $\Sigma\Delta$ M's SQNR using the range of quantizer gains that prevent the $\Sigma\Delta$ M from overloading. In Chapter 5, an analytical root locus method is used to determine the stability criteria for CT $\Sigma\Delta$ Ms that include exponential functions in their characteristic equations. This root locus method determines the range of quantizer gains for which a CT $\Sigma\Delta$ M is stable. These values can then be used to determine input signal and internal signal powers that prevent $\Sigma\Delta$ M from becoming unstable. Finally, Chapter 6 summarizes the work presented.

CHAPTER 2

FUNDAMENTALS OF CT $\Sigma\Delta$

Analog to digital conversion is a process that transforms analog signals which are continuous in time and amplitude into digital signals which are discrete in time and amplitude. Although this process can be implemented using a large variety of methods, the overall ADC process can be modeled mathematically by three simple systems. From this model, a mathematical definition of resolution can be defined so that the resolution of different ADC architectures can be compared.

Although different architectures exist for CT $\Sigma\Delta$ s, most single quantizer CT $\Sigma\Delta$ s can be described by a canonical feedback loop. This model allows CT $\Sigma\Delta$ s to be modeled mathematically so that their resolutions can be determined without the need for developing specific architectures. After developing a mathematical CT $\Sigma\Delta$ model that meets resolution specifications, the model can then be mapped to a specific CT $\Sigma\Delta$ architecture and implemented in hardware.

2.1 Performance of Analog to Digital Converters

The general ADC process can be modeled by three subsystems, an anti-aliasing filter (AAF), a sampler, and a quantizer. Each of these subsystems has a simple mathematical model that can be used to define general ADC metrics. An ADC's resolution is one such metric, and it is often defined in terms of effective number of bits (ENOB), SQNR, and dynamic range (DR).

2.1.1 Mathematical models of sampling and quantization

Fig 2.1 (a) shows a typical ADC process modeled by the three subsystems, an anti-aliasing filter (AAF), a sampler, and a quantizer. In this model, the AAF filters the analog input signal, $x(t)$. The sampler converts the filtered signal, $x_a(t)$, into the discrete signal, $x(n)$, such that $x(n)$

$=x_a(n \cdot T_s)$ where T_s is the sampling period. The third process, the quantizer, quantizes the amplitude of $x(n)$.

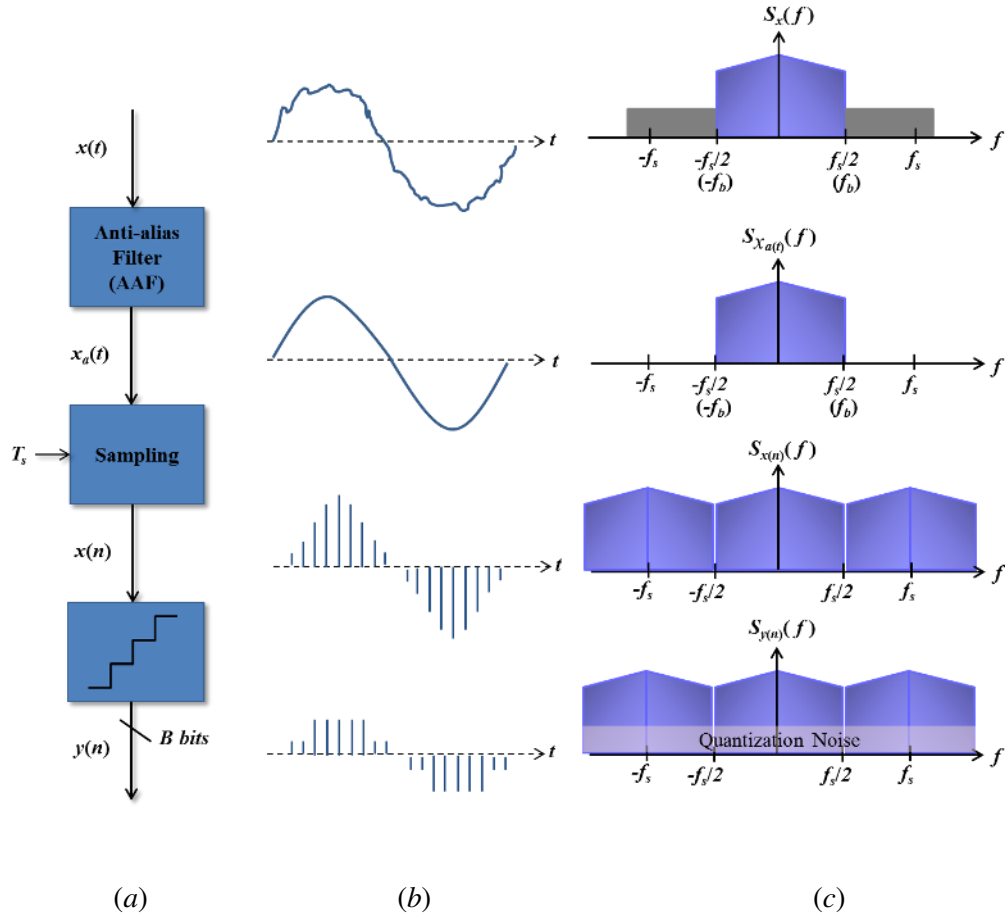


Figure 2.1 Operation principles of an ADC: (a) Block diagram of a classical analog to digital converter, (b) Time domain example, (c) Frequency domain example^[4]

Fig 2.1 (b) shows an example of this process in the time domain for a sinusoidal input signal, and Fig 2.1 (c) shows an example of this process in frequency domain for a wideband signal. As illustrated in Fig 2.1 (b) and (c), the AAF removes out of band frequency components which can fold into the signal band during the subsequent sampling process. Ideally, the AAF is an ideal (brick wall) lowpass filter (LPF) that has a cut-off frequency of f_c which equals the maximum bandwidth, f_b , of the signal of interest. As shown in Fig 2.1 (c), the filtered signal, $x_a(t)$, only contains frequency components between $-f_b$ and f_b . The filtered signal, $x_a(t)$ must be sampled at a

minimum sampling rate, f_s , of $2f_b$ to prevent aliasing and consequently information loss. When the sampler samples $x_a(t)$ with a period of T_s where $T_s = 1/f_s$, the sampler generates the discrete signal, $x(n)$ where $x(n) = x_a(n \cdot T_s)$. As illustrated in Fig 2.1 (c), sampling $x_a(t)$ with a period of $T_s = 1/2f_b$, generates a periodic extension of $S_{x_a(t)}(f)$ in the frequency domain as shown in the plot of $S_{x(n)}(f)$. The quantizer quantizes the amplitude of $x(n)$ into the digital signal, $y(n)$. In the time domain, the quantizer generates an amplitude error between $y(n)$ and $x(n)$. This quantization error between $y(n)$ and $x(n)$ depends on the quantization method (truncation or rounding) and the number of equally spaced quantization levels. A B -bit quantizer has 2^B equally spaced quantization levels. In the frequency domain, quantization adds noise to $S_{x(n)}(f)$. This noise limits the ADC's resolution.

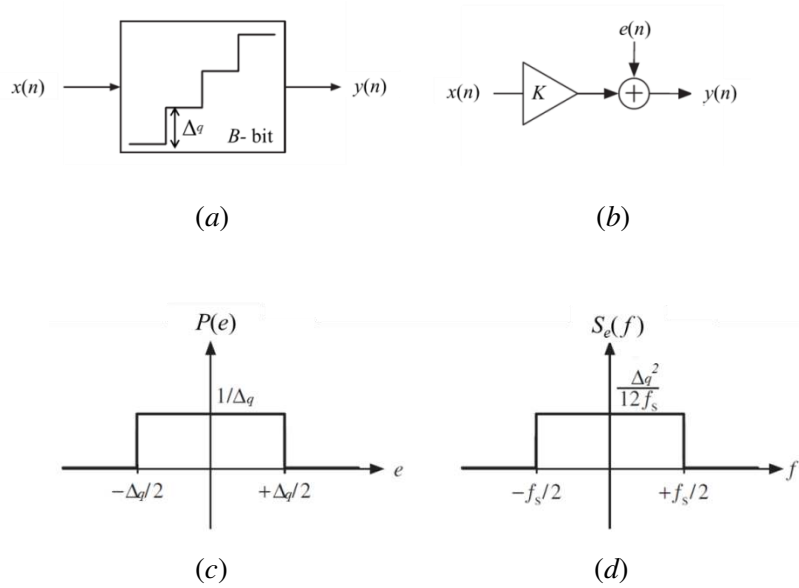


Figure 2.2 (a) B -bit quantizer block, (b) Equivalent linear model of quantizer (c) Probability density function of $e(n)$, (d) Power spectral density of $e(n)$ ^[51]

An ideal quantizer shown in Fig 2.2 (a) is often modeled linearly as a linear gain, K , and an additive quantization noise, or error, $e(n)$, as shown in Fig 2.2 (b); thus, a quantizer can be modeled as $y(n) = K \cdot x(n) + e(n)$ where $y(n)$ is the quantizer's output, $x(n)$ is the quantizer's input, and $e(n)$ is the quantizer error. The quantization error is generally modeled as a white random

process that has uniform distribution over the range of errors. Because the statistical mean for rounding is zero unlike the statistical mean for truncation and because the statistical variance for rounding is lower than it is for truncation, quantization is almost always performed by rounding instead of truncation.

Rounding errors have a range of $[-\Delta_q/2, +\Delta_q/2]$ where Δ_q is the quantization step size which is defined as the difference between adjacent digital output levels. Rounding errors can be modeled by a white random process that is uniformly distributed over the range of $[-\Delta_q/2, +\Delta_q/2]$. Because the quantization error, $e(n)$, is modeled as a uniformly distributed random process over the interval, $[-\Delta_q/2, +\Delta_q/2]$, the amplitude of the quantization noise's probability density function, $P(e)$, is $1/\Delta_q$ as shown in Fig 2.2 (c). Because the quantization noise has zero mean, the total quantization noise power, P_e , can be calculated as

$$\begin{aligned}
 P_e &= E(e^2) = \sigma_e^2 - E^2(e) = \sigma_e^2 \\
 &= \int_{-\infty}^{+\infty} e^2 \cdot P(e) de = \int_{-\frac{\Delta_q}{2}}^{+\frac{\Delta_q}{2}} e^2 \cdot \frac{1}{\Delta_q} de = \frac{\Delta_q^2}{12} .
 \end{aligned} \tag{2.1}$$

Because the total quantization noise is modeled as a white random process that is uniformly distributed over the frequency range of $[-f_s/2, f_s/2]$, the quantization error's power spectral density, $S_e(f)$, can be determined from

$$\sigma_e^2 = \int_{-f_s/2}^{+f_s/2} S_e(f) df = S_e(f) \cdot f_s = \frac{\Delta_q^2}{12} \tag{2.2}$$

which implies that

$$S_e(f) = \frac{\Delta_q^2}{12 \cdot f_s} . \tag{2.3}$$

2.1.2 Oversampling

The resolution of a B -bit ADC can be increased by a process called oversampling. If an ADC's

sampling frequency, f_s , exceeds twice the input signal's bandwidth, f_b , that is, $f_s > 2f_b$, a signal is said to be oversampled and the ADC is said to be an oversampling ADC. An ADC's oversampling ratio (OSR) is defined as

$$OSR = \frac{f_s}{2f_b} \quad (2.4)$$

To illustrate, an ADC operating with an $OSR = 1$ is a Nyquist rate ADC whereas an ADC operating with an $OSR = 2$ is an oversampling ADC.

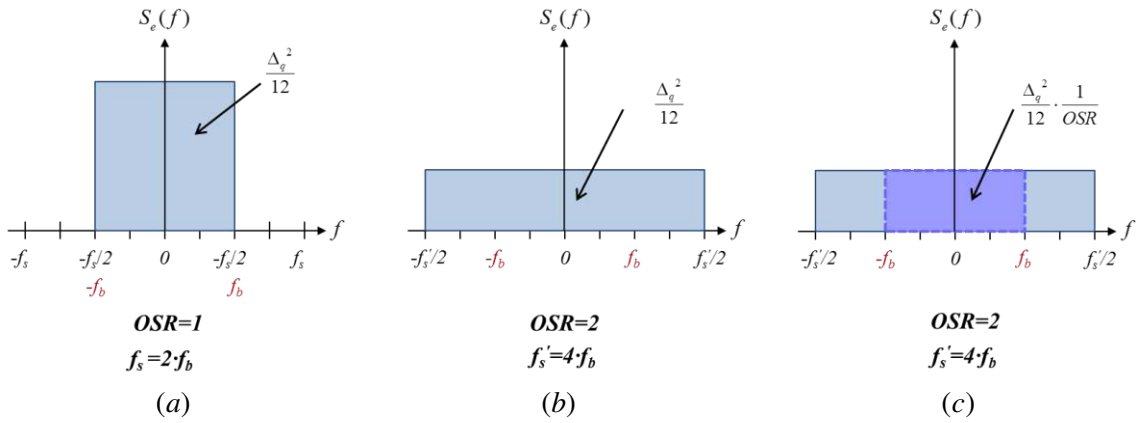


Figure 2.3 Power spectral density of the total quantization noise for (a) a Nyquist rate ADC, (b) an oversampling ADC with $OSR=2$, (c) power spectral density of the quantization noise power within signal bandwidth for an oversampling ADC with $OSR=2$

For both Nyquist rate converters and oversampling converters, the ADC's quantization noise power, σ_e^2 , is $\Delta_q^2 / 12$. However, the output of an oversampling ADC can be filtered below $-f_b$ and above f_b which implies that after filtering, the quantization noise power can be reduced to

$$\begin{aligned} \sigma_{e, \text{oversampling ADC}}^2 &= \int_{-f_b}^{+f_b} S_e(f) df \\ &= \int_{-f_s'/(2 \cdot OSR)}^{+f_s'/(2 \cdot OSR)} S_e(f) df = \int_{-f_s'/(2 \cdot OSR)}^{+f_s'/(2 \cdot OSR)} \frac{\Delta_q^2}{12 f_s'} df = \frac{\Delta_q^2}{12} \cdot \frac{1}{OSR} \end{aligned} \quad (2.5)$$

Fig 2.3 graphically illustrates this effect. Fig 2.3 (a) shows that the power spectral density (PSD)

of the quantization noise of a Nyquist rate ADC and Fig 2.3 (b) shows the PSD of the quantization noise of an equivalent ADC that is operated with $OSR = 2$. As illustrated in Fig 2.3 (c), the power of the quantization noise can be reduced by $1/OSR$ by filtering out signals outside the bandwidth of f_b , or $f_s/(2 \cdot OSR)$. Because the quantization noise power, σ_e^2 , of an oversampled ADC is inversely proportional to the ADC's OSR, an oversampling ADC's SQNR increases as its OSR increases.

2.1.3 Overload

Fig 2.4 shows the transfer characteristic for a typical B -bit quantizer with an input, x , and an output, y . Assuming that the ADC's maximum and minimum outputs are V and $-V$, respectively, the difference, Δ_q , between two adjacent output levels can be written as

$$\Delta_q = \frac{2 \cdot V}{2^B - 1} . \quad (2.6)$$

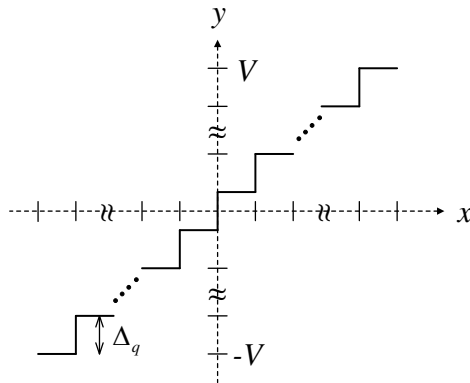


Figure 2.4 Transfer characteristic for a typical B -bit quantizer

When the quantizer's output is at $\pm V$ and the magnitude of the quantizer's error, e , exceeds half of Δ_q , that is, when $y = \pm V$ and

$$|e| \geq \frac{\Delta_q}{2}, \quad (2.7)$$

the ADC is said to be overloaded [6]. Therefore, for the an ADC with the transfer characteristic in Fig 2.4, the ADC is not overload when

$$-V - \frac{\Delta_q}{2} \leq x \leq +V + \frac{\Delta_q}{2}. \quad (2.8)$$

Using (2.6) and (2.8), the maximum input amplitude, x_{\max} , of a B -bit quantizer in the non-overload region is

$$x_{\max} = V + \frac{\Delta_q}{2} = \left(\frac{2^B}{2^B - 1} \right) \cdot V \quad (2.9)$$

and the minimum input amplitude, x_{\min} , of a B -bit quantizer in the non-overload region is

$$x_{\min} = -V - \frac{\Delta_q}{2} = -\left(\frac{2^B}{2^B - 1} \right) \cdot V. \quad (2.10)$$

2.1.4 Dynamic Range (DR)

The DR of an ADC is defined as the ratio between the power of the largest input signal that can be applied without significantly degrading the performance of the ADC and the power of the smallest detectable input signal at any frequency. The smallest detectable input signal is determined by the PSD of the ADC's noise floor. If the PSD of the noise floor is not uniform, the smallest detectable signal is determined where the noise floor's PSD is largest.

2.1.5 Signal to Quantization Noise Ratio (SQNR)

The SQNR of an ADC can be defined as the ratio of output signal power to quantization noise power; that is,

$$SQNR = \frac{P_y}{P_e} \quad (2.11)$$

where P_y is the ADC's output signal power and P_e is the ADC's output quantization noise power.

Assuming that the ADC's output and quantization noise have zero means,

$$P_y = E[y^2] = \sigma_y^2 \quad (2.12)$$

and

$$P_e = E[e^2] = \sigma_e^2 \quad (2.13)$$

and an ADC's SQNR in dB can be written as

$$SQNR(dB) = 10 \cdot \log \left(\frac{\sigma_y^2}{\sigma_e^2} \right) \text{ dB}. \quad (2.14)$$

For a full scale sinewave input, the output signal power, σ_y^2 , can be calculated as

$$\sigma_y^2 = \frac{x_{\max}^2}{2} = \frac{2^{2B-1}}{(2^B - 1)^2} \cdot V^2 \quad (2.15)$$

where x_{\max} is the maximum amplitude of the sinusoidal input signal. Substituting (2.2) into (2.6) and the resulting equation into (2.14), the SQNR of a Nyquist rate ADC can be written as

$$SQNR(dB)_{Nyquist\ ADC} \approx 1.76 + 6.02B \quad (2.16)$$

Eq. (2.16) shows that an ADC's SQNR is proportional to the number of bits, B , of the ADC's resolution. In practice, (2.16) is used to calculate the ADC's ENOB of resolution; that is,

$$ENOB = \frac{SQNR(dB) - 1.76}{6.02}. \quad (2.17)$$

Therefore, an ADC with a 6dB better SQNR has one additional bit of ENOB. This resolution metric defined as ENOB gives an indication of how many bits would be required in an ideal ADC to get the same performance.

The SQNR of an oversampled ADC can be calculated by substituting (2.5) and (2.15) into (2.14), which results in

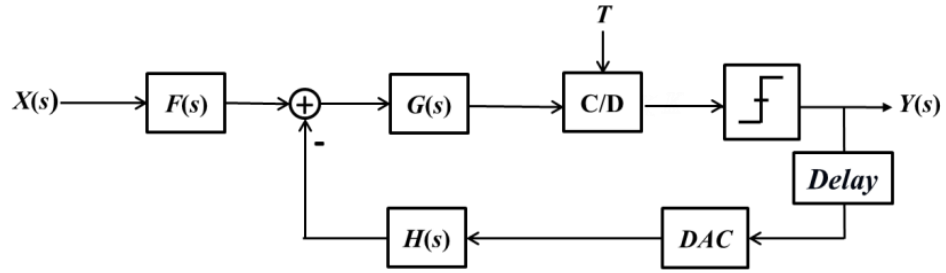
$$SQNR(dB)_{oversampling\ ADC} \approx 1.76 + 6.02B + 10 \cdot \log(OSR). \quad (2.18)$$

Eq. (2.18) shows that doubling an ADC's OSR increases its SQNR by 3dB. For example, an ADC with an OSR of 4 will have a 6dB better SQNR than the same ADC operated at the Nyquist rate. As a result, an ADC's ENOB can be increased by 1 bit by sampling the signal 4 times faster than its Nyquist rate.

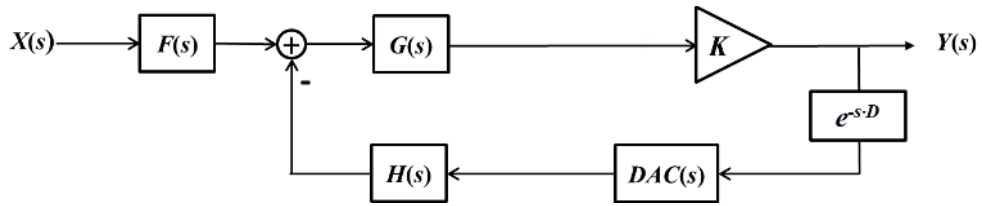
2.2 The Operation Principles of Sigma Delta Modulators

$\Sigma\Delta$ ADCs achieve a high resolution signal conversion by using a feedback loop filter and a low resolution quantizer that samples at rates much higher than the Nyquist rate. The loop filter is designed not only to shape the quantization noise so that it is attenuated over the frequency band of interest, but also to act as an AAF for the input signal. This is known as the “noise shaping technique”.

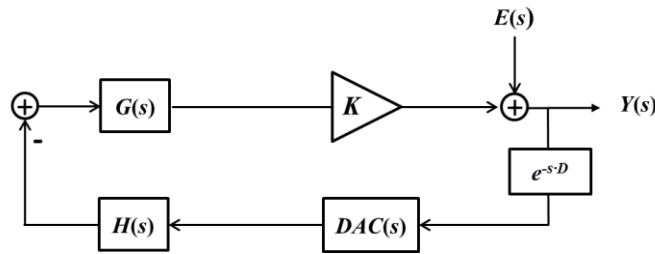
In a general, a CT $\Sigma\Delta$ can be modeled by the canonical feedback loop shown in Fig 2.5 (a) where $X(s)$ and $Y(s)$ are the Laplace transforms of the input signal and the output signal, respectively, and $F(s)$, $G(s)$ and $H(s)$ are the system functions of the pre-filter stage, the feedforward path and the feedback path, respectively. The continuous to discrete (C/D) block converts a continuous time signal into a discrete time signal. The C/D converter can be modeled by an impulse train modulator, followed by a block that converts the impulse train into a discrete time sequence [7]. Because the discrete time Fourier transform of the output of the C/D converter is identical to the Fourier transform of the input of the C/D converter if the input of C/D converter is bandlimited and oversampled, the system function of the C/D converter doesn't need to be included in the model. The quantizer block represents a clocked quantizer, and the DAC block represents a digital to analog converter (DAC). The quantizer delay and the DAC delay are often represented by a single delay block as they are in Fig 2.5 (a), and the combination of these two delays is often referred to as the $\Sigma\Delta$'s excess loop delay.



(a)



(b)



(c)

Figure 2.5 (a) Block diagram of a CT $\Sigma\Delta$ M, (b) A linear model for the CT $\Sigma\Delta$ M's STF, (c) A linear model for the CT $\Sigma\Delta$ M's NTF

Fig 2.5 (b) shows a linear model for the CT $\Sigma\Delta$ M's STF where the quantizer has been modeled by the variable gain, K . Fig 2.5 (c) shows a linear model for the CT $\Sigma\Delta$ M's NTF where the quantization error is modeled by the gain, K , and an additive quantization noise, $E(s)$. Because the block diagram models in Fig 2.5 (b) and (c) are linear, the $\Sigma\Delta$ M's output, $Y(s)$ can be written as

$$Y(s) = STF(s) \cdot X(s) + NTF(s) \cdot E(s) \quad (2.19)$$

where

$$STF(s) = Y(s) / X(s) , \text{ and } NTF(s) = Y(s) / E(s) . \quad (2.20)$$

Using Fig 2.5 (b), the $\Sigma\Delta\text{M}$'s STF can be written as

$$STF(s) = \frac{K \cdot F(s) \cdot G(s)}{1 + K \cdot e^{-sD} \cdot G(s) \cdot H(s) \cdot DAC(s)} , \quad (2.21)$$

and using Fig 2.5(c), the $\Sigma\Delta\text{M}$'s NTF can be written as

$$NTF(s) = \frac{1}{1 + K \cdot e^{-sD} \cdot G(s) \cdot H(s) \cdot DAC(s)} \quad (2.22)$$

where the exponential function, e^{-sD} is the Laplace transform of the excess loop delay, D .

In general, stable feedback loops minimize feedback error. Therefore, when calculating the output signal power, P_y , of the $\Sigma\Delta\text{M}$, the value of K is selected as the $\Sigma\Delta\text{M}$'s effective gain, K_{eff} , which is the value of K that minimizes the power, P_e , of the quantization noise [8]. Because $e(n) = y - K \cdot \psi$, the $\Sigma\Delta\text{M}$'s quantization noise power, P_e , can be written as

$$P_e = E[e^2(n)] = E[y^2(n)] - 2K \cdot E[y(n)\psi(n)] + K^2 \cdot E[\psi^2(n)]. \quad (2.23)$$

The necessary condition for K to minimize P_e is

$$\frac{\partial P_e}{\partial K} = -2 \cdot E[y(n)\psi(n)] + 2K_{eff} \cdot E[\psi^2(n)] = 0 \quad (2.24)$$

which implies that the K_{eff} that minimizes P_e is

$$K_{eff} = \frac{E[y(n)\psi(n)]}{E[\psi^2(n)]}. \quad (2.25)$$

Assuming $\psi(n)$ is a zero mean random process and assuming a single bit quantizer which implies $y(n) = \text{sgn}[\psi(n)]$, (2.25) can be written as

$$K_{eff} = \frac{E[|\psi(n)|]}{\sigma_{\psi}^2}. \quad (2.26)$$

To illustrate the operation of a $\Sigma\Delta\text{M}$, consider a NTF that is designed as a highpass Chebyshev Type 2 filter and a STF that has the lowpass characteristic shown in Fig 2.6. For low frequencies, the magnitude response of the NTF is almost zero, that is, $|NTF(j\omega)| \approx 0$ for $\omega < 2 \times 10^7$, so the quantization noise will be attenuated in that part of output spectrum. Also, for low frequencies, the magnitude response of the STF is approximately one which implies that the input signal is passed to the output without attenuation. However, for high frequencies, the NTF passes the quantization errors with a gain of one and the STF attenuates the input signal to reduce aliasing.

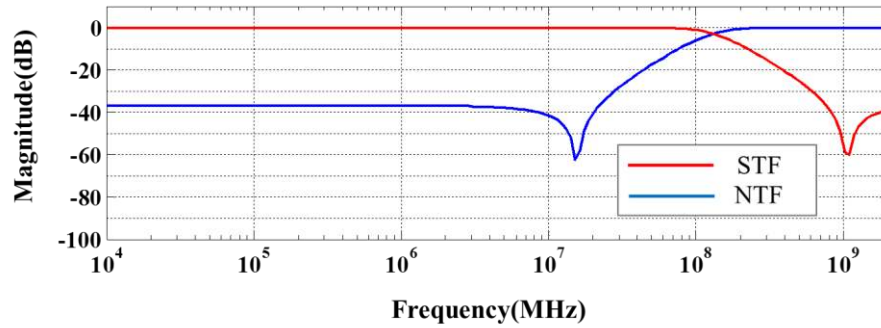


Figure 2.6 STF/NTF magnitude response designed with the Chebyshev2 filter

Fig 2.7 (a) shows an example of an input signal and the uniformly distributed quantization noise generated by the quantizer. Fig 2.7 (b) shows the output spectra of those signals after they have been filtering by the STF and the NTF, respectively. Because the spectrum of the quantization noise is shaped by the NTF, significant reduction of in-band quantization noise and improvement in SQNR occur.

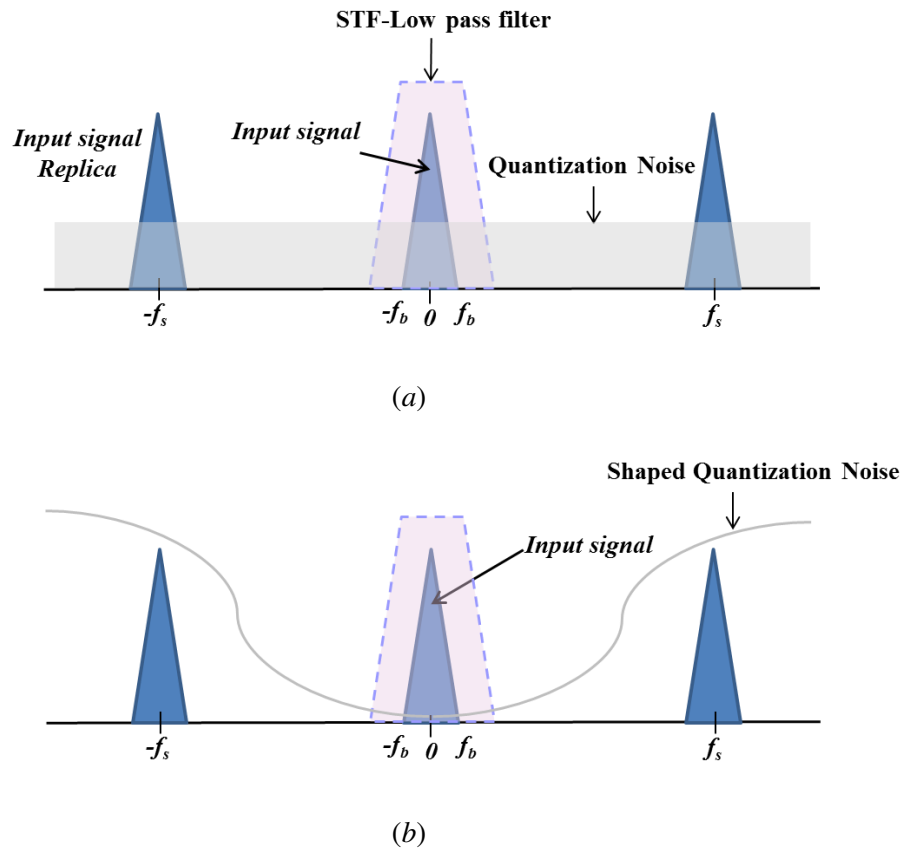


Figure 2.7 The spectra of the input signal and the quantization noise (a) before the noise shaping, (b) after the noise shaping

2.3 Classification of Sigma Delta Modulators

Many $\Sigma\Delta$ architectures have been suggested to improve the resolution of $\Sigma\Delta$ s. Many of these architectures are classified as described in Table 2.1.

Table 2.1 Classification of $\Sigma\Delta$ s

Criteria	Classification
▪ The number of bits in a quantizer	▪ Single-bit $\Sigma\Delta$ ▪ Multi-bit $\Sigma\Delta$
▪ The number of quantizers employed	▪ Single-loop $\Sigma\Delta$ ▪ Cascaded $\Sigma\Delta$
▪ The order of the loop filter	▪ 2 nd order $\Sigma\Delta$ ▪ High order $\Sigma\Delta$
▪ Signal transfer function (STF) characteristic	▪ Lowpass $\Sigma\Delta$ ▪ Bandpass $\Sigma\Delta$
▪ Loop filter circuitry	▪ Discrete time $\Sigma\Delta$ ▪ Continuous time $\Sigma\Delta$

2.3.1 Single-bit $\Sigma\Delta$ s versus Multi-bit $\Sigma\Delta$ s

$\Sigma\Delta$ s can be classified as single-bit $\Sigma\Delta$ s or multi-bit $\Sigma\Delta$ s depending on the number of bits in their quantizers. Single-bit $\Sigma\Delta$ s have the advantage that they are intrinsically linear quantizers because only two levels are used for quantization and mismatches of quantization step sizes do not exist. As a result, they can realize highly linear data conversion. On the other hand, $\Sigma\Delta$ s with multi-bit quantizers generate approximately 6dB less quantization noise for every additional bit. Therefore, the SQNR of $\Sigma\Delta$ s with multi-bit quantizers increases 6dB for every bit added to the quantizer. However, multi-bit $\Sigma\Delta$ s require more analog circuitry and are more difficult to design than single-bit $\Sigma\Delta$ s. Moreover, they exhibit some nonlinearities in their transfer characteristic due to mismatch of quantization step sizes. This can significantly influence a $\Sigma\Delta$'s performance.

2.3.2 Single-loop $\Sigma\Delta$ Ms versus Cascaded $\Sigma\Delta$ Ms

$\Sigma\Delta$ Ms employing only one quantizer are called single-loop $\Sigma\Delta$ Ms, whereas those employing several quantizers are often named Cascaded $\Sigma\Delta$ Ms or MASH $\Sigma\Delta$ Ms. Cascaded topologies use two or more low order $\Sigma\Delta$ Ms which are relatively stable and can achieve performances equivalent to higher order single loop architectures which can suffer from potential instability. However, the Cascaded topologies require tighter constraints on circuit specifications and mismatch than single-loop $\Sigma\Delta$ Ms [8].

2.3.3 2nd order $\Sigma\Delta$ Ms versus High order $\Sigma\Delta$ Ms

$\Sigma\Delta$ Ms can be categorized as 2nd order $\Sigma\Delta$ Ms or high order $\Sigma\Delta$ Ms. If the order of a $\Sigma\Delta$'s loop filter is greater than 2, the $\Sigma\Delta$ is called a high order $\Sigma\Delta$. As the order of the loop filter increases, the quantization noise can be suppressed more at low frequencies and a significant improvement in performance can be achieved. However, high order $\Sigma\Delta$ Ms are conditionally stable whereas 2nd order $\Sigma\Delta$ Ms can be designed to always be stable.

2.3.4 Lowpass $\Sigma\Delta$ Ms versus Bandpass $\Sigma\Delta$ Ms

Depending on a $\Sigma\Delta$'s NTF and STF characteristics, a $\Sigma\Delta$ can be classified as either a lowpass (LP) $\Sigma\Delta$ or a bandpass (BP) $\Sigma\Delta$. $\Sigma\Delta$ Ms that have NTFs with highpass shapes and that have STFs with lowpass shapes are considered LP $\Sigma\Delta$ Ms. $\Sigma\Delta$ Ms that have NTFs with bandstop shapes and that have STFs with bandpass shapes are called BP $\Sigma\Delta$ Ms.

2.3.5 Discrete Time $\Sigma\Delta$ Ms versus Continuous Time $\Sigma\Delta$ Ms

Finally, $\Sigma\Delta$ Ms can be classified as either discrete time (DT) $\Sigma\Delta$ Ms or continuous time (CT) $\Sigma\Delta$ Ms. $\Sigma\Delta$ Ms with a loop filter consisting of discrete time circuits such as switched capacitor or

switched current circuits are called DT $\Sigma\Delta$ s. Similarly, $\Sigma\Delta$ s with a loop filter consisting of continuous time circuits such as transconductors and integrators are called CT $\Sigma\Delta$ s.

2.3.6 $\Sigma\Delta$ s in this dissertation

Whereas DT $\Sigma\Delta$ s can be accurately simulated and analyzed using simple difference equations, CT $\Sigma\Delta$ s are more difficult to simulate and analyze due to the mixed signal nature of the feedback loop. Single loop, single-bit $\Sigma\Delta$ s have the advantage of being able to perform highly linear data conversion; however, they can become unstable for loop filter orders higher than two. In this dissertation, a stability criterion is developed for single loop CT $\Sigma\Delta$ s. This method is illustrated using single loop, single-bit $\Sigma\Delta$ s with loop filter orders ranging from 2 to 5. An overload criterion is also developed for single loop CT $\Sigma\Delta$ s. This method is also illustrated using single loop, single-bit $\Sigma\Delta$ s with loop filter orders ranging from 2 to 5. Also, CT $\Sigma\Delta$ s from 2nd order to 5th order are considered for comparison of simulation methods for CT $\Sigma\Delta$ s.

2.4 Topology Selection of the CT $\Sigma\Delta$ for simulations

After determining a desired NTF and STF, the NTF and STF coefficients need to be implemented in a hardware structure, such as a cascade of resonators feedback (CRFB), cascade of resonators feedforward (CRFF), cascade of integrator feedback (CIFB), and cascade of integrator feedforward (CIFF) implementations. Each of these feedback architectures feeds back the modulator output to each integrator. Because the amplifier nonlinearities generate harmonic distortion that depends on the input signal of the amplifier, single loop feedback architectures have signal distortion [9, 10, 11]. On the other hand, feedforward architectures sum all integrator outputs and the input signal at the input of the quantizer. These architectures have the benefit of lower signal distortion than feedback architectures. However, feedforward architectures require extra components for the summation before the quantizer, and thus these architectures have a

higher power consumption than feedback architectures [12]. In this dissertation, CT $\Sigma\Delta$ Ms are implemented using the CIFB architecture. These $\Sigma\Delta$ Ms are also typically designed using Chebyshev Type 2 NTFs.

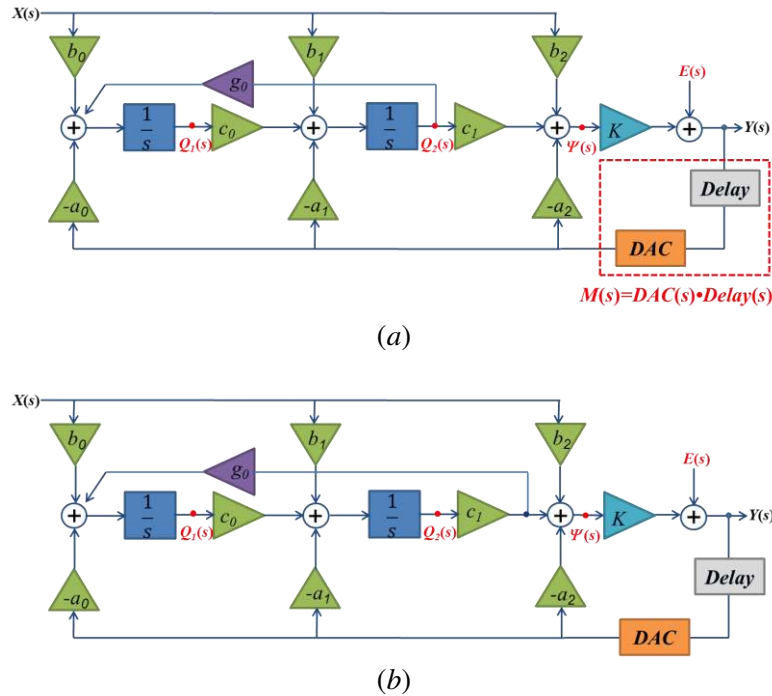


Figure 2.8 2nd order lowpass CT $\Sigma\Delta$ M block diagram
(a) RC implementation, (b) G_mC implementation

Fig 2.8 shows the block diagrams of CIFB implementations of a 2nd order CT $\Sigma\Delta$ M. Fig 2.8 (a) shows a CIFB block diagram where the integrators are implemented using RC integrators and Fig 2.8 (b) shows a CIFB block diagram where the integrators are implemented using G_mC integrators. In general, RC integrators have better linearity and larger signal swing than their G_mC counterparts [13]. However, linearization circuitry can be added to G_mC integrators to improve their linearity. The additional linearization circuitry adds phase to the feedback loop which negatively affects stability. RC integrators have drawbacks such as large die area, increased manufacturing price, low speed and high power consumption. G_mC integrators can be smaller and use less power; however, many G_mC integrator architectures use resistors to get a particular

transconductance, G_m , and the layout of these resistors can increase the G_mC integrator's die size significantly.

From inspection of the block diagram shown in Fig 2.8 (a), the $\Sigma\Delta M$'s states, $Q_1(s)$ and $Q_2(s)$, the quantizer's input, $\Psi(s)$, and the $\Sigma\Delta M$'s output, $Y(s)$ can be calculated as

$$Q_1(s) = \{b_0X(s) - a_0 \cdot M(s) \cdot Y(s) + g_0Q_2(s)\} \frac{1}{s} \quad (2.27)$$

$$Q_2(s) = \{b_1X(s) - a_1 \cdot M(s) \cdot Y(s) + c_0Q_1(s)\} \frac{1}{s} \quad (2.28)$$

$$\Psi(s) = b_2X(s) - a_2 \cdot M(s) \cdot Y(s) + c_1Q_2(s) \quad (2.29)$$

and

$$Y(s) = K \cdot \Psi(s) + E(s) \quad (2.30)$$

where $M(s) = DAC(s) \cdot Delay(s)$. Substituting (2.27) into (2.28) and solving for $Q_2(s)$, the resulting equation can be substituted into (2.29). Substituting that result into (2.30), the STF and the NTF for the RC implementation in Fig 2.8 (a) can be determined to be

$$STF(s) = \frac{K \cdot (b_2s^2 + b_1c_1s + b_0c_0c_1 - g_0b_2c_0)}{\{1 + K \cdot M(s) \cdot a_2\}s^2 + K \cdot M(s) \cdot a_1c_1s + \{K \cdot M(s) \cdot (a_0c_0c_1 - g_0a_2c_0) - g_0c_0\}} \quad (2.31)$$

and

$$NTF(s) = \frac{s^2 - g_0c_0}{\{1 + K \cdot M(s) \cdot a_2\}s^2 + K \cdot M(s) \cdot a_1c_1s + \{K \cdot M(s) \cdot (a_0c_0c_1 - g_0a_2c_0) - g_0c_0\}} \quad (2.32)$$

The gains, a_0 , a_1 , a_2 , b_0 , b_1 , b_2 , c_0 , c_1 and g_0 can be determined by equating the STF coefficients in (2.31) and the NTF coefficients in (2.32) with the desired STF and NTF coefficients, respectively.

Similarly, for the topology with the G_mC implementation shown in Fig. 2.8 (b), the $\Sigma\Delta M$'s states, $Q_1(s)$ and $Q_2(s)$, the quantizer's input, $\Psi(s)$, and the $\Sigma\Delta M$'s output, $Y(s)$ can be calculated

as

$$Q_1(s) = \{b_0 X(s) - a_0 \cdot M(s) \cdot Y(s) + g_0 c_1 Q_2(s)\} \frac{1}{s} \quad (2.33)$$

$$Q_2(s) = \{b_1 X(s) - a_1 \cdot M(s) \cdot Y(s) + c_0 Q_1(s)\} \frac{1}{s} \quad (2.34)$$

$$\Psi(s) = b_2 X(s) - a_2 \cdot M(s) \cdot Y(s) + c_1 Q_2(s) \quad (2.35)$$

and

$$Y(s) = K \cdot \Psi(s) + E(s) \quad (2.36)$$

where $M(s) = DAC(s) \cdot Delay(s)$. Substituting (2.33) into (2.34) and solving for $Q_2(s)$, the resulting equation can be substituted into (2.35). Substituting that result into (2.36), the STF and the NTF for the $G_m C$ implementation shown in Fig 2.8 (b) can be determined to be

$$STF(s) = \frac{K \cdot (b_2 s^2 + b_1 c_1 s + b_0 c_0 c_1 - g_0 b_2 c_0 c_1)}{\{1 + K \cdot M(s) \cdot a_2\} s^2 + K \cdot M(s) \cdot a_1 c_1 s + \{K \cdot M(s) \cdot (a_0 c_0 c_1 - g_0 a_2 c_0 c_1) - g_0 c_0 c_1\}} \quad (2.37)$$

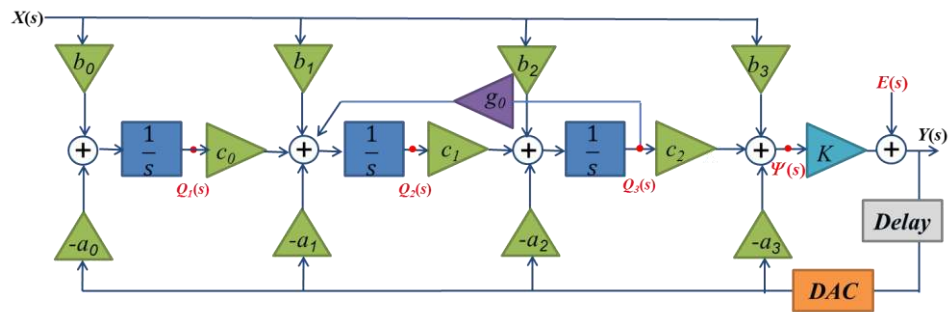
and

$$NTF(s) = \frac{s^2 - g_0 c_0 c_1}{\{1 + K \cdot M(s) \cdot a_2\} s^2 + K \cdot M(s) \cdot a_1 c_1 s + \{K \cdot M(s) \cdot (a_0 c_0 c_1 - g_0 a_2 c_0 c_1) - g_0 c_0 c_1\}} \quad (2.38)$$

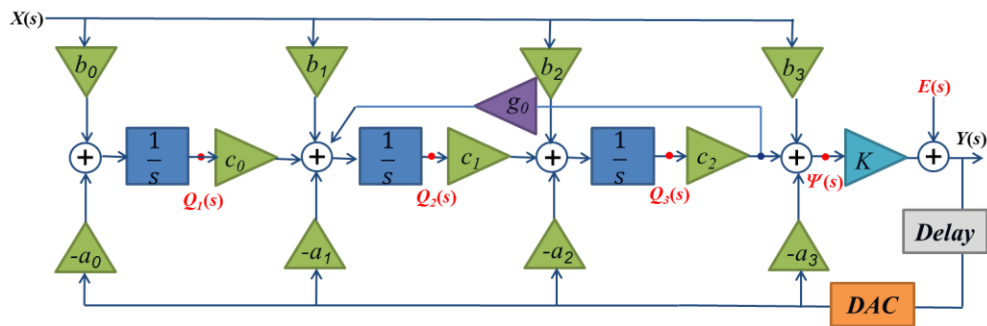
Fig 2.9, Fig 2.10, and Fig 2.11 show the block diagrams of CIFB implementations of 3rd order, 4th order, and 5th order CT $\Sigma\Delta$ Ms, respectively. Using techniques similar to the ones used to determine the STF and NTF of the 2nd order CIFB implementations, the STFs and NTFs for the CIFB implementations of the 3rd order through 5th order CT $\Sigma\Delta$ Ms can be determined as shown in Table 2.2 and Table 2.3. Table 2.2 shows the STF and NTF coefficients for the RC implementations and Table 2.3 shows the STF and NTF coefficients for the $G_m C$ implementations.

2.5 Conclusion

In this Chapter, the general ADC process was modeled mathematically, and from this model, SQNR, DR, and ENOB were defined. It was also shown that $\Sigma\Delta$ ADCs achieve a high resolution signal conversion by using an oversampling quantizer and a feedback loop filter. Various $\Sigma\Delta$ architectures can be used to implement CT $\Sigma\Delta$ s. For this dissertation, single loop, single-bit CT $\Sigma\Delta$ s with loop filter orders ranging from 2 to 5 are implemented using the CIFB architecture.

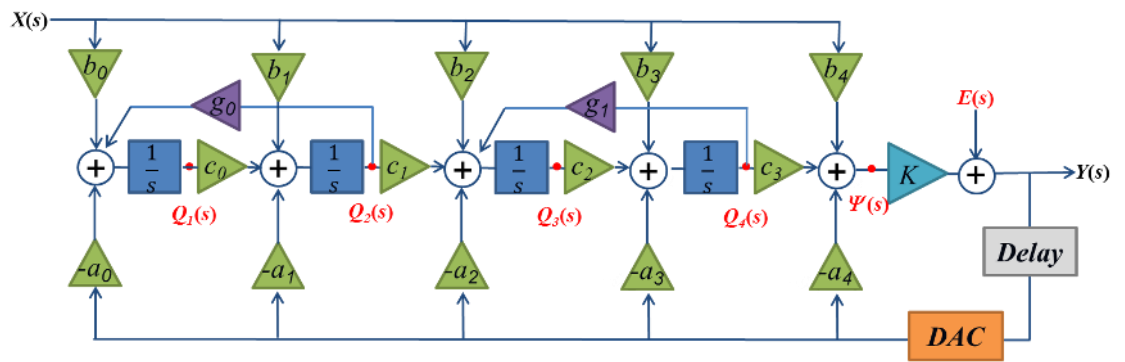


(a)

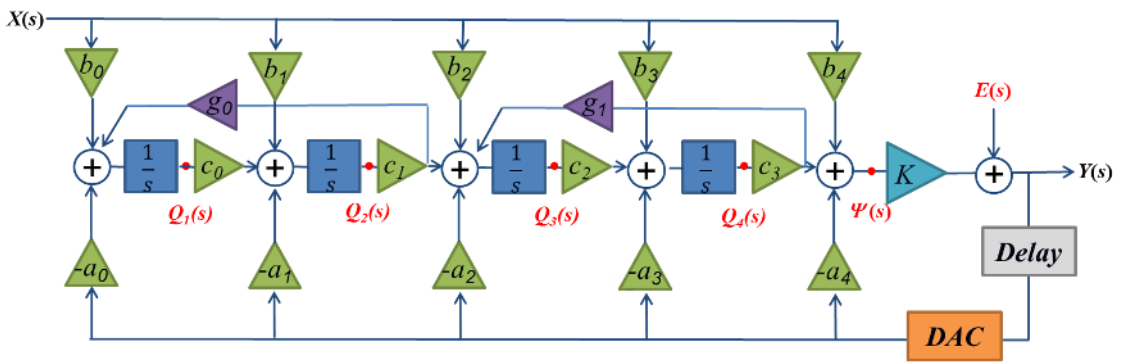


(b)

Figure 2.9 3rd order CT $\Sigma\Delta$ M block diagram
(a) RC implementation, (b) G_mC implementation

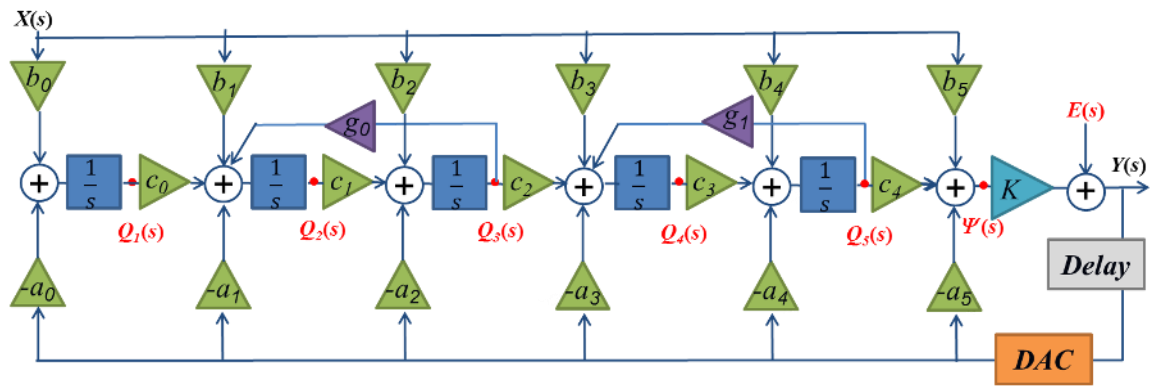


(a)

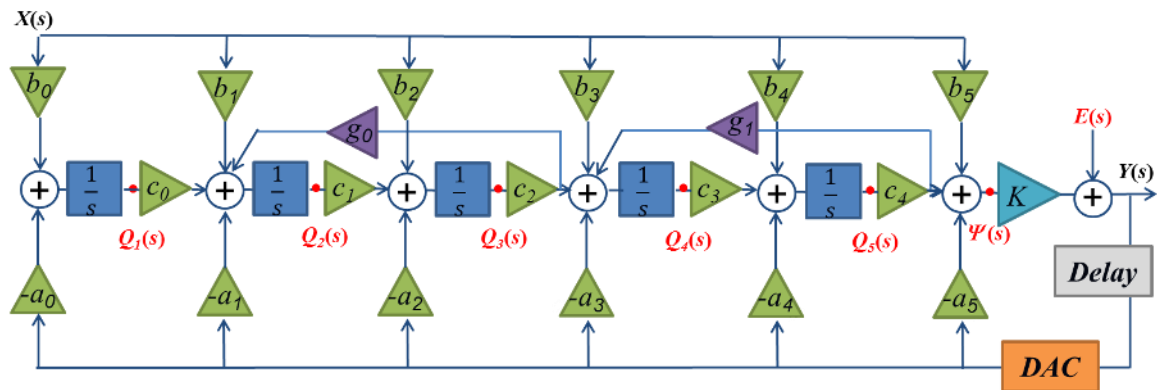


(b)

Figure 2.10 4th order CT $\Sigma\Delta M$ block diagram
 (a) RC implementation, (b) $G_m C$ implementation



(a)



(b)

Figure 2.11 5th order CT $\Sigma\Delta$ M block diagram
 (a) RC implementation, (b) G_mC implementation

Table 2.2 CT ΣAM STF and NTF coefficients for RC implementations

Order	RC implementation	
2nd	STF	$\frac{K \cdot (b_2 s^2 + b_1 c_1 s + b_0 c_0 c_1 - g_0 b_2 c_0)}{\{1 + K \cdot M(s) \cdot a_2\} s^2 + K \cdot M(s) \cdot a_1 c_1 s + \{K \cdot M(s) \cdot (a_0 c_0 c_1 - g_0 a_2 c_0) - g_0 c_0\}}$
	NTF	$\frac{s^2 - g_0 c_0 c_1}{\{1 + K \cdot M(s) \cdot a_2\} s^2 + K \cdot M(s) \cdot a_1 c_1 s + \{K \cdot M(s) \cdot (a_0 c_0 c_1 - g_0 a_2 c_0 c_1) - g_0 c_0 c_1\}}$
3rd	STF	$\frac{K \cdot (b_3 s^3 + b_2 c_1 s^2 + (b_1 c_1 c_2 - g_0 b_3 c_1) s + b_0 c_0 c_1 c_2)}{\{1 + K \cdot M(s) \cdot a_3\} s^3 + K \cdot M(s) \cdot a_2 c_2 s^2 + \{K \cdot M(s) \cdot (a_1 c_1 c_2 - g_0 a_3 c_1) - g_0 c_1\} s + K \cdot M(s) \cdot a_0 c_0 c_1 c_2}$
	NTF	$\frac{s(s^2 - g_0 c_1)}{\{1 + K \cdot M(s) \cdot a_3\} s^3 + K \cdot M(s) \cdot a_2 c_2 s^2 + \{K \cdot M(s) \cdot (a_1 c_1 c_2 - g_0 a_3 c_1) - g_0 c_1\} s + K \cdot M(s) \cdot a_0 c_0 c_1 c_2}$
4th	STF	$\frac{K \cdot \{b_4 s^4 + b_3 c_1 s^3 + (b_2 c_1 c_2 - g_0 b_4 c_2 - g_1 b_2 c_1) s^2 + (b_1 c_1 c_2 c_2 - g_0 b_3 c_1 c_2 - g_1 a_2 c_1 c_2 + g_0 g_1 b_2 c_1 c_2)\}}{\{1 + K \cdot M(s) \cdot a_4\} s^4 + K \cdot M(s) \cdot a_3 c_3 s^3 + \{K \cdot M(s) \cdot (a_2 c_2 c_3 - g_0 a_4 c_3 - g_1 a_2 c_2) - (g_0 c_3 + g_1 c_2)\} s^2 + K \cdot M(s) \cdot (a_1 c_1 c_3 - g_0 a_3 c_1 c_2) s + \{K \cdot M(s) \cdot (a_0 c_0 c_1 c_3 - g_0 a_4 c_0 c_2) + g_0 g_1 c_1 c_2\}}$
	NTF	$\frac{(s^2 - g_0 c_2)(s^2 - g_1 c_2)}{\{1 + K \cdot M(s) \cdot a_4\} s^4 + K \cdot M(s) \cdot a_3 c_3 s^3 + \{K \cdot M(s) \cdot (a_2 c_2 c_3 - g_0 a_4 c_3 - g_1 a_2 c_2) - (g_0 c_3 + g_1 c_2)\} s^2 + \{K \cdot M(s) \cdot (a_1 c_1 c_3 - g_0 a_3 c_1 c_2 - g_1 a_2 c_1 c_2) + g_0 g_1 a_2 c_1 c_2\} s + \{K \cdot M(s) \cdot (a_0 c_0 c_1 c_3 - g_0 a_4 c_0 c_2) + g_0 g_1 c_1 c_2\}}$
5th	STF	$\frac{K \cdot \{b_5 s^5 + b_4 c_1 s^4 + (b_3 c_1 c_2 - g_0 b_5 c_2 - g_1 b_3 c_1) s^3 + (b_2 c_1 c_2 c_2 - g_0 b_4 c_1 c_2 - g_1 a_3 c_1 c_2 + g_0 g_1 b_3 c_1 c_2) s^2 + (b_1 c_1 c_2 c_2 c_2 - g_0 b_3 c_1 c_2 c_2 - g_1 a_2 c_1 c_2 c_2 + g_0 g_1 b_2 c_1 c_2 c_2) s + (b_0 c_0 c_1 c_2 c_2 - g_0 a_4 c_0 c_2 c_2 - g_1 a_3 a_2 c_0 c_2 + g_0 g_1 b_1 c_0 c_2 c_2)\}}{\{1 + K \cdot M(s) \cdot a_5\} s^5 + K \cdot M(s) \cdot a_4 c_4 s^4 + \{K \cdot M(s) \cdot (a_3 c_3 c_4 - g_0 a_5 c_4 - g_1 a_3 c_3) - (g_0 c_4 + g_1 c_3)\} s^3 + K \cdot M(s) \cdot (a_2 c_2 c_4 - g_0 a_4 c_2 c_3 - g_1 a_3 a_2 c_2 c_3 + g_0 g_1 b_2 c_2 c_3) s^2 + \{K \cdot M(s) \cdot (a_1 c_1 c_4 - g_0 a_4 c_1 c_3 - g_1 a_3 a_2 c_1 c_3 + g_0 g_1 b_1 c_1 c_3) + g_0 g_1 a_2 c_1 c_3\} s + \{K \cdot M(s) \cdot (a_0 c_0 c_1 c_4 - g_0 a_5 c_0 c_3 - g_1 a_4 a_3 c_0 c_3 + g_0 g_1 b_0 c_0 c_3) + g_0 g_1 a_1 c_0 c_3\}}$
	NTF	$\frac{s^2(s^3 - g_0 c_3)(s^2 - g_1 c_3)}{\{1 + K \cdot M(s) \cdot a_5\} s^5 + K \cdot M(s) \cdot a_4 c_4 s^4 + \{K \cdot M(s) \cdot (a_3 c_3 c_4 - g_0 a_5 c_4 - g_1 a_3 c_3) - (g_0 c_4 + g_1 c_3)\} s^3 + \{K \cdot M(s) \cdot (a_2 c_2 c_4 - g_0 a_4 c_2 c_3 - g_1 a_3 a_2 c_2 c_3 + g_0 g_1 b_2 c_2 c_3) + g_0 g_1 a_2 c_2 c_3\} s^2 + \{K \cdot M(s) \cdot (a_1 c_1 c_4 - g_0 a_4 c_1 c_3 - g_1 a_3 a_2 c_1 c_3 + g_0 g_1 b_1 c_1 c_3) + g_0 g_1 a_2 c_1 c_3\} s + \{K \cdot M(s) \cdot (a_0 c_0 c_1 c_4 - g_0 a_5 c_0 c_3 - g_1 a_4 a_3 c_0 c_3 + g_0 g_1 b_0 c_0 c_3) + g_0 g_1 a_1 c_0 c_3\}}$

Table 2.3 CT ΣAM STF and NTF coefficients for G_mC implementations

Order	G_mC implementation	
2nd	STF	$\frac{K \cdot (b_2 s^2 + b_1 s + b_0 c_1 - g_0 b_2 c_1)}{\{1 + K \cdot M(s) \cdot a_2\} s^2 + K \cdot M(s) \cdot a_1 s + \{K \cdot M(s) \cdot (a_0 c_1 - g_0 a_2 c_1) - g_0 c_1\}}$
	NTF	$\frac{s^2 - g_0 c_1}{\{1 + K \cdot M(s) \cdot a_2\} s^2 + K \cdot M(s) \cdot a_1 s + \{K \cdot M(s) \cdot (a_0 c_1 - g_0 a_2 c_1) - g_0 c_1\}}$
3rd	STF	$\frac{K \cdot \{b_3 s^3 + b_2 c_2 s^2 + (b_1 c_2 - g_0 b_3 c_2) s + b_0 c_1 c_2\}}{\{1 + K \cdot M(s) \cdot a_3\} s^3 + K \cdot M(s) \cdot a_2 c_2 s^2 + \{K \cdot M(s) \cdot (a_1 c_2 - g_0 a_3 c_2) - g_0 c_2\} s + K \cdot M(s) \cdot a_0 c_1 c_2}$
	NTF	$\frac{s(s^2 - g_0 c_2)}{\{1 + K \cdot M(s) \cdot a_3\} s^3 + K \cdot M(s) \cdot a_2 c_2 s^2 + \{K \cdot M(s) \cdot (a_1 c_2 - g_0 a_3 c_2) - g_0 c_2\} s + K \cdot M(s) \cdot a_0 c_1 c_2}$
4th	STF	$\frac{K \cdot \{b_4 s^4 + b_3 c_3 s^3 + (b_2 c_3 - g_0 b_4 c_3 - g_0 b_3 c_2) s^2 + (b_1 c_3 - g_0 b_4 c_2 - g_0 b_3 c_1) s + (b_0 c_3 - g_0 b_4 c_1 - g_0 b_3 c_2) s + b_0 c_1 c_2\}}{\{1 + K \cdot M(s) \cdot a_4\} s^4 + K \cdot M(s) \cdot a_3 c_3 s^3 + \{K \cdot M(s) \cdot (a_2 c_3 - g_0 a_4 c_3) - (g_0 c_3 + g_0 c_2)\} s^2 + K \cdot M(s) \cdot (a_1 c_3 - g_0 a_4 c_2 - g_0 a_3 c_1) s + \{K \cdot M(s) \cdot (a_0 c_3 - g_0 a_4 c_1 - g_0 a_3 c_2) - (g_0 c_3 + g_0 c_2)\}}$
	NTF	$\frac{(s^2 - g_0 c_2)(s^2 - g_0 c_1)}{\{1 + M(s) \cdot a_4\} s^4 + K \cdot M(s) \cdot a_3 c_3 s^3 + \{K \cdot M(s) \cdot (a_2 c_3 - g_0 a_4 c_3) - (g_0 c_3 + g_0 c_2)\} s^2 + K \cdot M(s) \cdot (a_1 c_3 - g_0 a_4 c_2 - g_0 a_3 c_1) s + \{K \cdot M(s) \cdot (a_0 c_3 - g_0 a_4 c_1 - g_0 a_3 c_2) - (g_0 c_3 + g_0 c_2)\}}$
5th	STF	$\frac{K \cdot \{b_5 s^5 + b_4 c_4 s^4 + (b_3 c_4 - g_0 b_5 c_4 - g_0 b_4 c_3) s^3 + (b_2 c_4 - g_0 b_5 c_3 - g_0 b_4 c_2) s^2 + (b_1 c_4 - g_0 b_5 c_2 - g_0 b_4 c_1) s + (b_0 c_4 - g_0 b_5 c_1 - g_0 b_4 c_2) s + b_0 c_1 c_2\}}{\{1 + K \cdot M(s) \cdot a_5\} s^5 + K \cdot M(s) \cdot a_4 c_4 s^4 + \{K \cdot M(s) \cdot (a_3 c_4 - g_0 a_5 c_4) - (g_0 c_4 + g_0 c_3)\} s^3 + K \cdot M(s) \cdot (a_2 c_4 - g_0 a_5 c_3 - g_0 a_4 c_2) s^2 + \{K \cdot M(s) \cdot (a_1 c_4 - g_0 a_5 c_2 - g_0 a_4 c_1) + g_0 a_3 c_2\} s + K \cdot M(s) \cdot a_0 c_1 c_2}$
	NTF	$\frac{s^2(s^2 - g_0 c_2)(s^2 - g_0 c_1)}{\{1 + K \cdot M(s) \cdot a_5\} s^5 + K \cdot M(s) \cdot a_4 c_4 s^4 + \{K \cdot M(s) \cdot (a_3 c_4 - g_0 a_5 c_4) - (g_0 c_4 + g_0 c_3)\} s^3 + K \cdot M(s) \cdot (a_2 c_4 - g_0 a_5 c_3 - g_0 a_4 c_2) s^2 + \{K \cdot M(s) \cdot (a_1 c_4 - g_0 a_5 c_2 - g_0 a_4 c_1) + g_0 a_3 c_2\} s + K \cdot M(s) \cdot a_0 c_1 c_2}$

CHAPTER 3

A COMPARISON OF CT $\Sigma\Delta$ SIMULATION METHODS

Because DT $\Sigma\Delta$ s are simply made up of delays and gains, they can be accurately modeled using simple difference equations. On the other hand, CT $\Sigma\Delta$ s can be more difficult to simulate due to the mixed signal nature of the feedback loop. Several common approaches for simulating CT $\Sigma\Delta$ s have been developed and the representative methods include SPICE modeling, solving differential equations analytically and numerically, implementing difference equations based on impulse invariance transform and using Simulink. Each simulation method has a tradeoff between simplicity, speed and accuracy. In this chapter, the delta transform is used to determine difference equations that model CT $\Sigma\Delta$ s. These difference equations use the $\Sigma\Delta$'s input signal and the quantizer's feedback signal to determine the input at the quantizer's next sample time. However, unlike the other difference equation methods, the delta transform can be used to determine the loop filter signal values at times other than the sampling time. This method's modeling simplicity, accuracy and speed are compared to existing simulation methods by simulating several CT $\Sigma\Delta$ s.

3.1 The Conventional Approaches to Simulating CT $\Sigma\Delta$ s

CT $\Sigma\Delta$ s are most commonly simulated by using SPICE, solving differential equations, implementing difference equation based on the impulse invariance transform, and using Simulink/MATLAB.

3.1.1 *Macromodel in SPICE*

Simulating CT $\Sigma\Delta$ s using SPICE usually begins with macro level simulations using ideal components such as ideal voltage controlled voltage, or current, sources and ideal quantizers. These simulations are typically used to determine the $\Sigma\Delta$'s ideal performance. After the macro model has been designed to meet performance specifications, specific transistor level systems,

such as operational amplifiers, transconductance amplifiers, and DACs can be substituted for the macro level components to observe nonideal effects such as finite amplifier gains and bandwidths, parasitic capacitances and quantizer metastability. Full circuit level simulation using SPICE can usually be expected to give realistic results because transistor level models include nonideal effects such as finite transistor gains, finite amplifier bandwidths, and parasitic capacitances.

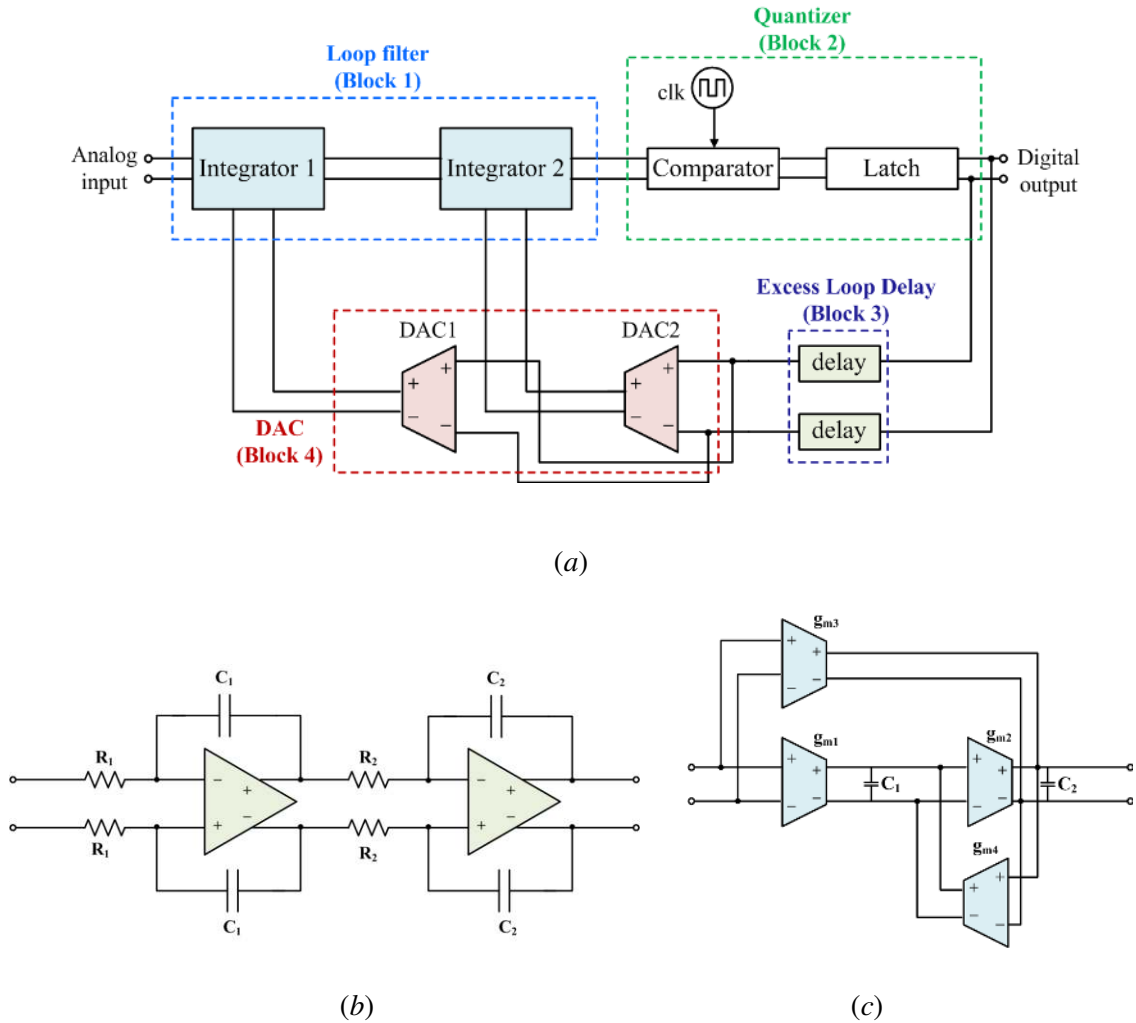


Figure 3.1 Macromodel of a 2nd order CT $\Delta\Sigma$ ^[15]
 (a) Functional blocks of a 2nd order CT $\Delta\Sigma$ M, (b) RC integrators implementation for a loop filter, (c) G_mC integrators implementation for a loop filter

As shown in Fig 3.1 (a), a CT $\Delta\Sigma$ M can be divided into functional blocks which can be further divided into individual circuits and sub-circuits. A loop filter can be implemented using RC

integrators or G_mC integrators. Fig 3.1 (b) shows an RC integrator macro model circuit for the integrators in Fig 3.1 (a). Fig 3.1 (c) shows a G_mC integrator macro model circuit for the integrators in Fig 3.1 (a). SPICE simulation can generate the most accurate simulation results because the nonideal effects can be reflected in the circuit. However, simulating CT $\Sigma\Delta$ Ms using SPICE can be time consuming even for macro models, and they are especially time consuming for higher order $\Sigma\Delta$ Ms [15].

3.1.2 Solving differential equations

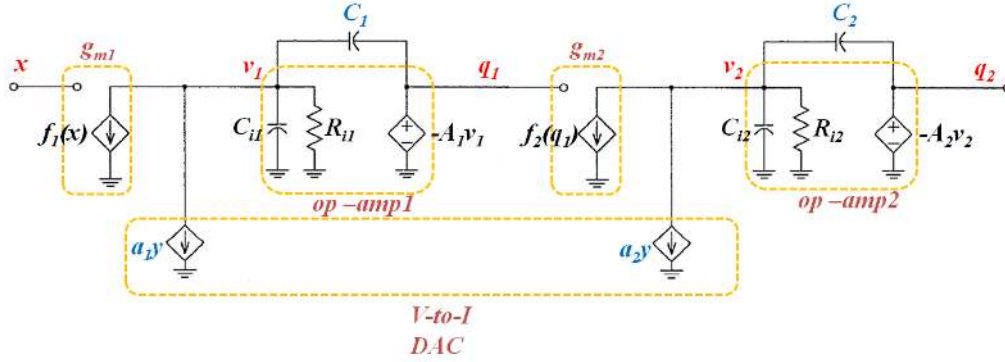


Figure 3.2 Circuit model of a 2nd order CT $\Sigma\Delta$ M^[4]

Alternatively, the simulation of the 2nd order CT $\Delta\Sigma$ M shown in Fig 3.1 can be approached by using the equivalent circuit depicted in Fig 3.2. A set of differential equations can be determined by writing the circuit's node equations. To illustrate, consider the single-ended circuit model of a 2nd order CT $\Delta\Sigma$ M shown in Fig 3.2 [17]. By applying Kirchoff's current law (KCL) to the nodes, v_1 and v_2 ,

$$g_{m1}x(t) + a_1y(n) + \left(sC_{i1} + \frac{1}{R_{i1}} \right) v_1(t) = sC_1 (q_1(t) - v_1(t)) \quad (3.1)$$

$$g_{m2}q_1(t) + a_2y(n) + \left(sC_{i2} + \frac{1}{R_{i2}} \right) v_2(t) = sC_2 (q_2(t) - v_2(t)) \quad (3.2)$$

where

$$v_1(t) = \frac{-q_1(t)}{A_1}, \quad v_2(t) = \frac{-q_2(t)}{A_2}$$

In the time domain, (3.1) and (3.2) can be written as

$$\frac{dq_1(t)}{dt} = \frac{g_{m1}x(t) + a_1y(n) - \frac{q_1(t)}{R_{i1}A_1}}{\frac{1}{A_1}(C_{i1} + C_1) + C_1} \quad (3.3)$$

and

$$\frac{dq_2(t)}{dt} = \frac{g_{m2}q_1(t) + a_2y(n) - \frac{q_2(t)}{R_{i2}A_2}}{\frac{1}{A_2}(C_{i2} + C_2) + C_2}, \quad (3.4)$$

respectively. This set of node equations can be written as linear state space equations and solved numerically to determine the system behavior as a function of time [16, 17, 18]. The node voltages, $q_1(t)$ and $q_2(t)$, which are the solution of the differential equations are composed of a zero input response (ZIR) which is a function of the initial condition, and a zero state response (ZSR) which is a function of the input, $x(t)$. A ZIR and a ZSR can be obtained using the resolvent matrix of the system [16, 17, 18].

This approach to modeling and simulating CT $\Delta\Sigma$ Ms allows nonideal effects such as finite amplifier gain (such as A_1 or A_2) and finite amplifier bandwidth to simply be added to the model and simulation. While this method can simulate a $\Sigma\Delta$ M much faster than using SPICE, it is not as fast or as simple as other methods.

3.1.3 Implementing difference equation (CT/DT equivalence)

Two other $\Sigma\Delta$ M simulation approaches use difference equations to model the $\Sigma\Delta$ M's loop filter. These difference equations use the $\Sigma\Delta$ M's input signal and the quantizer's feedback signal to determine the input at the quantizer's next sample time. This method then iterates these

calculations for each clock sample.

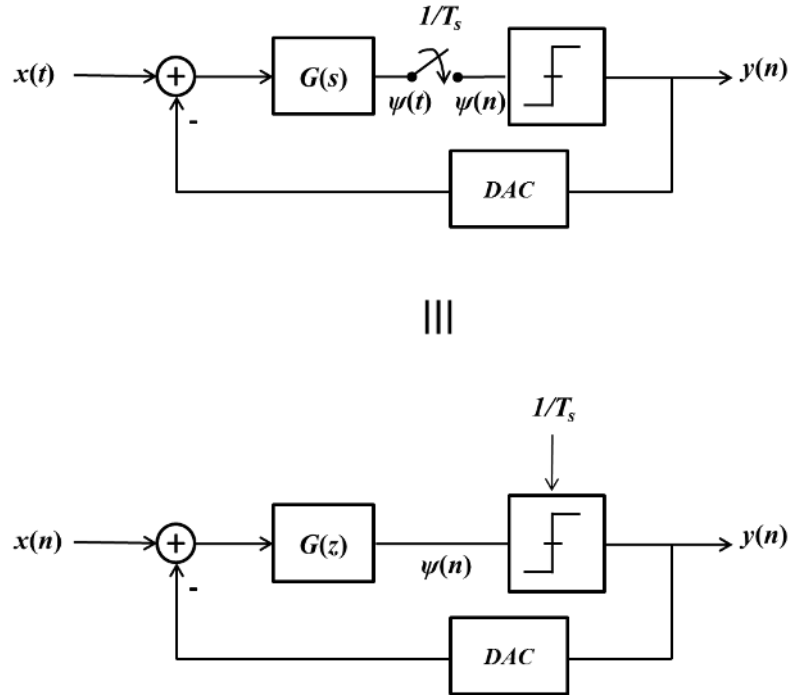


Figure 3.3 Equivalence between a CT $\Sigma\Delta$ M and a DT $\Sigma\Delta$ M

One of these methods determines the difference equations using the impulse invariance transformation. Fig 3.3 indicates that the equivalence between a CT $\Sigma\Delta$ M and a DT $\Sigma\Delta$ M for both $\Sigma\Delta$ Ms to have identical outputs. The quantizer inputs of both of the CT $\Sigma\Delta$ M and the DT $\Sigma\Delta$ M must be identical at sampling instants, $n \cdot T_s$ where n is the sample number and T_s is sampling period. This requires that the impulse responses of the CT $\Sigma\Delta$ M and the DT $\Sigma\Delta$ M are identical at the sampling instants, leading to the condition

$$\mathcal{Z}^{-1}\{G(z)\} = \mathcal{L}^{-1}\{DAC(s) \cdot G(s)\} \Big|_{t=n \cdot T_s} \quad (3.5)$$

or, in the time domain,

$$\psi(n) = [dac(t) * g(t)] \Big|_{t=n \cdot T_s} = \int_{-\infty}^{\infty} dac(t) g(t - \tau) d\tau \Big|_{t=n \cdot T_s} \quad (3.6)$$

where $dac(t)$ is the impulse response of the DAC and $g(t)$ is the impulse response of the $G(s)$ block. The transformation between the CT and DT impulse responses is called the impulse-invariance transformation [19]. This approach is much faster than SPICE simulation or solving the differential equations; however, it can be less accurate than SPICE simulations.

The other difference equation method uses a short SPICE transient simulation and numerically determines a difference equation that minimizes a 2 norm error between the SPICE data and the difference equation output. Although this method is faster than SPICE simulations and the differential equations method mentioned earlier, this method can be less accurate due to some guesswork to find the best difference equations.

3.1.4 MATLAB/Simulink

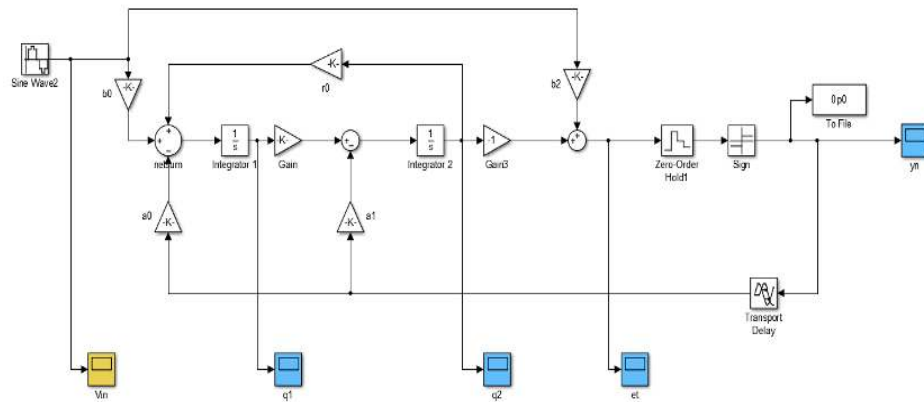


Figure 3.4 Simulink model for a 2nd order CT $\Sigma\Delta M$

MATLAB/Simulink is also commonly used to simulate CT $\Sigma\Delta M$ s. Fig 3.4 show a Simulink schematic of a 2nd order $\Sigma\Delta M$. Simulink schematics are quick and simple to create and Simulink's simulation times are relatively fast; however, Simulink's simulation accuracy is often dependent on the proper selection of Simulink models [20].

3.2 Simulating CT $\Sigma\Delta$ Ms Using the Delta Operator

In this section, the delta transform is used to determine difference equations that model CT $\Sigma\Delta$ Ms. These difference equations use the $\Sigma\Delta$ M's input signal and the quantizer's feedback signal to determine the input at the quantizer's next sample time. However, unlike the other difference equation methods, the delta transform calculates the loop filter signal values at times between the sampling times.

Because discrete systems are suitable for computer realization and continuous systems are not and because continuous systems are often described in the Laplace transform's s domain and discrete systems are often described in the \mathcal{Z} -transform's z domain, many transformations have been developed between the Laplace transform's s domain and the \mathcal{Z} -transform's z domain [21]. One such transformation is the delta transform or delta operator [22]. The discrete delta operator approximates the Euler derivative, and as the delta operator's sampling period is reduced, not only does the approximation improve, but the delta transform approaches the Laplace transform. As a result, the delta transform's poles and zeros, or the discrete system's poles and zeros, approach the Laplace transform's poles and zeros, or the continuous system's poles and zeros as the delta transform sample period approaches. Thus, unlike many other discrete models, a delta transform's discrete model of a continuous system can better represent an underlying continuous physical model by simply increasing the delta transform's sampling rate.

3.2.1 Definition of Delta Transform

The delta transform, Δ , of a function $f(t)$ is defined as

$$\Delta\{f(t)\} = T_{\Delta} \sum_{n=0}^{\infty} f(n \cdot T_{\Delta}) (1 + \delta \cdot T_{\Delta})^{-n} \quad (3.7)$$

where δ is a complex variable and T_{Δ} is the transform's sampling period. To show that $\Delta\{f(t)\} = \mathcal{L}\{f(t)\}$, where \mathcal{L} is the Laplace transform, as T_{Δ} approaches zero, consider

$$\mathcal{L}\{f(t)\} = \int_{t=0}^{\infty} f(t)e^{-st} dt = \lim_{\Delta t \rightarrow 0} \sum_{n=0}^{\infty} f(n \cdot \Delta t) e^{-sn \cdot \Delta t} \Delta t. \quad (3.8)$$

Letting $T_{\Delta} = \Delta t$, and replacing $e^{sT_{\Delta}}$ by its power series expansion, (3.8) can be written as

$$\mathcal{L}\{f(t)\} = \lim_{T_{\Delta} \rightarrow 0} T_{\Delta} \sum_{n=0}^{\infty} f(n \cdot T_{\Delta}) \left\{ 1 + (s \cdot T_{\Delta}) + \frac{(s \cdot T_{\Delta})^2}{2!} + \dots \right\}^{-n}. \quad (3.9)$$

Without the limit, $T_{\Delta} \rightarrow 0$, (3.9) can be approximated as

$$\mathcal{L}\{f(t)\} \cong T_{\Delta} \sum_{n=0}^{\infty} f(n \cdot T_{\Delta}) (1 + \delta \cdot T_{\Delta})^{-n} = T_{\Delta} \cdot \mathcal{Z}\{f(n \cdot T_{\Delta})\} \Big|_{z=1+\delta T_{\Delta}} \quad (3.10)$$

where $\mathcal{Z}\{f(n \cdot T_{\Delta})\}$ is \mathcal{Z} -transform of $f(n \cdot T_{\Delta})$ and δ is a complex variable where $\delta \rightarrow s$ as $T_{\Delta} \rightarrow 0$.

To develop a transformation between the Laplace transform's s domain, the delta transform's δ domain and the \mathcal{Z} -transform's z domain, consider Euler's forward difference equation that approximates the differential operator; that is, consider

$$\left. \frac{df(t)}{dt} \right|_{t=n \cdot T_{\Delta}} \cong \frac{f[(n+1) \cdot T_{\Delta}] - f(n \cdot T_{\Delta})}{T_{\Delta}}. \quad (3.11)$$

Because the delta transform approaches the Laplace transform and $\delta \rightarrow s$ as $T_{\Delta} \rightarrow 0$, (3.11)

implies that

$$\mathcal{L} \left\{ \left. \frac{df(t)}{dt} \right|_{t=n \cdot T_{\Delta}} \right\} = \lim_{T_{\Delta} \rightarrow 0} \Delta \left\{ \left. \frac{df(t)}{dt} \right|_{t=n \cdot T_{\Delta}} \right\} \cong \mathcal{Z} \left\{ \frac{f[(n+1) \cdot T_{\Delta}] - f(n \cdot T_{\Delta})}{T_{\Delta}} \right\} \quad (3.12)$$

and therefore as $T_{\Delta} \rightarrow 0$,

$$s \cdot F(s) = \delta \cdot F(\delta) \cong \frac{z-1}{T_{\Delta}} \cdot F(z). \quad (3.13)$$

Thus, the delta transform implies that

$$\frac{1}{s} \rightarrow \frac{1}{\delta} \rightarrow \frac{T_{\Delta} \cdot z^{-1}}{1 - z^{-1}} . \quad (3.14)$$

The transformation in (3.14) can be illustrated by the block diagrams in Fig 3.5.

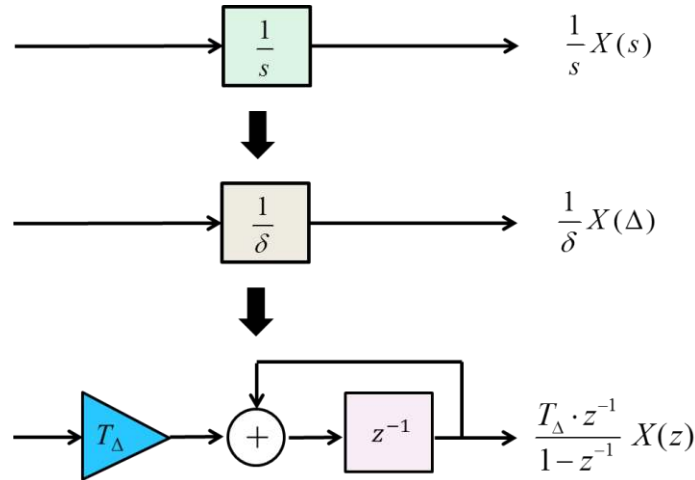


Figure 3.5 Delta operator block diagram

As illustrated in (3.14), the relationship between the delta transform and the \mathcal{Z} -transform is $z = 1 + \delta \cdot T_{\Delta}$. Because stability for the \mathcal{Z} -transform requires that all the system's poles lie within the region, $|z| < 1$, stability for the delta transform requires all the system's poles lie within the region, $|1 + \delta \cdot T_{\Delta}| < 1$ which defines a circle of radius, $1/T_{\Delta}$, centered at $-1/T_{\Delta}$. Therefore, as the sampling time, T_{Δ} approaches zero, the stability region of the delta transform becomes equivalent to that of the Laplace transform whereas the stable region of the \mathcal{Z} -transform is fixed to the interior of the unit circle. Fig 3.6 shows a comparison of stability regions for the \mathcal{Z} -transform, delta-transform, and Laplace domain. These plots illustrate the mapping between the continuous and discrete planes. It can be seen that as T_{Δ} approaches zero, the stability region for the delta transform will grow to approach that of the Laplace domain which is the whole left hand plane.

In summary, the delta-transform has the particular property that as the sample time, T_{Δ} , approaches zero, the delta-transform converges toward its continuous counterpart, the Laplace

transform. As a result, the delta-transform has superior performance at high sample rates compared to the \mathcal{Z} -transform because the continuous and discrete time models approach equivalence when the delta transform has a small sampling time.

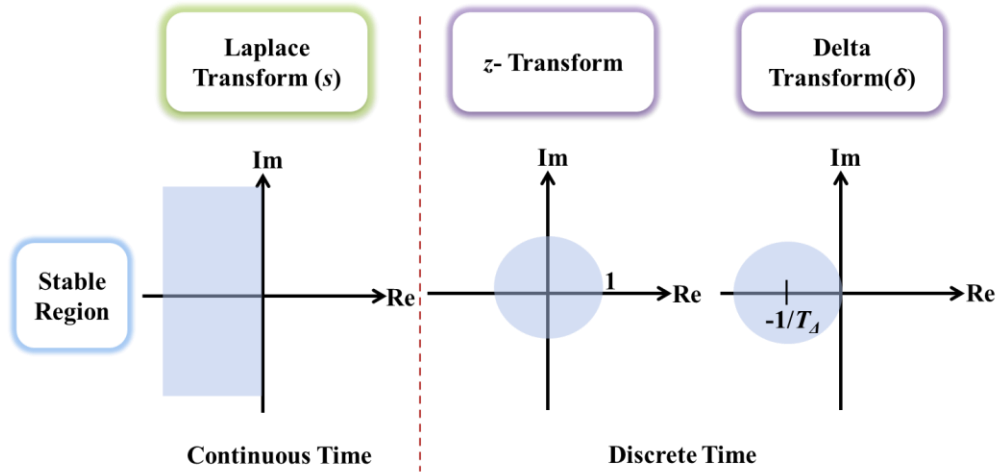


Figure 3.6 Stability regions for the continuous Laplace plane, and the discrete z -plane, delta-plane

3.2.2 Application of Delta Transform for CT $\Sigma\Delta$ Ms simulation

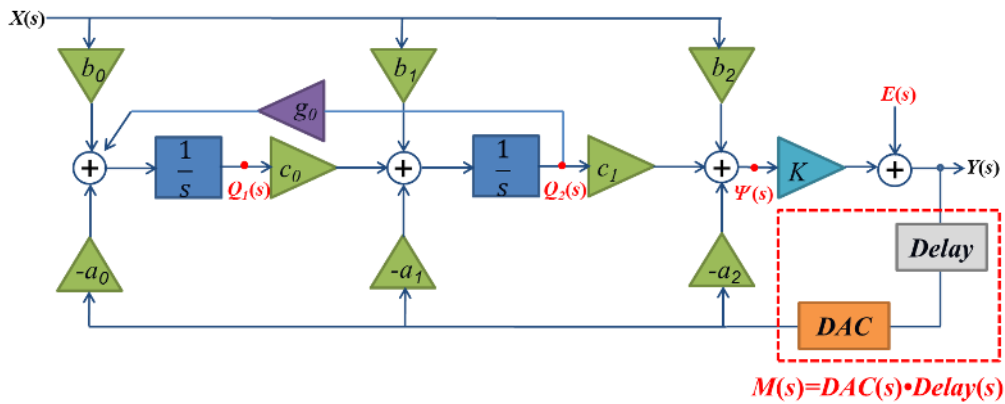


Figure 3.7 The 2nd order CT $\Sigma\Delta$ M block diagram

To apply the delta transform to the block diagram of a CT $\Sigma\Delta$ M, consider the block diagram of the CIFB implementation of a 2nd order CT $\Sigma\Delta$ M described in Chapter 2 and shown in Fig 3.7.

The block diagram in Fig 3.7 describes a 2nd order CT $\Sigma\Delta\text{M}$ where the $\Sigma\Delta\text{M}$'s STF and NTF are given by

$$STF(s) = \frac{K \cdot (b_2 s^2 + b_1 c_1 s + b_0 c_0 c_1 - g_0 b_2 c_0)}{\{1 + K \cdot M(s) \cdot a_2\} s^2 + K \cdot M(s) \cdot a_1 c_1 s + \{K \cdot M(s) \cdot (a_0 c_0 c_1 - g_0 a_2 c_0) - g_0 c_0\}} \quad (3.15)$$

$$NTF(s) = \frac{s^2 - g_0 c_0}{\{1 + K \cdot M(s) \cdot a_2\} s^2 + K \cdot M(s) \cdot a_1 c_1 s + \{K \cdot M(s) \cdot (a_0 c_0 c_1 - g_0 a_2 c_0) - g_0 c_0\}} \quad (3.16)$$

To determine the coefficients in (3.15) and (3.16), a desired NTF is designed and set equal to the NTF in (3.16). Throughout this dissertation, K is set equal to one unless otherwise noted. After determining the NTF, the numerator of a desired STF is determined and set equal to the STF in (3.15). In this dissertation, NTFs are designed as a highpass Chebyshev Type 2 filter with a cutoff frequency near the $\Sigma\Delta\text{M}$'s bandwidth. STFs are designed as a lowpass filter using the poles of the NTFs and the numerator of a lowpass Chebyshev Type 2 filter. The following MATLAB code shows an example of such a $\Sigma\Delta\text{M}$ that has a bandwidth of 20MHz and a sampling rate of 1GHz.

```
[NTFnum,NTFden]=cheby2(2,37,2*pi*22e6,'high','s');
NTF=tf(NTFnum,NTFden);

[STFnum,STFden]=cheby2(2,40,2*pi*750e6,'s');
STFnum=STFnum/STFnum(end)*NTFden(end);
STF=tf(STFnum,NTFden);
```

This code produces

$$STF(s) = \frac{0.01523s^2 + 6.764 \times 10^{17}}{s^2 + 1.155 \times 10^9 s + 6.764 \times 10^{17}} \quad (3.17)$$

and

$$NTF(s) = \frac{s^2 - 2.384 \times 10^{-7} s + 9.554 \times 10^{15}}{s^2 + 1.155 \times 10^9 s + 6.764 \times 10^{17}} \quad (3.18)$$

The gains, a_0 , a_1 , a_2 , b_0 , b_1 , b_2 , c_0 , c_1 and g_0 in (3.15) and (3.16) can be determined by equating the

STF in (3.15) with the desired STF coefficients in (3.17) and by equating the NTF in (3.16) with the desired NTF coefficients in (3.18), respectively.

To simulate the resulting $\Sigma\Delta\text{M}$, the integrators in Fig 3.7 are replaced by the expression in (3.14) where the sampling rate, T_Δ , is chosen to be less than the sampling rate, T , of the $\Sigma\Delta\text{M}$. Fig. 3.8 shows a block diagram of the CT $\Sigma\Delta\text{M}$ represented in Fig 3.7 where the integrators have been replaced by the delta transform equivalents.

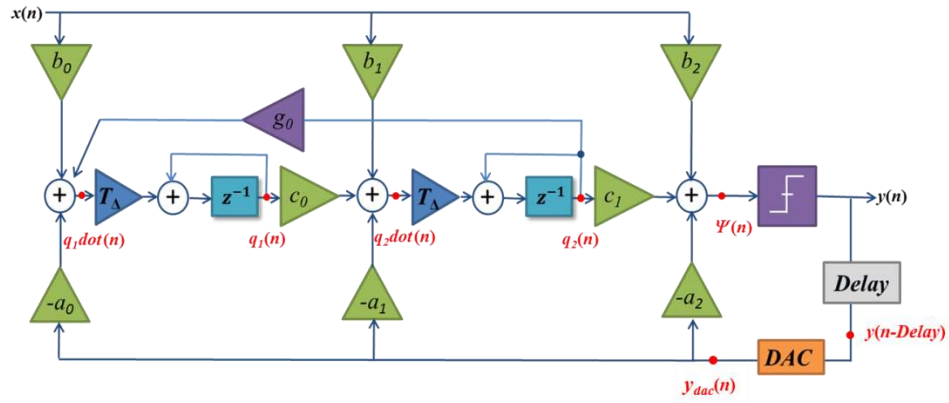


Figure 3.8 2nd order DT model $\Sigma\Delta\text{M}$ using delta transform

By inspection of the block diagram in Fig. 3.8, the difference equations describing the states can be determined as

$$y_{dac}(n) = \text{DAC}[y(n - \text{Delay})] \quad (3.19)$$

$$q_1\text{dot}(n) = b_0 \cdot x(n) - a_0 \cdot y_{dac}(n) + g_0 \cdot q_2(n) \quad (3.20)$$

$$q_1(n) = T_\Delta \cdot q_1\text{dot}(n-1) + q_1(n-1) \quad (3.21)$$

$$q_2\text{dot}(n) = b_1 \cdot x(n) - a_1 \cdot y_{dac}(n) + c_0 \cdot q_1(n) \quad (3.22)$$

$$q_2(n) = T_\Delta \cdot q_2\text{dot}(n-1) + q_2(n-1) \quad (3.23)$$

$$\psi(n) = b_2 \cdot x(n) - a_2 \cdot y_{dac}(n) + c_1 \cdot q_2(n) \quad (3.24)$$

if $n = T / T_\Delta$,

$$y(n) = \text{sgn}\{\psi(n)\} \quad (3.25)$$

where DAC is a function that maps $y(n-Delay)$ to a DAC output. This can be implemented in Matlab using the following code:

```
% Analysis of 2nd Order sigma delta modulator(RC implementation)
for n = start:finish,
    % First state
    qdot(n,1) = b0*x(n) - a0*ydac(n-1) + g0*q(n-1,2);
    q(n,1) = Delta*qdot(n,1) + q(n-1,1);

    % Second state
    qdot(n,2) = b1*x(n) - a1*ydac(n-1) + c0*q(n,1);
    q(n,2) = Delta*qdot(n,2) + q(n-1,2);

    % Input to quantizer
    et(n) = b2*x(n) + c1*q(n,2) - a2*ydac(n-1);

    % Quantizer
    yq(n) = sign(et(n));

    % DAC
    y(n)=y(n-1);

    if rem(n,DeltaOSR) == 0, % Update quantizers every Delta samples
        y(n) = yq(n);
    end

    ydac(n) = y(n-D); % excess loop delay between quantizer and DAC
end
```

As T_{Δ} decreases, this model converges towards its continuous counterpart and the simulation results converge towards a simulation based on the differential equations describing the $\Sigma\Delta M$. Also, because this discrete model uses difference equations, it can simulate more quickly than a continuous time domain model. The delta transform can be easily applied to higher order CT $\Sigma\Delta M$ s.

3.3 Simulation Comparison

To compare the delta transform simulation methods with the four other simulation methods mentioned earlier, six 2nd order, six 3rd order, six 4th order and six 5th order CT $\Sigma\Delta M$ s were simulated.

Each of the CT $\Sigma\Delta$ Ms was designed using an RC implementation and a Chebyshev Type 2 highpass NTF which met the specifications listed in Table 3.1. The delta transform's sampling rate, T_A , was chosen as $T/10$ where T is the $\Sigma\Delta$ M's sampling period. For each $\Sigma\Delta$ M order, the excess loop delays were chosen as $0, 0.5T, T, 1.5T, 2T$ and $2.5T$.

Fig 3.9 (a) shows the five output power spectra generated by simulating the 2nd order CT $\Sigma\Delta$ M with an excess loop delay of zero using each of the five different simulation methods. While the output signal power spectra are mostly coincident, some discrepancy between the simulation results exists; however, little difference between each simulation's SQNR exists for this example. Fig 3.9 (b) shows the five output power spectra of the 2nd order CT $\Sigma\Delta$ M with an excess loop delay of $0.5T$. In this example, the output signal power spectra vary, and a discrepancy between the SQNRs exist. In particular, the output power spectrum from Simulink is noticeably different from the others. Fig 3.9 (c) shows the five output power spectra of the 2nd order CT $\Sigma\Delta$ M with an excess loop delay of T . For this case, the output signal power spectra vary remarkably, and in particular, the output power spectrum using the CT/DT transformation varies from the others. Fig 3.9 (d), (e) and (f) show the five output power spectra of the 2nd order CT $\Sigma\Delta$ M with an excess loop delay of $1.5T, 2T$ and $2.5T$, respectively. The output power spectrum from Simulink varies the most compared to the other spectra, and a discrepancy exists between the SQNR of five output power spectra.

Table 3.1 Simulation Condition

Specification	
Order of loop filter	2, 3, 4, 5
Sampling frequency ($1/T$)	1 GHz
Input frequency	3 MHz
Bandwidth	20 MHz
Excess loop delay	$0, 0.5T, T, 1.5T, 2T, 2.5T$

Fig 3.10 (a) summarizes the simulated SQNRs of the 2nd order CT $\Sigma\Delta$ Ms with respect to the change in excess loop delay. The Simulink simulation results vary the most compared to the other

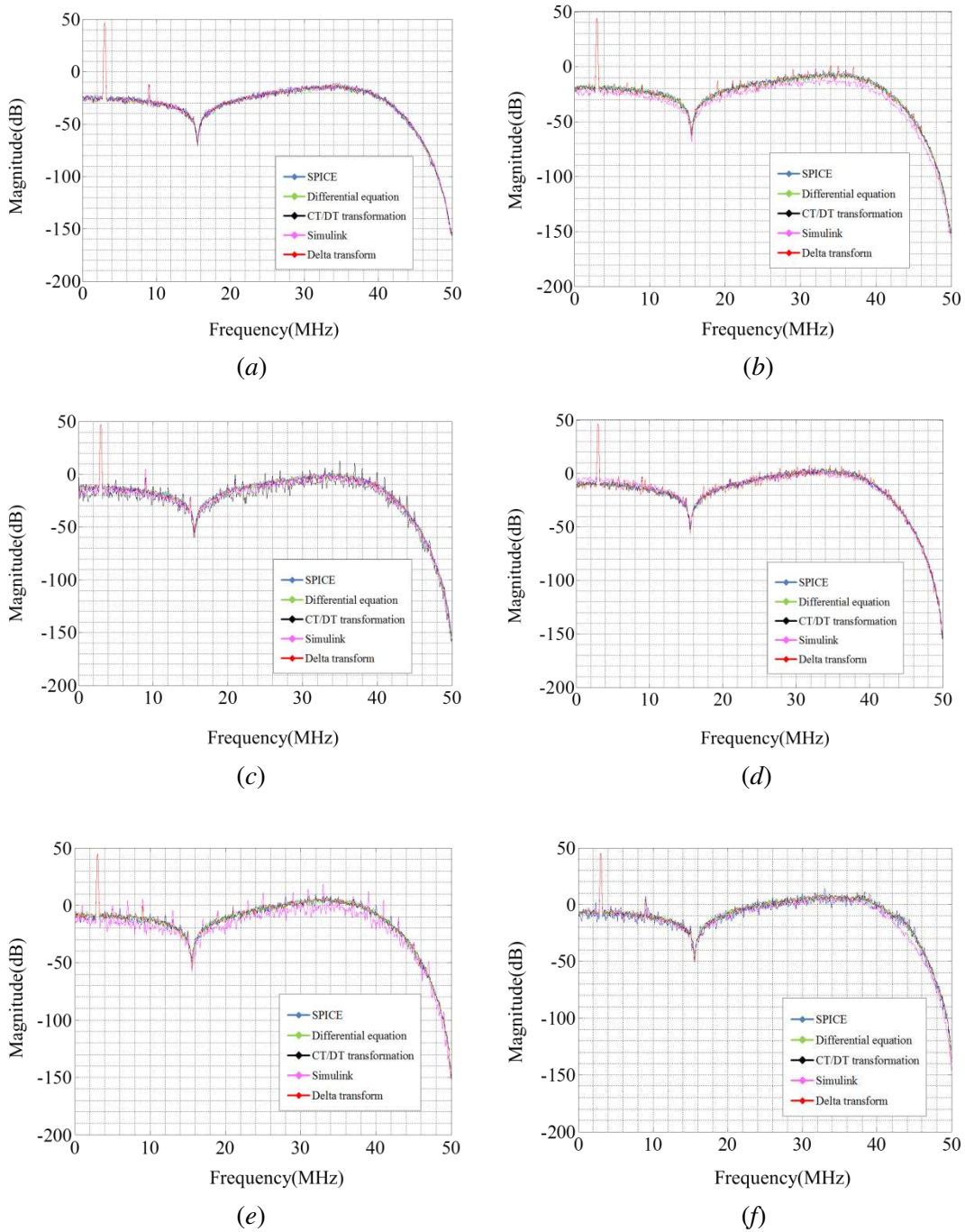


Figure 3.9 The output power spectra comparison for the simulation methodologies for 2nd order CT $\Sigma\Delta$ Ms with an excess loop delay of (a) zero, (b) $0.5T$, (c) T , (d) $1.5T$, (e) $2T$, (f) $2.5T$

simulation methods especially when the excess loop delay time is not a multiple integer of the sampling period (T) such as $0.5T$, $1.5T$ and $2.5T$. The simulation method based on solving

differential equations is the method that has results closest to those of the SPICE simulations which are assumed to be the most accurate. The CT/DT transform simulation results are similar to those of the SPICE simulations; however, for this example, the delta transform simulation results are closer to SPICE's SQNR results than the CT/DT transform simulation results.

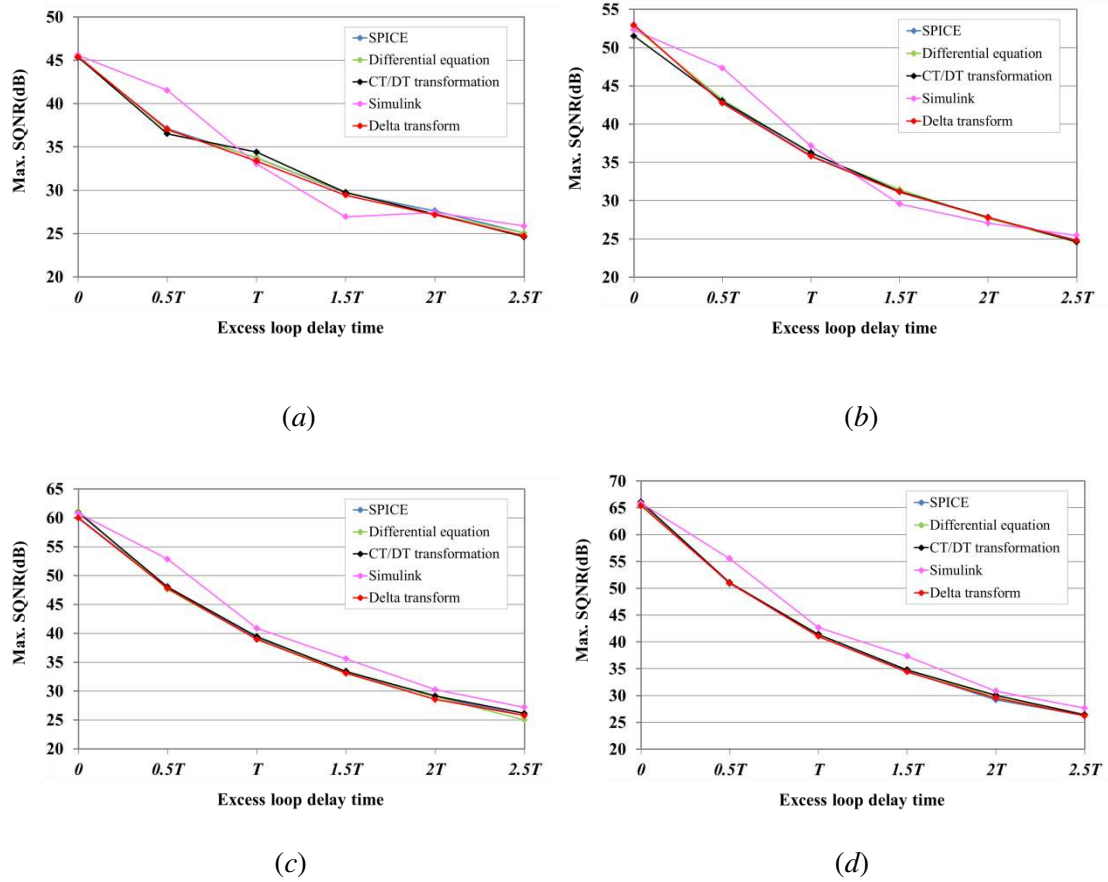


Figure 3.10 Simulation comparison of the maximum SQNR for (a) 2nd order CT $\Sigma\Delta$ Ms, (b) 3rd order CT $\Sigma\Delta$ Ms, (c) 4th order CT $\Sigma\Delta$ Ms, (d) 5th order CT $\Sigma\Delta$ Ms

Fig 3.10 (b) shows the simulated SQNRs of the 3rd order CT $\Sigma\Delta$ Ms with respect to the change in excess loop delay. The results of the 3rd order $\Sigma\Delta$ simulations are similar to those of the 2nd order $\Sigma\Delta$ simulations. The SQNR of the Simulink simulation varies from the other SQNRs and are the least accurate. The SQNRs determined by solving the differential equations are the closest SQNRs to those of the SPICE simulations. The SQNRs simulated using the delta transform are

consistent with the SQNRs generated by solving the differential equations and the SQNRs generated using the CT/DT transformation.

Fig 3.10 (c) and (d) show the simulated SQNRs of the 4th order CT $\Sigma\Delta$ Ms and the 5th order CT $\Sigma\Delta$ Ms with respect to the changes in excess loop delay, respectively. Compared to the simulated SQNRs of the 2nd order CT $\Sigma\Delta$ Ms or the 3rd order CT $\Sigma\Delta$ Ms, little difference is apparent between the SQNRs generated by the four different simulation methods except for the Simulink simulations.

Table 3.2 The SQNR comparison of simulation methods for the 4th order CT $\Sigma\Delta$ Ms

(a) Simulated SQNR

Simulation Methods \ Delay Time		[dB]					
		0	$0.5T$	T	$1.5T$	$2T$	$2.5T$
SPICE		60.05	47.78	39.14	33.21	28.76	25.76
Differential equation		60.12	47.82	39.02	33.32	29.02	25.65
CT/DT transformation		60.88	48.04	39.44	33.42	29.16	26.14
Simulink		60.80	52.85	40.89	35.60	30.24	27.19
Delta transform		59.94	47.79	38.94	33.09	28.54	25.78

(b) The SQNR difference from the SQNR of SPICE

Simulation Methods \ Delay Time		[dB]					
		0	$0.5T$	T	$1.5T$	$2T$	$2.5T$
SPICE		-	-	-	-	-	-
Differential equation		0.07	0.04	-0.12	0.11	0.26	-0.11
CT/DT transformation		0.83	0.26	0.3	0.21	0.4	0.38
Simulink		0.75	5.07	1.75	2.39	1.48	1.43
Delta transform		-0.11	0.01	-0.2	-0.12	-0.22	0.02

(c) The percentage of SQNR difference

Simulation Methods \ Delay Time		[%]					
		0	$0.5T$	T	$1.5T$	$2T$	$2.5T$
SPICE		-	-	-	-	-	-
Differential equation		0.12	0.08	-0.31	0.33	0.90	-0.43
CT/DT transformation		1.38	0.54	0.77	0.63	1.39	1.48
Simulink		1.25	10.61	4.47	7.20	5.15	5.55
Delta transform		-0.18	0.02	-0.51	-0.36	-0.76	0.08

Table 3.3 The SQNR comparison of simulation methods for the 5th order CT $\Sigma\Delta$ Ms

(a) Simulated SQNR

Simulation Methods \ Delay Time		[dB]					
		0	$0.5T$	T	$1.5T$	$2T$	$2.5T$
SPICE		65.59	50.82	41.11	34.58	29.76	26.12
Differential equation		65.63	50.88	41.29	34.76	29.65	26.27
CT/DT transformation		66.07	51.05	41.38	34.80	30.05	26.42
Simulink		65.85	55.51	42.65	37.32	30.83	27.62
Delta transform		65.40	50.94	41.01	34.41	29.55	26.19

(b) The SQNR difference from the SQNR of SPICE

Simulation Methods \ Delay Time		[dB]					
		0	$0.5T$	T	$1.5T$	$2T$	$2.5T$
SPICE		-	-	-	-	-	-
Differential equation		0.04	0.06	0.18	0.18	-0.11	0.15
CT/DT transformation		0.48	0.23	0.27	0.22	0.29	0.3
Simulink		0.26	4.69	1.54	2.74	1.07	1.50
Delta transform		-0.19	0.12	-0.1	-0.17	-0.21	0.07

(c) The percentage of SQNR difference

Simulation Methods \ Delay Time		[%]					
		0	$0.5T$	T	$1.5T$	$2T$	$2.5T$
SPICE		-	-	-	-	-	-
Differential equation		0.06	0.12	0.44	0.52	-0.37	0.57
CT/DT transformation		0.73	0.45	0.66	0.64	0.97	1.15
Simulink		0.40	9.23	3.75	7.92	3.60	5.74
Delta transform		-0.29	0.24	-0.24	-0.49	-0.71	0.27

Table 3.2 and Table 3.3 show and compare the SQNR simulation results for the 4th order CT $\Sigma\Delta$ Ms and 5th order CT $\Sigma\Delta$ Ms, respectively. Table 3.2 (a) and Table 3.3 (a) list the SQNRs for each of simulation methods. Table 3.2 (b) and Table 3.3 (b) list the differences between the SQNRs of the four different simulation methods from the SQNRs of the SPICE simulations which are assumed to be the most accurate. Table 3.2 (c) and Table 3.3 (c) list the percentage differences of the SQNRs of the four different simulation methods from the SQNRs of SPICE simulations. The SQNRs generated by solving the differential equations are the most similar to those generated by SPICE simulation; however, for some excess loop delay times, the SQNRs obtained by using the delta transform are closer to the SQNRs obtained from SPICE simulation

rather than the SQNRs obtained solving the differential equations. The SQNRs generated using the CT/DT transformation and Simulink show some notable difference when compared with the SPICE simulations.

The earlier simulated CT $\Sigma\Delta$ Ms can also be designed using G_mC implementations. To compare the simulation results of the RC implementation to the G_mC implementation, a G_mC implementation of the 2nd order CT $\Sigma\Delta$ M with the specifications listed in Table 3.1 was simulated using the five methods.

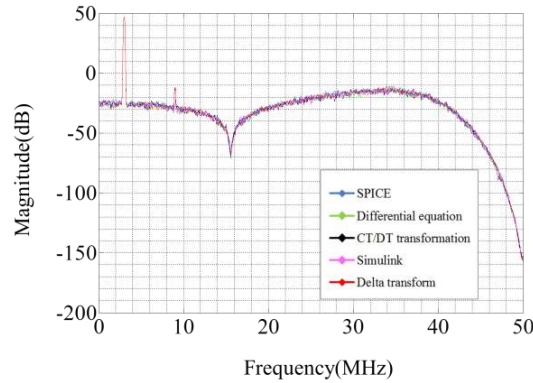


Figure 3.11 The output power spectra for the G_mC implementation for the 2nd order CT $\Sigma\Delta$ Ms with an excess loop delay of zero

Fig 3.11 shows the five output power spectra generated by simulating the 2nd order CT $\Sigma\Delta$ M with an excess loop delay of zero using the G_mC implementation and each of the five different simulation methods. As shown in Fig 3.11 and Fig 3.9 (a), the five output power spectra of the G_mC implementation are the same as the output power spectra of the RC implementation.

Table 3.4 shows the SQNRs of the 2nd order RC implementation simulations shown in Fig 3.9 (a) and 2nd order G_mC implementation simulations shown in Fig 3.11. As shown in Table 3.4, the simulated SQNRs obtained using the G_mC implementation are the same as the simulated SQNRs obtained using RC implementation. The simulated SQNRs are the same for both implementations because the mathematical models for RC implementation and G_mC implementation are the same.

Table 3.4 The SQNRs comparison between RC implementation and $G_m C$ implementation for each of simulation methods

Simulation Methods	[dB]	
	RC implementation	$G_m C$ implementation
SPICE	45.31	45.31
Differential equation	45.39	45.39
CT/DT transformation	45.49	45.49
Simulink	45.58	45.58
Delta transform	45.41	45.41

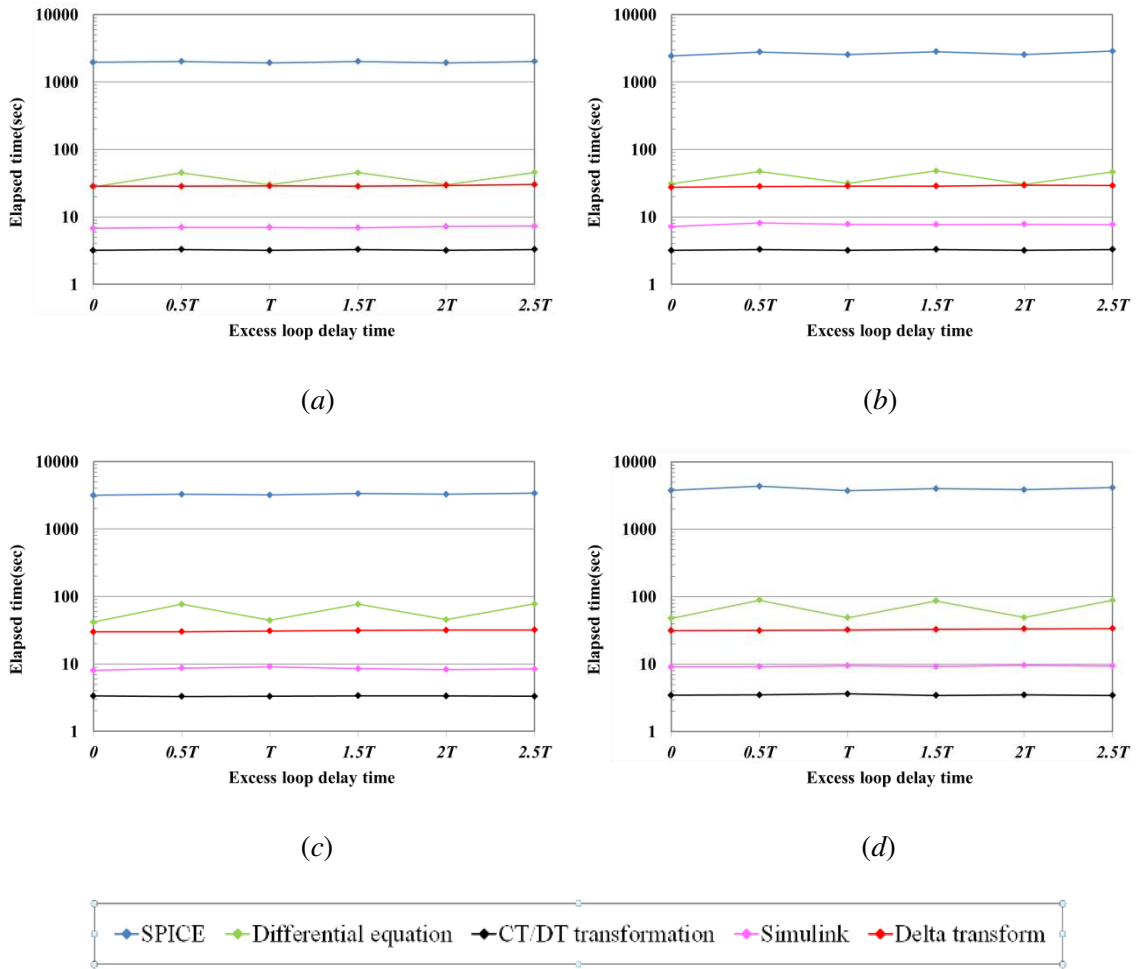


Figure 3.12 Simulation comparison of the elapsed time to complete the simulation for (a) 2nd order CT ΣAMs, (b) 3rd order CT ΣAMs, (c) 4th order CT ΣAMs, (d) 5th order CT ΣAMs

Fig 3.12 (a) compares the elapsed time for each of the 2nd order CT $\Sigma\Delta$ simulations generated with *RC* implementations. The CT/DT transform simulations were consistently the fastest simulations taking only a few seconds to complete. Simulink was the next fastest method. The simulation times for the delta transform method and the differential equation method were both about ten times as long as the simulation times using CT/DT transform method. The simulation times for the delta transform method were more consistent than for the differential equation method since the simulation time for the differential equation method increased when the excess loop delay time was $0.5T$, $1.5T$, or $2.5T$. SPICE simulation was by far the slowest method of simulation.

Fig 3.12 (b), (c) and (d) compare the elapsed time for each of the 3rd order CT $\Sigma\Delta$ simulations, the 4th order CT $\Sigma\Delta$ simulations, and the 5th order CT $\Sigma\Delta$ simulations, respectively. Similar to the 2nd order CT $\Sigma\Delta$ simulations, the fastest simulation method is CT/DT transformation and the slowest simulation method is SPICE simulation. Whereas the elapsed times for SPICE simulation and solving differential equations increase as the order of loop filters increase, the elapsed times for the CT/DT transformation, Simulink and the delta transform method are nearly constant regardless of the order of the loop filter.

Table 3.5 The elapsed time comparison between *RC* implementation and *G_mC* implementation for each of simulation methods

	[sec]	
Simulation Methods	<i>RC</i> implementation	<i>G_mC</i> implementation
SPICE	1958	1975
Differential equation	27.9	28.9
CT/DT transformation	3.2	3.2
Simulink	6.8	7.4
Delta transform	28.5	28.7

Table 3.5 compares the elapsed times between the *RC* implementation simulations and the *G_mC* implementation simulations. For the 2nd order CT $\Sigma\Delta$ with an excess loop delay of zero, little or no difference exists between the simulation times as shown in Table 3.5.

Table 3.6 Performance comparison of simulation methods

Simulation Methods \ Performance	SPICE	Differential equation	CT/DT transformation	Simulink	Delta transform
Simplicity	***	*	****	*****	****
Accuracy	*****	****	***	*	****
Speed	*	**	*****	****	***

Table 3.6 compares the performance of the different simulation methods. It is assumed that SPICE simulations produce the most accurate results, and SPICE simulations are also a moderately simple method because macro models of circuit can be added easily. It also has the advantage that circuit schematics can be substituted for the macro models as the CT $\Sigma\Delta$ circuits are developed. The method's major disadvantage is that the simulations are very time consuming especially for higher order CT $\Sigma\Delta$ s. Also, the method lacks a mathematical model which can be used for various analyses. Solving the CT $\Sigma\Delta$'s differential equations results in a mathematical model for analysis, and the method is much faster than using SPICE. The method also produces accurate results. However, the method is not as fast or simple as the other methods. While the CT/DT transformation method is the fastest method and is moderately simple because the CT $\Sigma\Delta$ can be implemented using the difference equations, the CT/DT transform method is less accurate than both SPICE simulations and solving the differential equations. Also the method only calculates nodes at the sample times. Simulink is simplest of the methods for simulating CT $\Sigma\Delta$ s, and it is relatively fast. However, Simulink's accuracy is dependent on the proper selection of Simulink models; therefore, it can be less accurate as illustrated by the results presented in this chapter. The delta transform method takes more time to complete than the two faster methods because it calculates loop filter signal values at times other than the $\Sigma\Delta$'s sampling times. However, the method resulted in simulations almost as accurate as SPICE. Also, it is a simple method because CT $\Sigma\Delta$ s can be simulated using difference equations. In other

words, the delta transform method is very simple and effective to get accurate results at reasonable speeds.

CHAPTER 4

OVERLOAD ANALYSIS OF CT $\Sigma\Delta$ MS

A quantizer is said to be overloaded when the input of the quantizer generates a quantizer error of more than half a quantization step size above or below the quantizer's maximum or minimum output, respectively. When the quantizer in a $\Sigma\Delta$ M is overloaded, the $\Sigma\Delta$ M's output signal no longer increases linearly with the input signal, and the $\Sigma\Delta$ M is said to be overloaded. Overload is often described as a $\Sigma\Delta$ M instability because it affects the $\Sigma\Delta$ M's resolution.

In this chapter, the necessary conditions that prevent quantizers in $\Sigma\Delta$ Ms from overloading are presented. Using these conditions, the maximum input signal power that prevents a CT $\Sigma\Delta$ M from overloading can be determined, and the CT $\Sigma\Delta$ M's maximum SQNR can be determined.

4.1 Definition of Overload for a Single-bit Quantizer

The transfer characteristic of a single-bit quantizer is

$$y(\psi) = \frac{\Delta_q}{2} \cdot \text{sgn}(\psi) = \begin{cases} \frac{\Delta_q}{2} & \text{for } \psi > 0 \\ -\frac{\Delta_q}{2} & \text{for } \psi < 0 \end{cases} \quad (4.1)$$

where ψ is quantizer's input, y is quantizer's output and Δ_q is the quantizer's step size. Fig 4.1 (a) shows (4.1) graphically where $\Delta_q = 2$. Such a quantizer is considered to be overloaded when $|\psi| > \Delta_q$ which implies that the quantizer's error, e , exceeds $\Delta_q/2$ which is half of the quantizer's quantization step size, Δ_q ; that is, a $\Sigma\Delta$ M's quantizer is considered to be overloaded when

$$|e| > \frac{\Delta_q}{2} \quad (4.2)$$

and is not considered to be overloaded when

$$|e| \leq \frac{\Delta_q}{2}. \quad (4.3)$$

The input signal range for which a quantizer is not overloaded is called the no-overload input range, or simply, input range [25].

In this dissertation, Δ_q is normalized to 2 which implies that

$$y = \text{sgn}(\psi) = \begin{cases} 1 & \text{for } \psi > 0 \\ -1 & \text{for } \psi < 0 \end{cases}. \quad (4.4)$$

Therefore, when the quantizer is not overloaded, the quantizer error has the range

$$-1 \leq e \leq +1, \quad (4.5)$$

and the quantizer's no-overload input range is

$$-2 \leq \psi \leq +2. \quad (4.6)$$

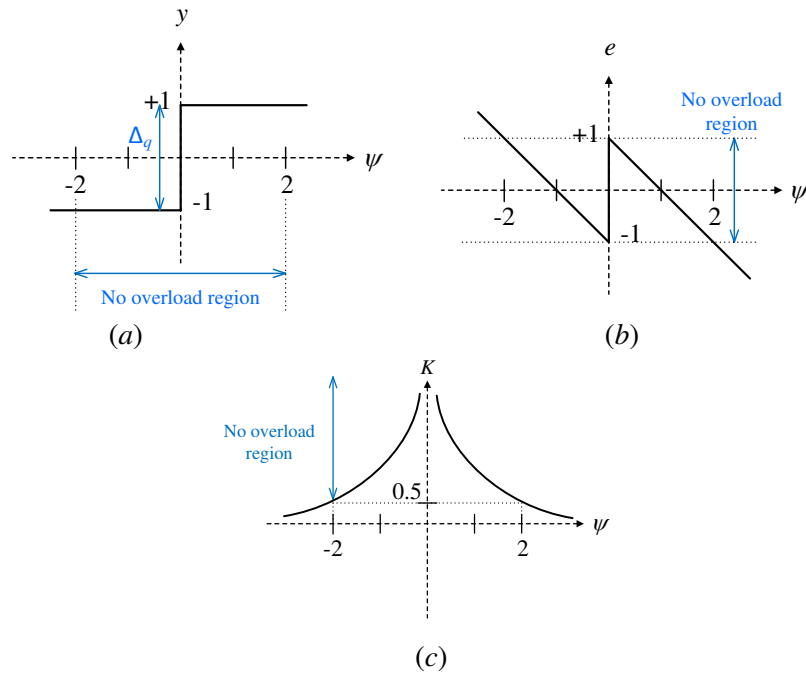


Figure 4.1 (a) The transfer characteristic for a single-bit quantizer (b) quantization error, e of a single-bit quantizer, (c) quantizer gain, K of a single-bit quantizer

Fig 4.1(a) shows the overload input range of a single-bit quantizer where $\Delta_q = 2$. Because $y = \psi + e$, $e = y - \psi$. Also, because the output, y , of a single-bit quantizer is ± 1 , the quantization error, e , of a single-bit quantizer can be written as

$$e = \begin{cases} 1 - \psi & \text{for } \psi > 0 \text{ or } y = 1 \\ -1 - \psi & \text{for } \psi < 0 \text{ or } y = -1 \end{cases} . \quad (4.7)$$

Fig 4.1 (b) depicts the quantization error, e , for a single-bit quantizer as a function of the quantizer's input, ψ .

A quantizer's gain, K , can be defined as the ratio of the quantizer's output amplitude to the quantization's input amplitude which implies that $K = y/\psi$. For a single-bit quantizer,

$$K = \begin{cases} \frac{1}{\psi} & \text{for } \psi > 0 \text{ or } y = 1 \\ -\frac{1}{\psi} & \text{for } \psi < 0 \text{ or } y = -1 \end{cases} . \quad (4.8)$$

Fig 4.1 (c) shows the plot of (4.8). Because the quantizer's maximum input, $\psi_{\max O}$, that prevents overloading is

$$\psi_{\max O} = 2 \quad (4.9)$$

as shown in (4.6), the minimum quantizer gain, $K_{\min O}$, that prevents overloading is

$$K_{\min O} = 0.5. \quad (4.10)$$

4.2 Overload Analysis

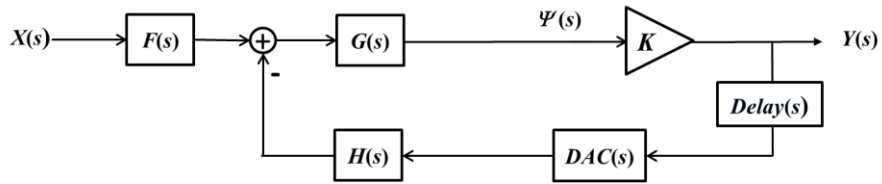
To determine the maximum input signal power, $P_{\max O}$, that prevents a $\Sigma\Delta M$ from overloading, consider the STF and NTF models shown in Fig 4.2 (a) and (b) and assume that the quantizer's input, ψ , is a zero mean random process. Because ψ is a zero mean random process, the

quantizer's input signal power, P_ψ , can be written as $P_\psi = \sigma_\psi^2$ where σ_ψ is the standard deviation of ψ . To prevent overload, $\psi_{\max O} < 2$ where $\psi_{\max O}$ is the maximum quantizer's input amplitude that prevents overload. This condition is assumed to be true when $\mu \cdot \sigma_\psi < \psi_{\max O}$ or equivalently when

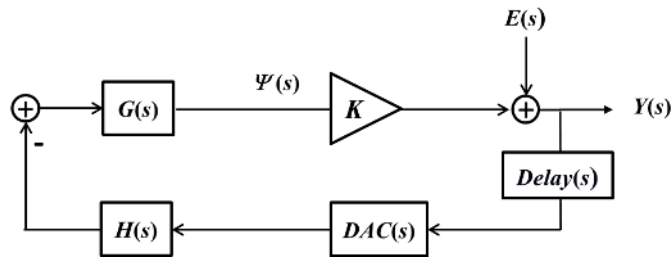
$$\sigma_{\psi_{\max O}}^2 = \left(\frac{\psi_{\max O}}{\mu} \right)^2 = \left(\frac{1}{\mu \cdot K_{\min O}} \right)^2 \quad (4.11)$$

where μ is the standard deviation coefficient of σ_ψ as shown in Fig 4.3. Based on the empirical simulation results, μ is chosen as 3.6. For a quantizer with the characteristic function, $y(n) = \text{sgn}[\psi(n)]$, the minimum quantizer gain, $K_{\min O}$, that prevents quantizer overload is 0.5 which implies that (4.11) can be written as

$$P_{\psi_{\max O}} = \sigma_{\psi_{\max O}}^2 = \left(\frac{1}{\mu \cdot K_{\min O}} \right)^2 = \frac{4}{\mu^2} \approx 0.309. \quad (4.12)$$



(a)



(b)

Figure 4.2 (a) Block diagram of a CT $\Sigma\Delta M$'s STF, (b) Block diagram of a CT $\Sigma\Delta M$'s NTF

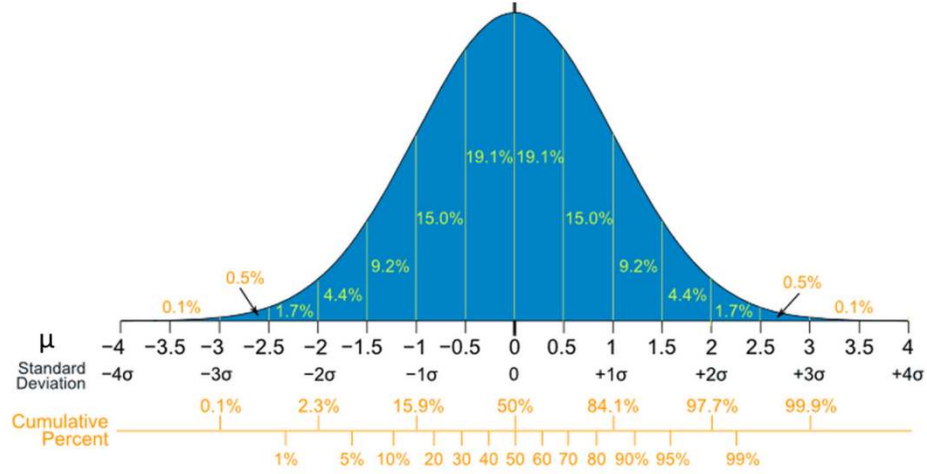


Figure 4.3 Bell curve of the standard normal distribution [22]

From the block diagrams in Fig 4.2, the quantizer's input power, σ_{ψ}^2 , can be written as

$$\sigma_{\psi}^2 = \frac{\sigma_x^2}{f_s} \cdot \frac{1}{K^2} \int_{-f_s/2}^{f_s/2} |STF(f)|_{K=K_{eff}}^2 df + \frac{\sigma_e^2}{f_s} \int_{-f_s/2}^{f_s/2} \left| \frac{G \cdot H \cdot DAC \cdot Delay}{1 + K \cdot G \cdot H \cdot DAC \cdot Delay}(f) \right|_{K=K_{eff}}^2 df. \quad (4.13)$$

where $K_{eff} = E[|\psi(n)|] / \sigma_{\psi}^2$. When $\sigma_{\psi}^2 = \sigma_{\psi_{maxO}}^2$, $K_{eff} = K_{des}$ where K_{des} is the value of K used to design the $\Sigma\Delta M$. Therefore, the quantizer's maximum input power, $\sigma_{\psi_{maxO}}^2$, that prevents a $\Sigma\Delta M$ from overloading can be written as

$$\sigma_{\psi_{maxO}}^2 = \frac{\sigma_{x_{maxO}}^2}{f_s} \cdot \frac{1}{K^2} \int_{-f_s/2}^{f_s/2} |STF(f)|_{K=K_{des}}^2 df + \frac{\sigma_{e_{maxO}}^2}{f_s} \int_{-f_s/2}^{f_s/2} \left| \frac{G \cdot H \cdot DAC \cdot Delay}{1 + K \cdot G \cdot H \cdot DAC \cdot Delay}(f) \right|_{K=K_{des}}^2 df \quad (4.14)$$

where $\sigma_{x_{maxO}}^2$ is the maximum input power that prevents overload and $\sigma_{e_{maxO}}^2$ is the quantization noise power when $\sigma_x^2 = \sigma_{x_{maxO}}^2$ and $\sigma_{\psi}^2 = \sigma_{\psi_{maxO}}^2$. Assuming that the $\Sigma\Delta M$'s input, output and quantization noise signals have means of zero, the $\Sigma\Delta M$'s output signal power, P_y , can be calculated as

$$P_y = E[y^2] = \sigma_y^2 = \frac{\sigma_x^2}{f_s} \int_{-fs/2}^{fs/2} |STF(f)|^2_{K=K_{eff}} df + \frac{\sigma_e^2}{f_s} \int_{-fs/2}^{fs/2} |NTF(f)|^2_{K=K_{eff}} df . \quad (4.15)$$

Therefore, at the maximum values of σ_x^2 and σ_e^2 that prevent overload,

$$\sigma_y^2 = \frac{\sigma_{x_{maxO}}^2}{f_s} \int_{-fs/2}^{fs/2} |STF(f)|^2_{K=K_{des}} df + \frac{\sigma_{e_{maxO}}^2}{f_s} \int_{-fs/2}^{fs/2} |NTF(f)|^2_{K=K_{des}} df . \quad (4.16)$$

Subtracting (4.14) from (4.16) and solving the resulting equation for σ_e^2 , the quantization noise power, σ_e^2 , can be determined as

$$\sigma_e^2 = \frac{\sigma_y^2 - \sigma_{\psi}^2}{\frac{1}{f_s} \left[\int_{-fs/2}^{fs/2} |NTF(f)|^2_{K=K_{eff}} df - \int_{-fs/2}^{fs/2} \left| \frac{G \cdot H \cdot DAC \cdot Delay}{1 + K \cdot G \cdot H \cdot DAC \cdot Delay}(f) \right|^2_{K=K_{eff}} df \right]} \quad (4.17)$$

Therefore, the maximum quantization noise power, $\sigma_{e_{maxO}}^2$, that prevents a $\Sigma\Delta M$ from overloading can be determined as

$$\sigma_{e_{maxO}}^2 = \frac{\sigma_y^2 - \sigma_{\psi_{maxO}}^2}{\frac{1}{f_s} \left[\int_{-fs/2}^{fs/2} |NTF(f)|^2_{K=K_{des}} df - \int_{-fs/2}^{fs/2} \left| \frac{G \cdot H \cdot DAC \cdot Delay}{1 + K \cdot G \cdot H \cdot DAC \cdot Delay}(f) \right|^2_{K=K_{des}} df \right]} \quad (4.18)$$

Using (4.16), the maximum input power, $P_{x_{maxO}}$, that prevents a $\Sigma\Delta M$ from overloading can be determined as

$$P_{x_{maxO}} = \sigma_{x_{maxO}}^2 = \frac{\sigma_y^2 - \frac{\sigma_{e_{maxO}}^2}{f_s} \int_{-fs/2}^{fs/2} |NTF(f)|^2_{K=K_{des}} df}{\frac{1}{f_s} \int_{-fs/2}^{fs/2} |STF(f)|^2_{K=K_{des}} df} \quad (4.19)$$

where σ_y^2 is 1 for a single-bit quantizer and $\sigma_{e_{maxO}}^2$ is given in (4.18).

4.3 Example

To illustrate this method for determining the maximum input signal power that prevents overload, consider the 2nd order CT $\Sigma\Delta$ that has a sampling frequency of 1GHz, a Chebyshev Type 2 NTF with attenuation of 35dB and an excess loop delay of $D = 0$. Unlike higher order $\Sigma\Delta$ s, 2nd order $\Sigma\Delta$ s are typically stable for arbitrary inputs. This can be illustrated by examining the root locus of a 2nd order $\Sigma\Delta$. Fig 4.4 shows the root locus of a 2nd order $\Sigma\Delta$ with a sampling frequency of 1GHz and Chebyshev Type 2 NTF for $D = 0$, $D = 0.5T$, and $D = T$. As shown in Fig 4.4, the minimum quantizer gain required for stability is zero which implies that the $\Sigma\Delta$ never goes unstable, but instead the $\Sigma\Delta$ will overload when the input signal power becomes large enough. This is typical behavior for 2nd order $\Sigma\Delta$ s.

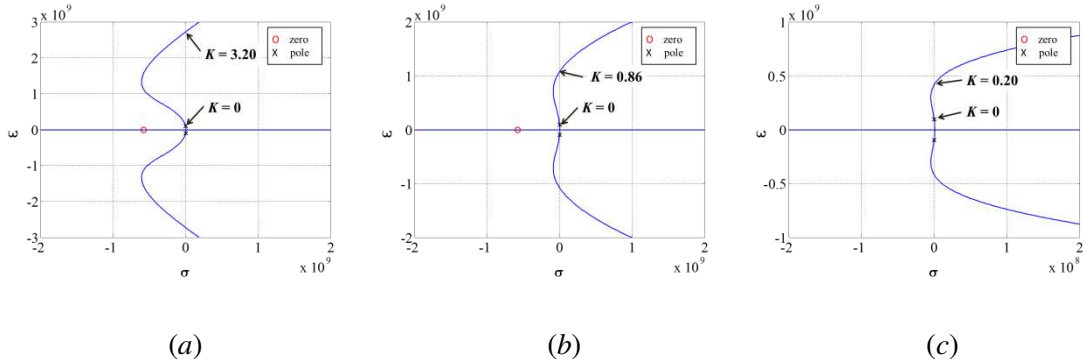


Figure 4.4 The root locus of a 2nd order CT $\Sigma\Delta$ M with a sampling frequency, f_s , where $f_s = 1/T$, of 1GHz and Chebyshev Type 2 NTF for (a) $D = 0$, (b) $D = 0.5T$, (c) $D = T$

Using (4.12), quantizer's maximum input power, $\sigma_{\psi_{\max O}}^2$, is

$$\sigma_{\psi_{\max O}}^2 = \frac{4}{3.6^2} = 0.309. \quad (4.20)$$

Using (4.18) and (4.20), the maximum quantization noise power, $\sigma_{e_{\max O}}^2$, that prevents a $\Sigma\Delta$ M from overloading can be determined as

$$\sigma_{e_{\max O}}^2 = \frac{1 - 0.309}{3.220 - 0.703} = 0.275 \quad (4.21)$$

where the term $\frac{1}{f_s} \int_{-fs/2}^{fs/2} |NTF(f)|^2_{K=K_{des}} df$ and the term

$\frac{1}{f_s} \int_{-fs/2}^{fs/2} \left| \frac{G \cdot H \cdot DAC \cdot Delay}{1 + K \cdot G \cdot H \cdot DAC \cdot Delay}(f) \right|^2_{K=K_{des}} df$ were calculated using the following Matlab code

and K_{des} was set to one in this example.

```
% The coefficients of transfer function F(s),G(s),and H(s)
% F(s)=F2*s^2+F1*s+F0;
% G(s)=1/(s^2+G0)
% H(s)=H2*s^2+H1*s+H0

% fs: Sampling frequency
% T=1/fs: Sampling period
% D: Excess loop delay

NTFsq=@(f)abs(((j.*2*pi.*f).^2+G0).*(j.*2*pi.*f.*T)/(((j.*2*pi.*f).^2+G0).*(j.*2*pi.*f.*T)+K.*(H1.*(j.*2*pi.*f)+H0)).*(1-exp(j.*2*pi.*f.*T)).*exp(j.*2*pi.*f.*D)).^2;

NTF=integral(NTFsq,-fs/2,fs/2)/fs;

GHDACsq=@(f)abs(((H1.*(j.*2*pi.*f)+H0).*(1-exp(-(j.*2*pi.*f).*T)).*exp(-(j.*2*pi.*f).*D))./(((j.*2*pi.*f).^2+G0).*(j.*2*pi.*f.*T)+K.*(H1.*(j.*2*pi.*f)+H0)).*(1-exp(-(j.*2*pi.*f).*T)).*exp(-(j.*2*pi.*f).*D))).^2;

GHDAC=integral(GHDACsq,-fs/2,fs/2)/fs;
```

Using (4.19) and (4.21), the maximum input power, $P_{x_{maxO}}$, that prevents the $\Sigma\Delta M$ from overloading is

$$P_{x_{maxO}} = \sigma_{x_{maxO}}^2 = 1 - 0.275 \cdot 3.220 = 0.114. \quad (4.22)$$

where the term $\frac{1}{f_s} \int_{-fs/2}^{fs/2} |STF(f)|^2_{K=K_{des}} df$ was calculated using the following Matlab code.

```
% F(s)=F2*s^2+F1*s+F0;
% G(s)=1/(s^2+G0)
% H(s)=H2*s^2+H1*s+H0

STFsq=@(f)abs((K.*(F2.*(j.*2*pi.*f).^2+F1.*(j.*2*pi.*f)+F0)).*(j.*2*pi.*f).*T)/(((j.*2*pi.*f).^2+G0).*(j.*2*pi.*f.*T)+K.*(H1.*(j.*2*pi.*f)+H0)).*(1-exp(-j.*2*pi.*f.*T)).*exp(-j.*2*pi.*f.*D))).^2;

STF=integral(STFsq,-fs/2,fs/2)/fs;
```

Assuming a sinusoidal input signal,

$$P_{x_{\max O}} = \sigma_{x_{\max O}}^2 = x_{\max O}^2 / 2 \quad (4.23)$$

where $x_{\max O}$ is the $\Sigma\Delta M$'s maximum input amplitude that prevents the quantizer from overloading. Using (4.22) and (4.23), $x_{\max O}$ is estimated to be 0.478 (-6.4dB).

Fig 4.5 shows the simulated SQNR and minimum quantizer gain for the 2nd order CT $\Sigma\Delta M$. When the input amplitude is greater than -6dB, the $\Sigma\Delta M$'s SQNR no longer increases linearly with the input signal power because the minimum quantizer gain drops below 0.5 which implies that the $\Sigma\Delta M$ is overloaded.

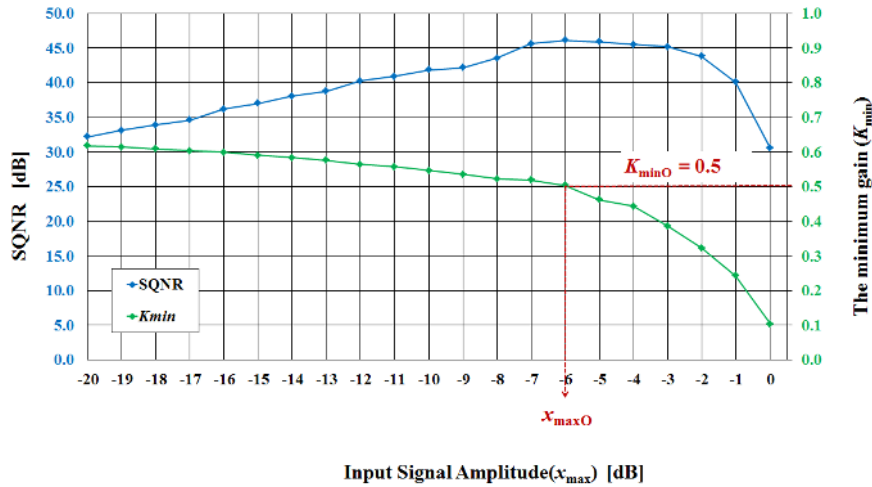


Figure 4.5 Simulated SQNR and the minimum quantizer gain (K_{\min}) using a sinusoidal input for the 2nd order CT $\Sigma\Delta M$ in example

4.4 Other Simulation Results

To illustrate this methodology's accuracy for predicting overload, six 2nd order, six 3rd order, four 4th order, and one 5th order CT $\Sigma\Delta M$ s were simulated to determine their overload points and these overload points are compared to their predicted overload points. Table 4.1 shows the specification for each CT $\Sigma\Delta M$.

Fig 4.6 (a), (b), (c), and (d) show the simulated SQNRs and the quantizer gains as a function of

the amplitude of a sinusoidal input signal for a 2nd order, a 3rd order, a 4th order, and a 5th order CT $\Sigma\Delta$ with $D = 0$, respectively. Fig 4.6 shows that SQNR increases linearly almost before the $\Sigma\Delta$ is overloaded, and the SQNR degrades or increases nonlinearly when the quantizer is overloaded. Fig 4.7 (a), (b), and (c) show the simulated SQNRs and quantizer gains as a function of sinusoidal input signal amplitude for a 2nd order, a 3rd order, and a 4th order CT $\Sigma\Delta$ with $D = T$, respectively.

Table 4.1 Specification for each CT $\Sigma\Delta$

(a) Common specification

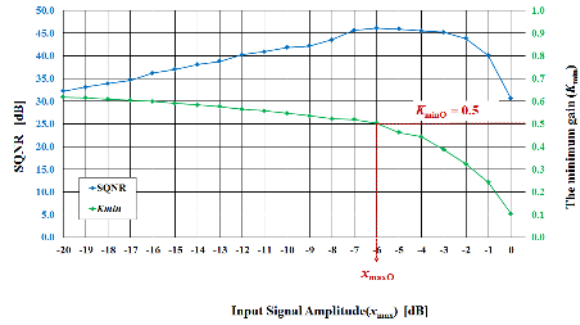
Specification	
Sampling frequency	1GHz
Sinusoidal Input frequency	0.1MHz
Signal Bandwidth	20MHz

(b) NTF attenuation for each CT $\Sigma\Delta$

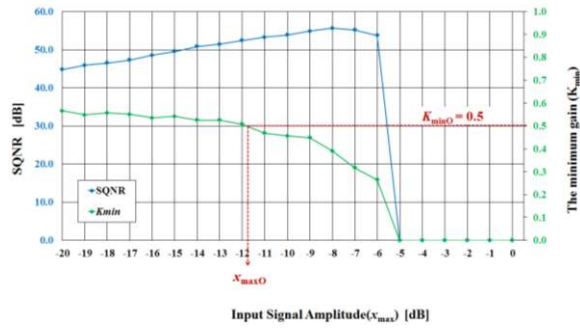
Excess loop delay (D)	NTF attenuation [dB]					
	0	$0.5T$	T	$1.5T$	$2T$	$2.5T$
2nd order CT $\Sigma\Delta$ s	35	28	25	21	18	15
3rd order CT $\Sigma\Delta$ s	47	37	30	25	21	18
4th order CT $\Sigma\Delta$ s	53	41	32	25	-	-
5th order CT $\Sigma\Delta$ s	59	-	-	-	-	-

Table 4.2 compares the theoretical minimum quantizer gain of 0.5 that prevents overload with the simulated minimum quantizer gains obtained when the simulated input signal is a sinusoidal signal that has an amplitude of $x_{\max O}$ which is the maximum predicted amplitude that prevents overload. Table 4.3 compares the predicted maximum input signal amplitude with the simulated maximum input signal amplitude that prevents overloading for the $\Sigma\Delta$ s.

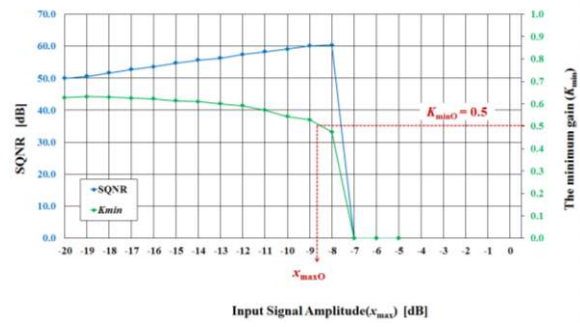
Because $\Sigma\Delta$'s SQNR depends on the input frequency, the maximum input signal amplitudes vary for different frequencies of the input signal [32, 33]. This is especially true for low input frequencies close to DC where a $\Sigma\Delta$'s SQNR can degrade at smaller input amplitudes. It may therefore be possible that the discrepancies between the predicted $x_{\max O}$ and the simulated $x_{\max O}$ might be a result of the chosen input frequency.



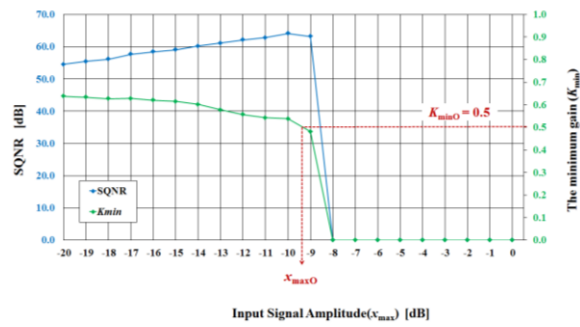
(a)



(b)

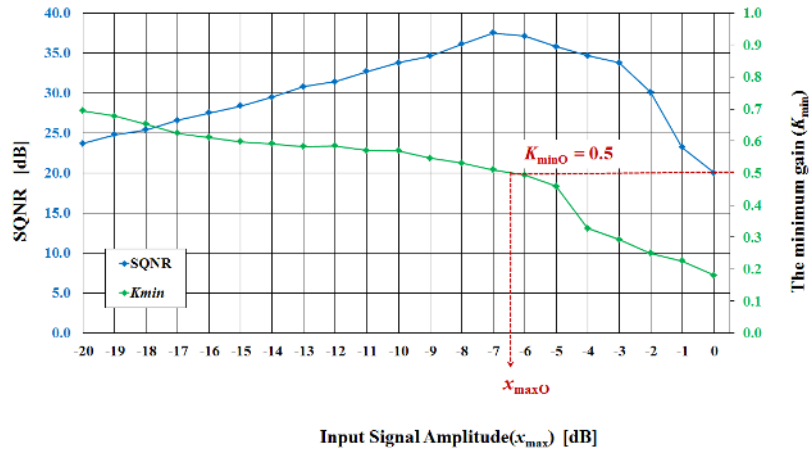


(c)

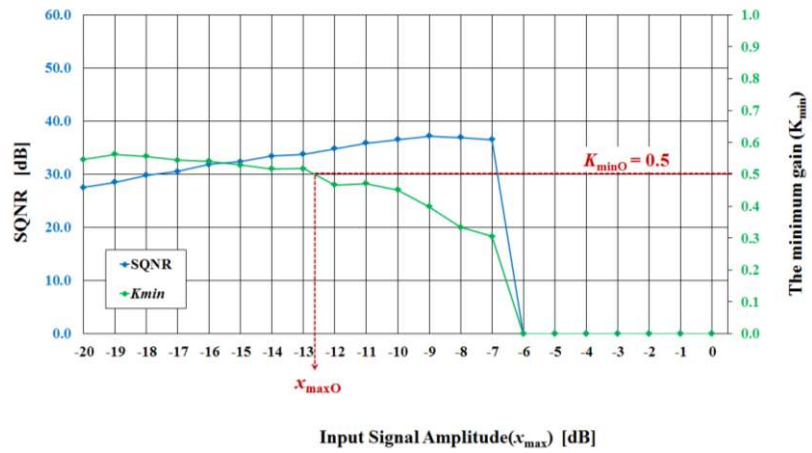


(d)

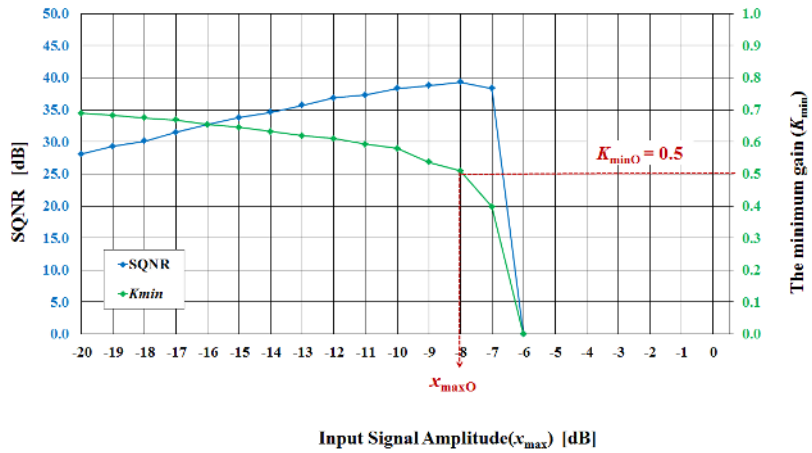
Figure 4.6 Simulated SQNR and the minimum quantizer gain (K_{min}) using a sinusoidal input
 (a) for a 2nd order CT $\Sigma\Delta M$, (b) for a 3rd order CT $\Sigma\Delta M$,
 (c) for a 4th order CT $\Sigma\Delta M$, (d) for a 5th order CT $\Sigma\Delta M$ with $D = 0$



(a)



(b)



(c)

Figure 4.7 Simulated SQNR and the minimum quantizer gain (K_{\min}) using a sinusoidal input
 (a) for a 2nd order CT $\Sigma\Delta M$, (b) for a 3rd order CT $\Sigma\Delta M$,
 (c) for a 4th order CT $\Sigma\Delta M$ with $D = T$

Table 4.2 Comparison of the theoretical minimum quantizer gains and the simulated minimum quantizer gains at predicted $x_{\max O}$

Simulated $K_{\min O}$	Excess loop delay (D)					
	0	$0.5T$	T	$1.5T$	$2T$	$2.5T$
2nd order	0.507	0.505	0.510	0.502	0.501	0.501
3rd order	0.504	0.504	0.506	0.501	0.508	0.504
4th order	0.513	0.502	0.504	0.502	-	-
5th order	0.508	-	-	-	-	-
Predicted $K_{\min O}$	0.5	0.5	0.5	0.5	0.5	0.5

Table 4.3 Comparison of the predicted maximum sinusoidal input amplitude with the simulated maximum sinusoidal input amplitude that prevents overloading for the $\Sigma\Delta$ Ms in Table 4.1

		Excess loop delay (D)						[dB]
		0	$0.5T$	T	$1.5T$	$2T$	$2.5T$	
2nd order	Predicted $x_{\max O}$	-6.4	-6.5	-6.8	-11.1	-12.5	-10.2	
	Simulated $x_{\max O}$	-6.0	-7.0	-6.5	-12.9	-13.0	-9.0	
3rd order	Predicted $x_{\max O}$	-12.1	-12.7	-13.2	-17.0	-17.3	-53.1	
	Simulated $x_{\max O}$	-11.8	-11.4	-12.7	-15.9	-18.8	-51.2	
4th order	Predicted $x_{\max O}$	-9.0	-8.8	-8.4	-8.1	-	-	
	Simulated $x_{\max O}$	-8.8	-8.4	-8.0	-8.0	-	-	
5th order	Predicted $x_{\max O}$	-9.6	-	-	-	-	-	
	Simulated $x_{\max O}$	-9.5	-	-	-	-	-	

4.5 Predicting the SQNR of a $\Sigma\Delta$ M

The most significant metric of a $\Sigma\Delta$ M is its SQNR, which gives an estimate of modulator's performance [28, 29, 30]. However, the estimation of a $\Sigma\Delta$ M's SQNR is normally based on a $\Sigma\Delta$ M's output bitstream which is obtained by simulations which are usually time consuming tasks. Some approximations of the expected SQNR have been suggested, but they are limited to ideal low order $\Sigma\Delta$ Ms [29, 30, 31]. In this section, a method for estimating the SQNR of an arbitrary $\Sigma\Delta$ M is derived. This method provides estimated SQNRs without requiring simulations. Examples are provided that compare the method's estimated SQNRs with simulated SQNRs.

4.5.1 Derivation of SQNR Approximation when operating in no-overload input range

Consider a CT $\Sigma\Delta$ modeled by the block diagrams in Fig 4.2 where the block diagram in Fig 4.2 (a) models the $\Sigma\Delta$'s STF and the block diagram in Fig 4.2 (b) models the $\Sigma\Delta$'s NTF. Assuming a zero mean input, the SQNR of a CT $\Sigma\Delta$ modeled by Fig 4.2 can be calculated as

$$SQNR \text{ [dB]} = 10 \cdot \log_{10} \left(\frac{P_y}{P_n} \right) = 10 \cdot \log_{10} \left(\frac{\sigma_y^2}{\sigma_n^2} \right) \quad (4.24)$$

where P_y and σ_y^2 are the output signal power and P_n and σ_n^2 are the quantization noise power over the output signal's bandwidth. Because the power spectral density, $S_e(f)$, of the unshaped quantization noise is σ_e^2 / f_s , the quantization noise, σ_n^2 , in the signal's bandwidth, f_B , is

$$\sigma_n^2 = \int_{-f_B}^{f_B} S_e(f) |NTF(f)|^2_{K=K_{eff}} df = \int_{-f_B}^{f_B} \frac{\sigma_e^2}{f_s} |NTF(f)|^2_{K=K_{eff}} df \quad (4.25)$$

where σ_e^2 is given by (4.18). Substituting (4.26) into (4.25), the SQNR of a CT $\Sigma\Delta$ can be written as

$$SQNR \text{ [dB]} = 10 \cdot \log_{10} \left(\frac{\sigma_y^2}{\int_{-f_B}^{f_B} \frac{\sigma_e^2}{f_s} |NTF(f)|^2_{K=K_{eff}} df} \right) = 10 \cdot \log_{10} \left(\frac{\frac{\sigma_x^2}{f_s} \int_{-f_s}^{f_s} |STF(f)|^2 df}{\int_{-f_B}^{f_B} \frac{\sigma_e^2}{f_s} |NTF(f)|^2_{K=K_{eff}} df} \right). \quad (4.26)$$

Assuming that that $|STF(f)|=1$ at the input signal's frequency and that the input signal is sinusoidal which implies that $\sigma_x^2 = x_{\max}^2 / 2$, then $\sigma_y^2 = \sigma_x^2 = x_{\max}^2 / 2$, and the SQNR of a CT $\Sigma\Delta$ with a sinusoidal input can be written as

$$SQNR \text{ [dB]} = 10 \cdot \log_{10} \left(\frac{\frac{x_{\max}^2}{2}}{\frac{1}{f_s} \int_{-f_B}^{f_B} \sigma_e^2 |NTF(f)|^2_{K=K_{eff}} df} \right) \quad (4.27)$$

where σ_e is given by (4.17).

To determine K_{eff} , it is assumed that $E[|\psi(n)|]$ is proportional to its standard deviation; that is, it is assumed that

$$E[|\psi(n)|] = \alpha \cdot \sigma_\psi \quad (4.28)$$

where α is a constant. Eq. (4.28) implies that

$$K_{eff} = \frac{E[|\psi(n)|]}{\sigma_\psi^2} = \frac{\alpha}{\sigma_\psi}. \quad (4.29)$$

When $\sigma_\psi^2 = \sigma_{\psi_{maxO}}^2$, $K_{eff} = K_{des}$ which implies that

$$\alpha = K_{eff} \cdot \sigma_\psi = K_{des} \cdot \sigma_{\psi_{maxO}}. \quad (4.30)$$

Substituting (4.12) into (4.30),

$$\alpha = \frac{K_{des}}{\mu \cdot K_{minO}} \quad (4.31)$$

K_{eff} can then be estimated for the power of other input signals using an iteration method. This method begins by using (4.13) to estimate σ_ψ^2 for an input power of σ_x^2 ; that is,

$$\sigma_\psi^2(n) = \frac{\sigma_x^2}{f_s} \cdot \frac{1}{K^2} \int_{-fs/2}^{fs/2} |STF(f)|_{K=K_{eff}(n)}^2 df + \frac{\sigma_e^2(n)}{f_s} \int_{-fs/2}^{fs/2} \left| \frac{G \cdot H \cdot DAC \cdot Delay}{1 + K \cdot G \cdot H \cdot DAC \cdot Delay}(f) \right|_{K=K_{eff}(n)}^2 df \quad (4.32)$$

where $K_{eff}(0) = K_{des}$ and $\sigma_e^2(0) = \sigma_{e_{maxO}}^2$. Using (4.29),

$$K_{eff}(n+1) = \frac{\alpha}{\sigma_\psi(n)}. \quad (4.33)$$

Using (4.17),

$$\sigma_e^2(n+1) = \frac{1 - \sigma_\psi^2(n)}{\frac{1}{f_s} \left[\int_{-fs/2}^{fs/2} |NTF(f)|_{K=K_{eff}(n+1)}^2 df - \int_{-fs/2}^{fs/2} \left| \frac{G \cdot H \cdot DAC \cdot Delay}{1 + K \cdot G \cdot H \cdot DAC \cdot Delay}(f) \right|_{K=K_{eff}(n+1)}^2 df \right]} \quad (4.34)$$

Eq. (4.32), (4.33), and (4.34) are repeated until K_{eff} and σ_e^2 converge. These values can be substituted into (4.27) to calculate the $\Sigma\Delta M$'s SQNR when the input power is the σ_x^2 in (4.32).

4.5.2 Prediction of the SQNR of $\Sigma\Delta M$ in Overload

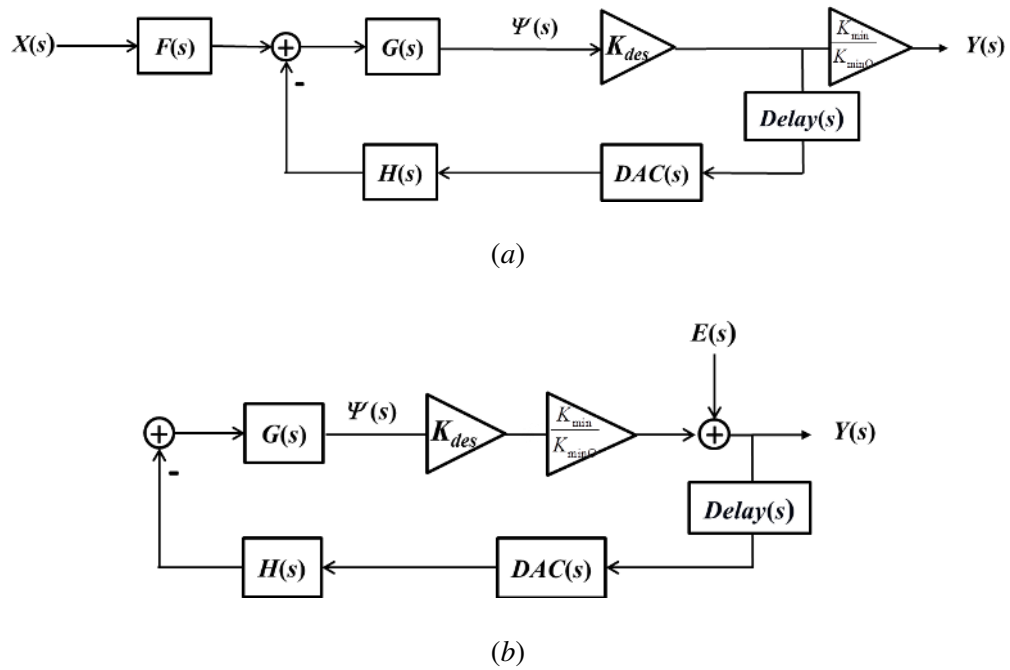


Figure 4.8 (a) A linear model for the CT $\Sigma\Delta M$'s STF in overload,
(b) A linear model for the CT $\Sigma\Delta M$'s NTF in overload

When the CT $\Sigma\Delta M$ in Fig 4.2 is operating in overload, the linear models in Fig 4.2 are no longer valid, and modified block diagram models need to be used to reflect the effects of overload. When the $\Sigma\Delta M$ is overloaded, the output signal's amplitude is limited and the quantization error

range increases. Fig 4.8 (a) shows a linear model for a CT $\Sigma\Delta M$'s STF in overload. This linear model has $K_{\min}/K_{\min O}$ at the output to reflect the $\Sigma\Delta M$'s output bitstream's inability to realize larger amplitudes. Fig 4.8 (b) shows a linear model for a CT $\Sigma\Delta M$'s NTF in overload. This linear model has a quantizer gain of $K_{\min}/K_{\min O}$ to reflect that overload increases quantization noise range from $|e| < 1$ to $|e| < K_{\min O}/K_{\min}$. K_{\min} can be estimated using (4.11) which implies that

$$K_{\min} = \frac{1}{\mu \cdot \sigma_{\psi}} \quad (4.35)$$

where σ_{ψ} can be calculated using the iterative method in (4.32), (4.33), and (4.34).

Using Fig 4.8 (a), the $\Sigma\Delta M$'s STF in overload can be written as

$$STF(s) = \frac{K_{\min}}{K_{\min O}} \cdot \frac{K_{des} \cdot F(s) \cdot G(s)}{1 + K_{des} \cdot G(s) \cdot H(s) \cdot DAC(s) \cdot Delay(s)} \quad (4.36)$$

and using Fig 4.8 (b), the $\Sigma\Delta M$'s NTF in overload can be written as

$$NTF(s) = \frac{1}{1 + K_{des} \cdot \frac{K_{\min}}{K_{\min O}} \cdot G(s) \cdot H(s) \cdot DAC(s) \cdot Delay(s)} \quad (4.37)$$

Modifying (4.27) and (4.17), the SQNR of a CT $\Sigma\Delta M$ that is operating in overload and has a sinusoidal input signal is

$$SQNR \text{ [dB]} = 10 \cdot \log_{10} \left(\frac{\frac{x_{\max}^2}{2} \cdot \left(\frac{K_{\min}}{K_{\min O}} \right)^2}{\int_{-f_B}^{f_B} \frac{\sigma_e^2}{f_s} \left| \frac{1}{1 + K_{des} \cdot \frac{K_{\min}}{K_{\min O}} \cdot G \cdot H \cdot DAC \cdot Delay} \right|^2 (f) df} \right) \quad (4.38)$$

where

$$\sigma_e^2 = \frac{1 - \sigma_\psi^2}{\frac{1}{f_s} \left[\int_{-fs/2}^{fs/2} \left| \frac{1}{1 + K_{des} \cdot \frac{K_{min}}{K_{min0}} \cdot G \cdot H \cdot DAC \cdot Delay} \right|^2 (f) df - \int_{-fs/2}^{fs/2} \left| \frac{G \cdot H \cdot DAC \cdot Delay}{1 + K_{des} \cdot \frac{K_{min}}{K_{min0}} \cdot G \cdot H \cdot DAC \cdot Delay} \right|^2 (f) df \right]} \quad (4.39)$$

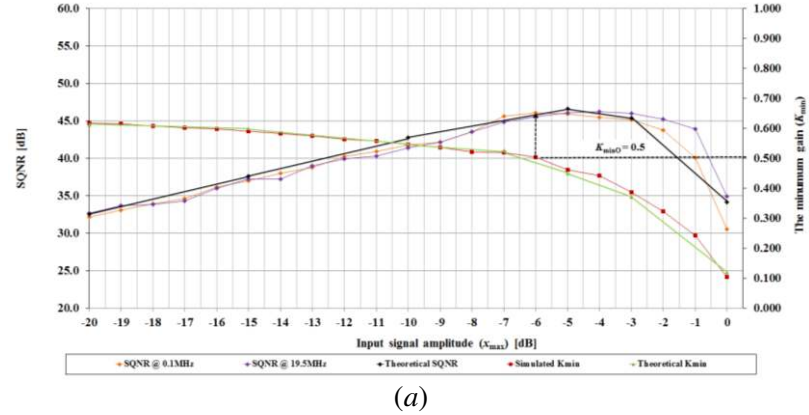
4.5.3 Simulation results

To determine the validity of the SQNR predicted by (4.27) and (4.17) when the $\Sigma\Delta M$ is not overloaded and by (4.38) and (4.39) when the $\Sigma\Delta M$ is overloaded, six 2nd order CT $\Sigma\Delta M$ s, six 3rd order CT $\Sigma\Delta M$ s, and four 4th order CT $\Sigma\Delta M$ s were simulated. Table 4.1 shows the specification for each CT $\Sigma\Delta M$ using a sinusoidal input with a frequency of 0.1MHz and 19.5MHz.

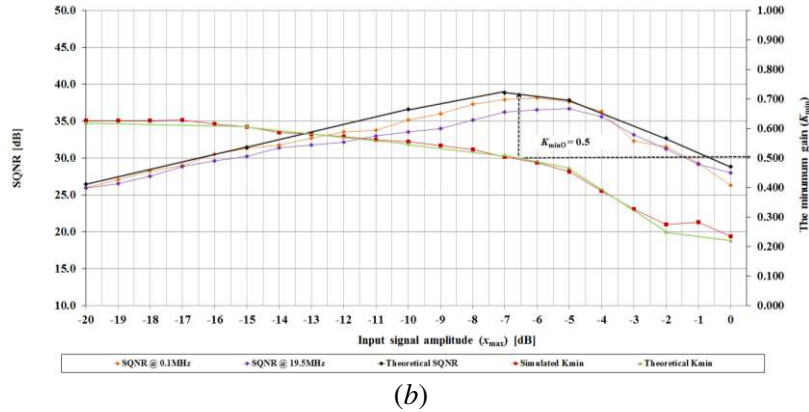
Fig 4.9 (a), (b), (c), (d), (e) and (f) compare the simulated SQNRs with the predicted SQNRs for a 2nd order CT $\Sigma\Delta M$ with $D = 0$, $D = 0.5T$, $D = T$, $D = 1.5T$, $D = 2T$, and $D = 2.5T$, respectively. Simulation results show that while the $\Sigma\Delta M$ is not overloaded, the SQNR increases linearly as input amplitude increases. The simulations also show that $\Sigma\Delta M$ s' SQNRs degrade or increase nonlinearly when the $\Sigma\Delta M$ s are overloaded.

To validate the SQNR prediction in overload for higher order $\Sigma\Delta M$ s, six 3rd order CT $\Sigma\Delta M$ s and four 4th order CT $\Sigma\Delta M$ were simulated and compared with the predicted SQNRs. Fig 4.10 (a), (b), (c), (d), (e) and (f) compare the simulated SQNRs with the predicted SQNRs for a 3rd order CT $\Sigma\Delta M$ with $D = 0$, $D = 0.5T$, $D = T$, $D = 1.5T$, $D = 2T$, and $D = 2.5T$, respectively. Similar to the 2nd order $\Sigma\Delta M$ s in Fig 4.9, simulation results show the SQNR increases linearly when the $\Sigma\Delta M$ is not overloaded and the SQNRs stop increasing linearly and degrade when the $\Sigma\Delta M$ is overloaded. Fig 4.11 (a), (b), (c), and (d) compare the simulated SQNRs with the predicted SQNRs for a 4th order CT $\Sigma\Delta M$ with $D = 0$, $D = 0.5T$, $D = T$, and $D = 1.5T$, respectively. The simulation results show the SQNRs degrade when the $\Sigma\Delta M$ is overloaded. Also,

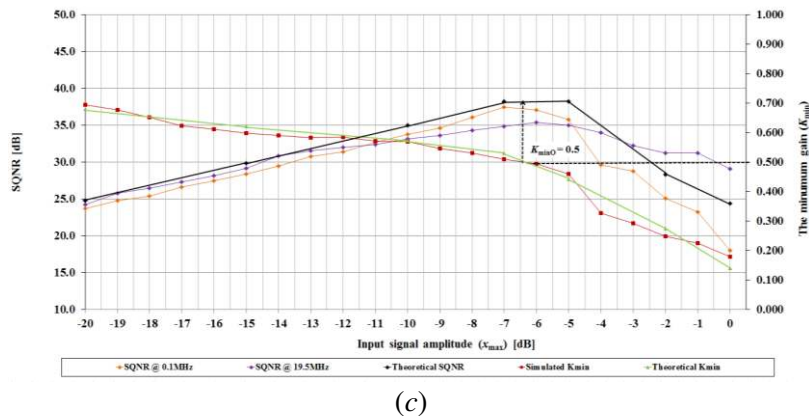
the SQNRs for an input frequency of 0.1MHz is closer to the estimated SQNRs than the SQNRs for an input frequency of 19.5MHz. Because $\Sigma\Delta\text{M}$'s SQNRs depend on the input frequency, the $\Sigma\Delta\text{M}$'s SQNRs can degrade at smaller input amplitudes for the low input frequencies close to DC.



(a)

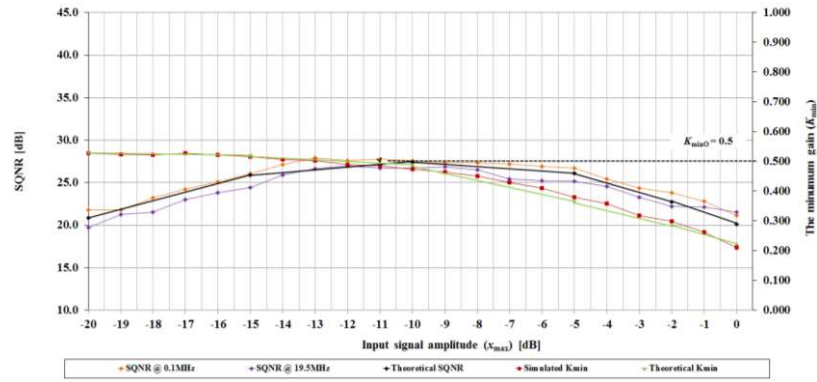


(b)

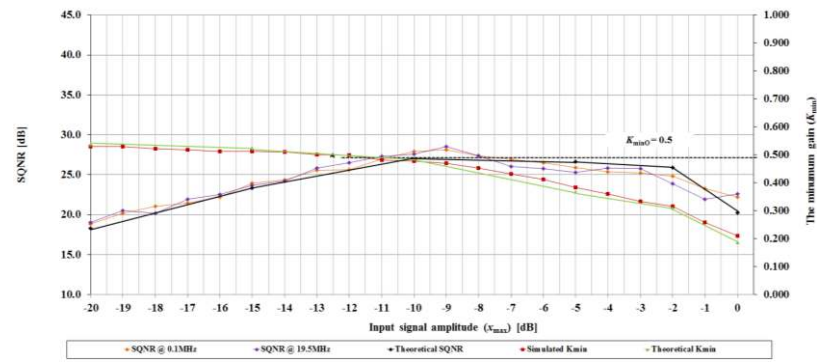


(c)

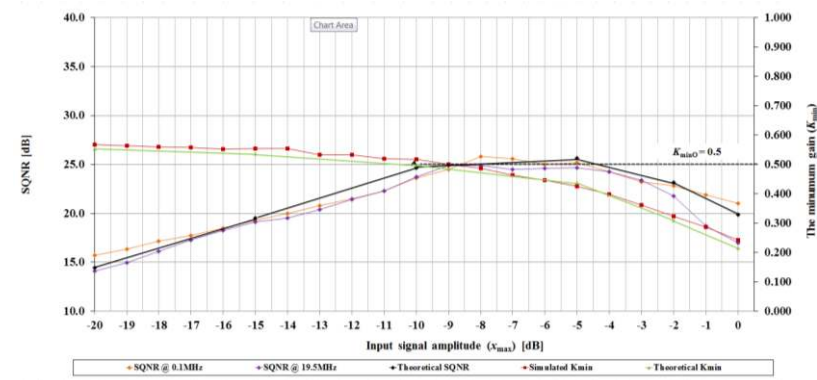
Figure 4.9 Simulated SQNR and estimated SQNR for the 2nd order CT $\Sigma\Delta\text{M}$ with
 (a) $D = 0$, (b) $D = 0.5T$, (c) $D = T$



(d)

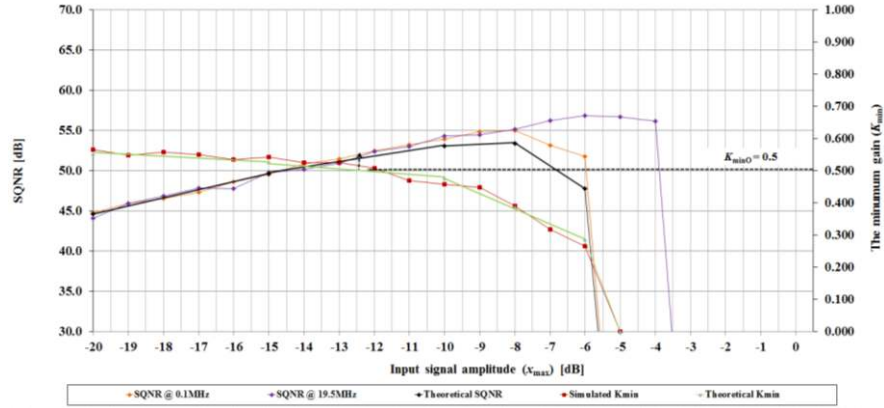


(e)

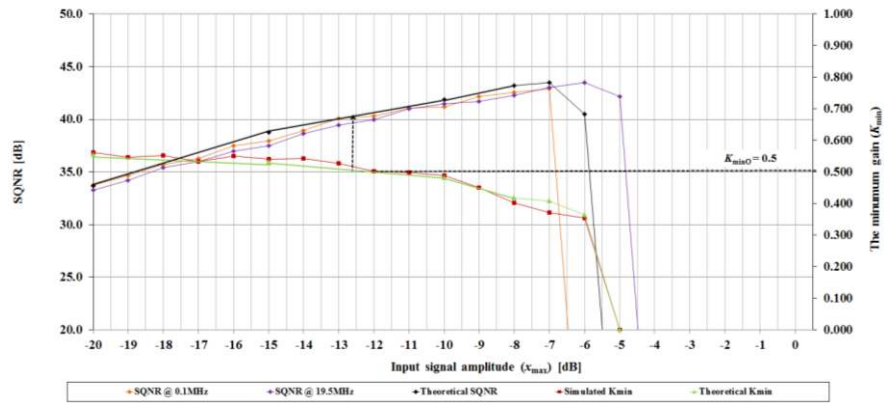


(f)

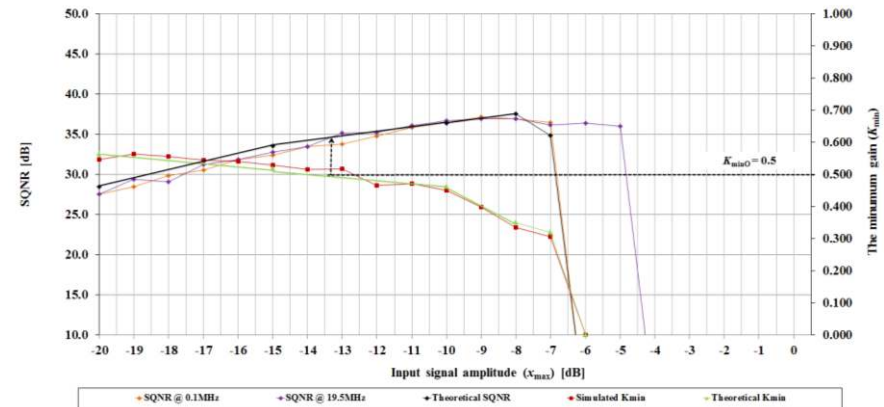
Figure 4.9 (Continued) Simulated SQNR and estimated SQNR for the 2nd order CT $\Sigma\Delta$ M with (d) $D = 1.5T$, (e) $D = 2T$, (f) $D = 2.5T$



(a)

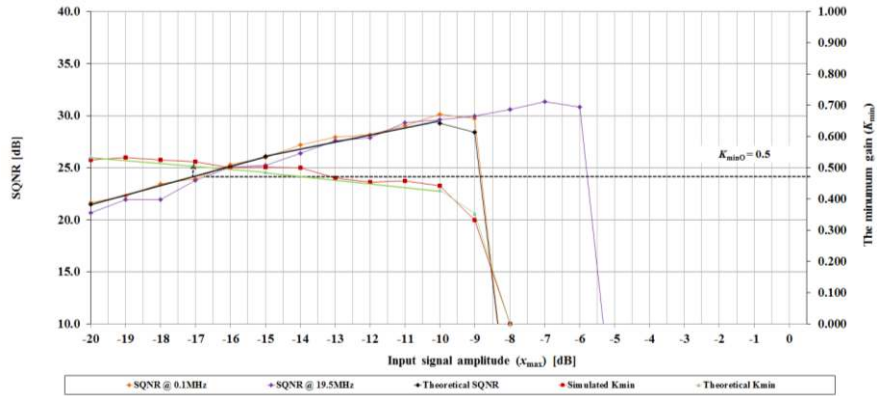


(b)

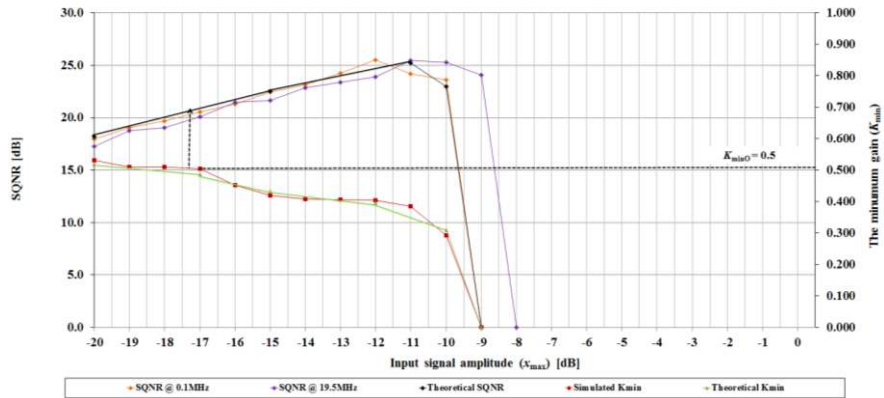


(c)

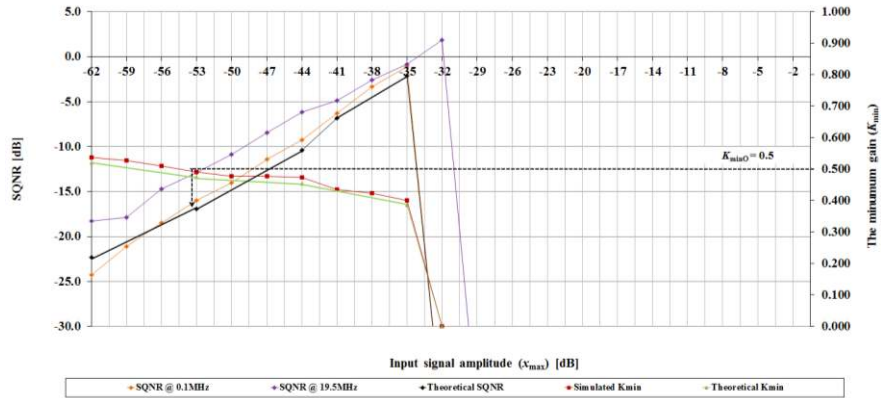
Figure 4.10 Simulated SQNR and estimated SQNR for the 3rd order CT $\Sigma\Delta M$ with
 (a) $D = 0$, (b) $D = 0.5T$, (c) $D = T$



(d)

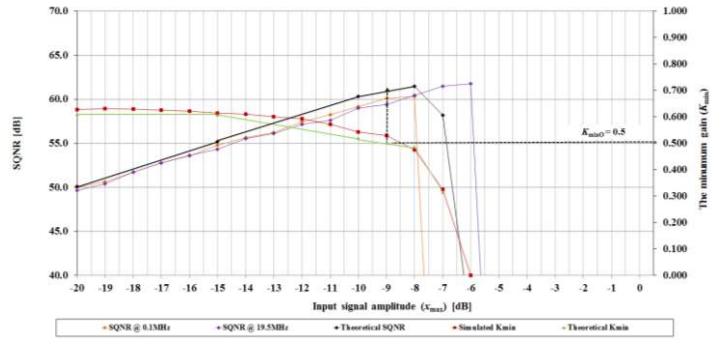


(e)

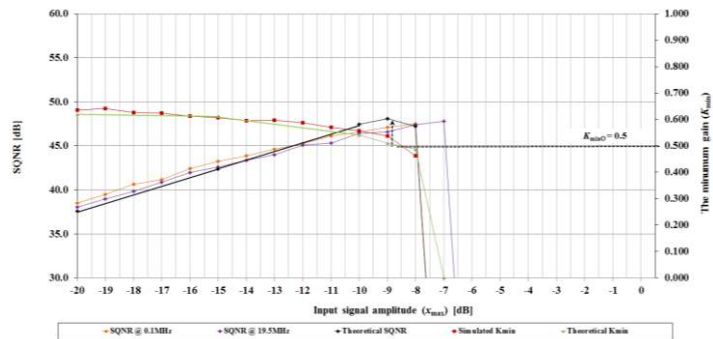


(f)

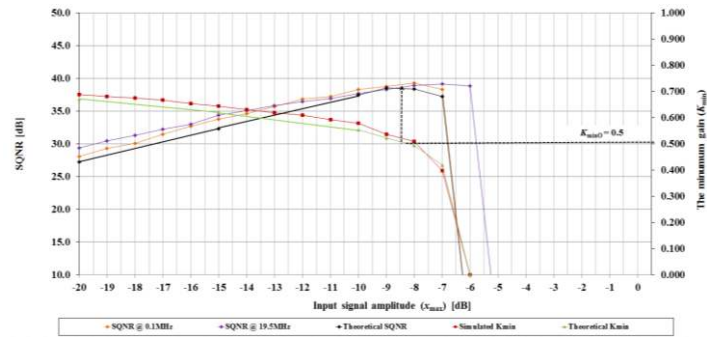
Figure 4.10 (Continued) Simulated SQNR and estimated SQNR for the 3rd order CT $\Sigma\Delta\text{M}$ with
 (d) $D = 1.5T$, (e) $D = 2T$, (f) $D = 2.5T$



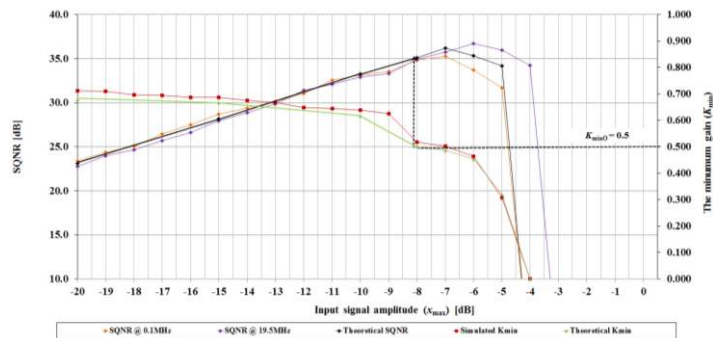
(a)



(b)



(c)



(d)

Figure 4.11 Simulated SQNR and estimated SQNR for the 4th order CT $\Sigma\Delta M$ with (a) $D = 0$, (b) $D = 0.5T$, (c) $D = T$, (d) $D = 1.5T$

CHAPTER 5

STABILITY ANALYSIS OF CT $\Sigma\Delta$ MS

Because a $\Sigma\Delta$ M's output is typically the output of the $\Sigma\Delta$ M's quantizer, $\Sigma\Delta$ Ms cannot be unstable in the bounded input bounded output (BIBO) sense. Instead, a $\Sigma\Delta$ M is considered to have become unstable when the amplitude of a $\Sigma\Delta$ M's input is increased over a value which causes the $\Sigma\Delta$ M's output SQNR to decrease dramatically and the $\Sigma\Delta$ M's output SQNR cannot be restored to its previous values even when the $\Sigma\Delta$ M's input is decreased to its previous amplitudes. In this chapter, a root locus method is used to analyze and predict the maximum input signal parameters that keep a CT $\Sigma\Delta$ M stable.

Root locus methods have been successfully used to determine the stability of DT $\Sigma\Delta$ Ms; however, because the denominator terms of both the STF and NTF of a CT $\Sigma\Delta$ M contain exponential functions, traditional root locus methods cannot be used for determining the stability of CT $\Sigma\Delta$ Ms. Instead, several other methods have been developed for predicting the stability of CT $\Sigma\Delta$ Ms. One such method models the nonlinear quantizer using two linear gains, one for the signal gain and one for quantization noise gain [35]. This approach has not received much attention because of its complexity and because it cannot predict stability for several classes of $\Sigma\Delta$ Ms. Other approaches predict CT $\Sigma\Delta$ M stability by assuming that the $\Sigma\Delta$ M has a DC input and then by performing a simple stability analysis. These methods are effective for predicting stability for lower order $\Sigma\Delta$ Ms but not for higher order $\Sigma\Delta$ Ms [35, 36, 37, 38, 39, 40, 41]. Another method attempts to determine $\Sigma\Delta$ M's stability by using a one-norm of the $\Sigma\Delta$ M's NTF to determine stability in a BIBO sense. It has been shown that the one-norm condition is available only for second order lowpass modulators [43]. Therefore, a mixture of one-norm, two-norm and infinity-norm constraints have been proposed to predict the stability of higher order modulators [44]. Lee's rule is another method used to determine the stability of $\Sigma\Delta$ Ms [45]. Lee's rule states that a

$\Sigma\Delta\text{M}$ will be stable if the gain of the $\Sigma\Delta\text{M}$'s NTF is less than two for all frequencies. It has been shown that Lee's rule is neither a necessary nor a sufficient condition to ensure stability in $\Sigma\Delta\text{Ms}$ [46]. In this chapter, an analytical root locus method is used to determine the stability criteria for CT $\Sigma\Delta\text{Ms}$ that include exponential functions in their characteristic equations. This root locus method determines the range of quantizer gains for which a CT $\Sigma\Delta\text{M}$ is stable. These values can then be used to determine input signal power and other internal signal powers that prevent the $\Sigma\Delta\text{M}$ from becoming unstable.

5.1 Analytical Root Locus

5.1.1 Root locus equation and Gain equation

The poles of a system are the roots of the system's characteristic equation, and these roots provide valuable insight concerning the stability and the response of a system. Root locus analysis is a method for examining how the poles of a system change as function of a certain system parameter. This method is commonly used to determine the stable region of feedback systems as a function of open loop gain by plotting the poles of the system's closed loop transfer function as a function of the system's open loop gain.

As shown in (2.20), CT $\Sigma\Delta\text{Ms}$ typically have characteristic equations of the form

$$1 + K \cdot e^{-sD} \cdot G(s) \cdot H(s) \cdot DAC(s) = 0 \quad (5.1)$$

where D is the $\Sigma\Delta\text{M}$'s excess loop delay and $DAC(s)$ is the system function of a DAC which usually contains at least one exponential function. The root locus analysis of a CT $\Sigma\Delta\text{M}$ that has a characteristic equation like the one in (5.1) can be performed using standard graphical analysis methods [47] or using an analytical method [48, 49] only when $D = 0$ and $DAC(s) = 1$. Although the DAC is not explicitly modeled, a typical zero order hold (ZOH) DAC would have the system function

$$DAC(s) = \frac{1 - e^{-sT}}{s \cdot T} \quad (5.2)$$

where T is the $\Sigma\Delta M$'s sampling period. Most other DACs are also typically modeled using exponential functions. When $D \neq 0$ or $DAC(s)$ contains at least one exponential function, root locus analysis of the characteristic equation in (5.1) cannot be performed using the standard graphical or analytical methods. Instead, the root locus analysis can be performed using an extended graphical analysis method [50, 51, 52] or using the analytical method in [53].

To illustrate the analytical method in [53], the term $e^{-sD} \cdot G(s) \cdot H(s) \cdot DAC(s)$ in (5.1) is written as

$$e^{-sD} \cdot G(s) \cdot H(s) \cdot DAC(s) = \frac{N(s)}{D(s)} \quad (5.3)$$

which implies that (5.1) can be written as

$$D(s) + K \cdot N(s) = 0. \quad (5.4)$$

Solving (5.4) for K ,

$$K = -\frac{D(s)}{N(s)} = -\frac{\text{Re}\{D(s)\} + j \text{Im}\{D(s)\}}{\text{Re}\{N(s)\} + j \text{Im}\{N(s)\}}. \quad (5.5)$$

In standard form, (5.5) can be written as

$$K = \frac{-\text{Re}\{D(s)\} \cdot \text{Re}\{N(s)\} - \text{Im}\{D(s)\} \cdot \text{Im}\{N(s)\}}{(\text{Re}\{N(s)\})^2 + (\text{Im}\{N(s)\})^2} + j \frac{\text{Re}\{D(s)\} \cdot \text{Im}\{N(s)\} - \text{Im}\{D(s)\} \cdot \text{Re}\{N(s)\}}{(\text{Re}\{N(s)\})^2 + (\text{Im}\{N(s)\})^2} \quad (5.6)$$

Because the quantizer's variable gain, K , is real, (5.6) implies that

$$K = \frac{-\text{Re}\{D(s)\} \cdot \text{Re}\{N(s)\} - \text{Im}\{D(s)\} \cdot \text{Im}\{N(s)\}}{(\text{Re}\{N(s)\})^2 + (\text{Im}\{N(s)\})^2} \quad (5.7)$$

and that

$$\text{Re}\{D(s)\} \cdot \text{Im}\{N(s)\} - \text{Im}\{D(s)\} \cdot \text{Re}\{N(s)\} = 0. \quad (5.8)$$

Plotting (5.8) in the s -plane renders the root locus of (5.1) for $-\infty < K < \infty$.

5.1.2 Illustrative example of analytical root locus

To illustrate this analytical root locus method, consider a 3rd order CT $\Sigma\Delta M$ implemented using an RC CIFB implementation as shown in Fig 2.9 (a). From Table 2, the STF and NTF of this CT $\Sigma\Delta M$ are

$$STF(s) = \frac{\frac{K \cdot \{b_3 s^3 + b_2 c_2 s^2 + (b_1 c_1 c_2 - g_0 b_3 c_1) s + b_0 c_0 c_1 c_2\}}{s(s^2 - g_0 c_1)}}{1 + \frac{K \cdot M(s) \cdot \{a_3 s^3 + a_2 c_2 s^2 + (a_1 c_1 c_2 - g_0 a_3 c_1) s + a_0 c_0 c_1 c_2\}}{s(s^2 - g_0 c_1)}}} \quad (5.9)$$

and

$$NTF(s) = \frac{1}{1 + \frac{K \cdot M(s) \cdot \{a_3 s^3 + a_2 c_2 s^2 + (a_1 c_1 c_2 - g_0 a_3 c_1) s + a_0 c_0 c_1 c_2\}}{s(s^2 - g_0 c_1)}}} \quad (5.10)$$

Comparing the STF in (2.21) with (5.9) and NTF in (2.22) with (5.10), it can be seen that

$$F(s) = b_3 s^3 + b_2 c_2 s + (b_1 c_1 c_2 - g_0 b_3 c_1) s + b_0 c_0 c_1 c_2 \quad (5.11)$$

$$G(s) = \frac{1}{s(s^2 - g_0 c_1)} \quad (5.12)$$

$$H(s) = a_3 s^3 + a_2 c_2 s^2 + (a_1 c_1 c_2 - g_0 a_3 c_1) s + a_0 c_0 c_1 c_2 \quad (5.13)$$

Using (5.1), (5.2), (5.12) and (5.13), $N(s)$ and $D(s)$ can be determined to be

$$N(s) = \{a_3 s^3 + a_2 c_2 s^2 + (a_1 c_1 c_2 - g_0 a_3 c_1) s + a_0 c_0 c_1 c_2\} \cdot (1 - e^{-sT}) \cdot e^{-sD} \quad (5.14)$$

and

$$D(s) = (s^2 - g_0 c_1) \cdot s^2 \cdot T \quad (5.15)$$

Substituting $\sigma + j\omega$ for s where $\sigma = \text{Re}\{s\}$ and $\omega = \text{Im}\{s\}$,

$$\text{Re}\{D(s)\} = T \cdot (\sigma^4 - g_0 c_1 \sigma^2 - 3\sigma^2 \omega^2 + \omega^4 + g_0 c_1 \omega^2 - 3\sigma^2 \omega^2) \quad (5.16)$$

$$\text{Im}\{D(s)\} = T \cdot (\sigma^3 \omega - g_0 c_1 \sigma \omega - 3\sigma \omega^3 - \sigma \omega^3 - g_0 c_1 \sigma \omega + 3\sigma^3 \omega) \quad (5.17)$$

$$\begin{aligned} \text{Re}\{N(s)\} = & \left\{ a_3 \sigma^3 - 3a_3 \sigma \omega^2 + a_2 c_2 \sigma^2 - a_2 c_2 \omega^2 + (a_1 c_1 c_2 - g_0 a_3 c_1) \sigma + a_0 c_0 c_1 c_2 \right\} \\ & \cdot \left\{ e^{-D\sigma} \cos(D\omega) - e^{-(T+D)\sigma} \cos((T+D)\omega) \right\} \\ & - \left\{ 3a_3 \sigma^2 \omega - a_3 \omega^3 + 2a_2 c_2 \sigma \omega + (a_1 c_1 c_2 - g_0 a_3 c_1) \omega \right\} \\ & \cdot \left\{ -e^{-D\sigma} \sin(D\omega) + e^{-(T+D)\sigma} \sin((T+D)\omega) \right\} \end{aligned} \quad (5.18)$$

and

$$\begin{aligned} \text{Im}\{N(s)\} = & \left\{ a_3 \sigma^3 - 3a_3 \sigma \omega^2 + a_2 c_2 \sigma^2 - a_2 c_2 \omega^2 + (a_1 c_1 c_2 - g_0 a_3 c_1) \sigma + a_0 c_0 c_1 c_2 \right\} \\ & \cdot \left\{ -e^{-D\sigma} \sin(D\omega) + e^{-(T+D)\sigma} \sin((T+D)\omega) \right\} \\ & + \left\{ 3a_3 \sigma^2 \omega - a_3 \omega^3 + 2a_2 c_2 \sigma \omega + (a_1 c_1 c_2 - g_0 a_3 c_1) \omega \right\} \\ & \cdot \left\{ e^{-D\sigma} \cos(D\omega) - e^{-(T+D)\sigma} \cos((T+D)\omega) \right\}. \end{aligned} \quad (5.19)$$

Substituting (5.16), (5.17), (5.18) and (5.19) into (5.8), the root locus of the 3rd order CT $\Sigma\Delta\text{M}$ using an *RC* implementation can be plotted for $-\infty < K < \infty$.

Similarly, comparing the STF and the NTF for each order CT $\Sigma\Delta\text{M}$ shown in Table 2.2 and Table 2.3 with (2.20) and (2.21), respectively, the $F(s)$, $G(s)$ and $H(s)$ for each order CT $\Sigma\Delta\text{M}$ can be determined. Table 5.1 and Table 5.2 show the results. Table 5.1 shows $F(s)$, $G(s)$ and $H(s)$ for an *RC* implementation, and Table 5.2 shows $F(s)$, $G(s)$ and $H(s)$ for a $G_m C$ implementation. Using Table 5.1 and Table 5.2, $D(s)$ and $N(s)$ for each order CT $\Sigma\Delta\text{M}$ can be easily determined to get the analytical root locus and the quantizer gain value. Table 5.3 and Table 5.4 show $\text{Re}\{D(s)\}$, $\text{Im}\{D(s)\}$, $\text{Re}\{N(s)\}$ and $\text{Im}\{N(s)\}$ for *RC* implementations and $G_m C$ implementations, respectively.

Fig 5.1 (a), (b), (c), (d), (e) and (f) show the root locus or the plot of (5.8), for six lowpass 3rd order CT $\Sigma\Delta\text{M}$ s that have sampling frequencies of 1GHz, Chebyshev Type 2 NTFs with 30dB

attenuation in the stopband, and excess loop delays of $D = 0$, $D = 0.5T$, $D = T$, $D = 1.5T$, $D = 2T$, and $D = 2.5T$, respectively. The plots in Fig 5.1 include both the positive gain ($K > 0$) root locus and the negative gain ($K < 0$) root locus.

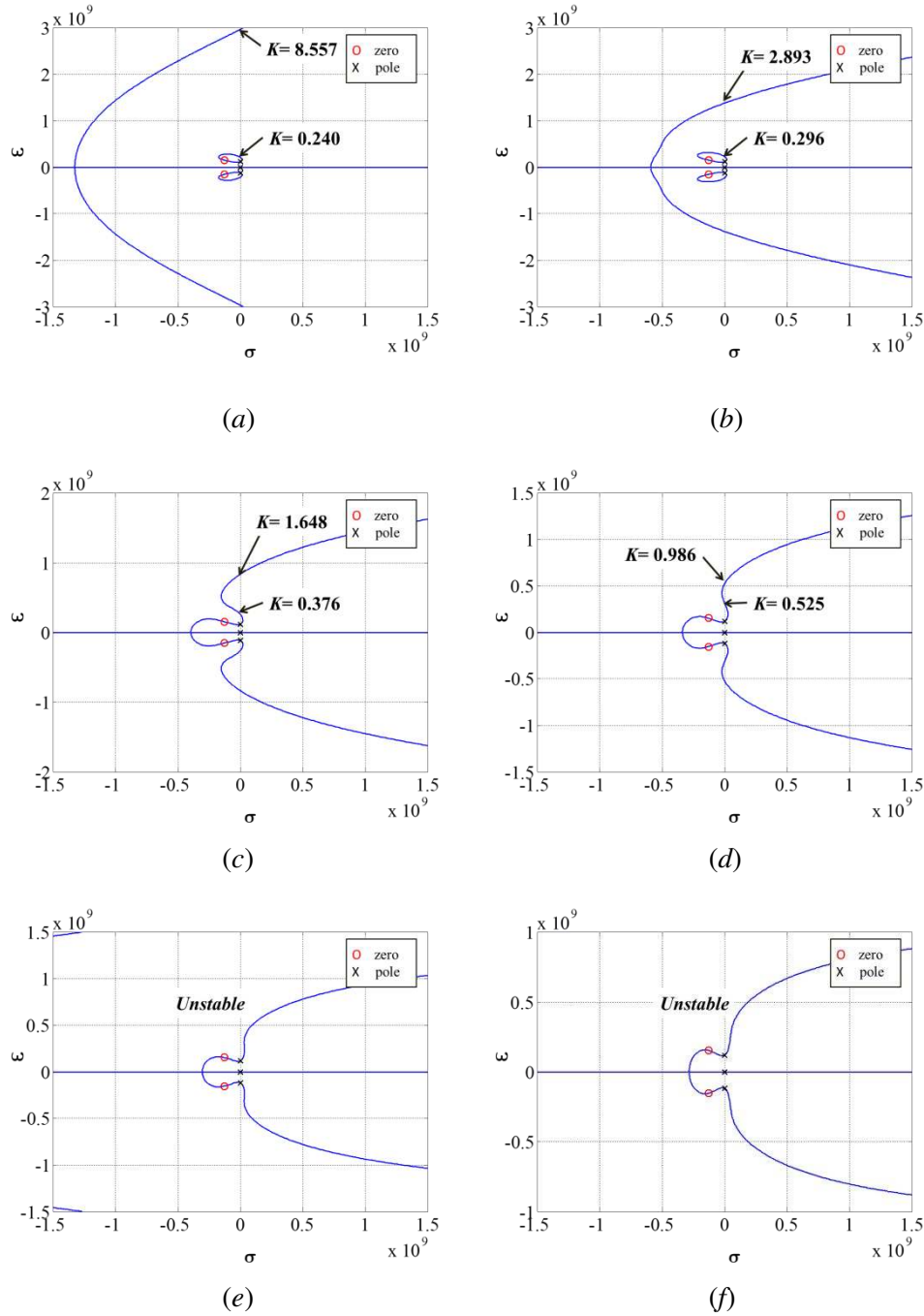


Figure 5.1 The root locus of six lowpass 3rd order CT $\Sigma\Delta$ Ms that have Chebyshev Type 2 NTFs with 30dB attenuation in stopband, a sampling frequency of 1GHz, for and excess loop delays of (a) $D = 0$, (b) $D = 0.5T$, (c) $D = T$, (d) $D = 1.5T$, (e) $D = 2T$, (f) $D = 2.5T$

According to the plots in Fig 5.1, the CT $\Sigma\Delta$ Ms with $D = 0$, $D = 0.5T$, $D = T$, and $D = 1.5T$ are stable for $0.240 < K < 8.557$, $0.296 < K < 2.893$, $0.376 < K < 1.648$, and $0.525 < K < 0.986$, respectively. Although the root locus plots show that the CT $\Sigma\Delta$ Ms with $D = 0$, $D = 0.5T$, $D = T$, and $D = 1.5T$ are unstable for $K > 8.557$, $K > 2.893$, $K > 1.648$, and $K > 0.986$, respectively, none of the modulators show a degradation in SQNR when K enters those ranges because when the modulator enters unstable regions for large values of quantizer gain, K , the feedback signal increases which reduces the quantizer gain, K , and moves the poles back into a stable region. However, when $K < 0.240$, $K < 0.296$, $K < 0.376$, and $K < 0.525$ for the CT $\Sigma\Delta$ Ms with $D = 0$, $D = 0.5T$, $D = T$, and $D = 1.5T$, respectively, the modulator shows a degradation in SQNR because when the modulator enters those unstable regions the feedback signal increases which further reduces the quantizer gain, K , and consequently moves the poles further from the stable region. Therefore, a CT $\Sigma\Delta$ M will remain stable if its quantizer gain, K , remains above its minimum stable value, $K_{\min S}$, as determined from the $\Sigma\Delta$ M's root locus plot.

Fig 5.1 (e) and (f) show the root locus plots for the 3rd order CT $\Sigma\Delta$ Ms with $D = 2T$, and $D = 2.5T$, respectively. These plots show that for both of the cases no quantizer gain, K , exists that can stabilize the $\Sigma\Delta$ Ms. For these cases, a NTF with less attenuation should be chosen. The root loci in Fig 4.1 also show that the range of the quantizer gains that prevent a $\Sigma\Delta$ M from becoming unstable is reduced as the excess loop delay time, D , increases.

Besides root locus plots, Bode plots can also be used to compute the range of quantizer gains over which a CT $\Sigma\Delta$ M is stable. For example, Fig 5.2 shows the Bode plot for the 3rd order CT $\Sigma\Delta$ Ms that has a sampling frequency of 1GHz, uses a Chebyshev Type 2 NTF with 30dB attenuation in the stopband and has an excess loop delay time, D , of zero. The root locus for this $\Sigma\Delta$ M is shown in Fig 5.1 (a). From Fig 5.2, it can be seen that the lowest stable quantizer gain is -12.39dB (0.240) and the highest stable quantizer gain is 18.65 dB (8.55). Both of these values are consistent with the values obtained from the root locus plot in Fig 5.1 (a).

Table 5.1 $F(s)$, $G(s)$ and $H(s)$ for RC implementations

2nd order CT $\Sigma\Delta\Delta$	
$F(s)$	$b_2s^2 + b_1c_1s + b_0c_0c_1 - g_0b_2c_0$
$G(s)$	$\frac{1}{s^2 - g_0c_0}$
$H(s)$	$a_2s^2 + a_1c_1s + (a_0c_0c_1 - g_0a_2c_0)$
3rd order CT $\Sigma\Delta\Delta$	
$F(s)$	$b_3s^3 + b_2c_2s^2 + (b_1c_1c_2 - g_0b_3c_1)s + b_0c_0c_1c_2$
$G(s)$	$\frac{1}{s(s^2 - g_0c_1)}$
$H(s)$	$a_3s^3 + a_2c_2s^2 + (a_1c_1c_2 - g_0a_3c_1)s + a_0c_0c_1c_2$
4th order CT $\Sigma\Delta\Delta$	
$F(s)$	$b_4s^4 + b_3c_3s^3 + (b_2c_2c_3 - g_0b_4c_0 - g_1b_4c_2)s^2 + (b_1c_1c_2c_3 - g_0b_3c_0c_3)s + (b_0c_0c_1c_2c_3 - g_0b_2c_0c_2c_3 + g_0g_1b_4c_0c_2)$
$G(s)$	$\frac{1}{(s^2 - g_0c_1)(s^2 - g_1c_2)}$
$H(s)$	$a_4s^4 + a_3c_3s^3 + (a_2c_2c_3 - g_0a_4c_0 - g_1a_4c_2)s^2 + (a_1c_1c_2c_3 - g_0a_3c_0c_3)s + (a_0c_0c_1c_2c_3 - g_0a_2c_0c_2c_3 + g_0g_1a_4c_0c_2)$
5th order CT $\Sigma\Delta\Delta$	
$F(s)$	$b_5s^5 + b_4c_4s^4 + (b_3c_3c_4 - g_0b_5c_1 - g_1b_5c_3)s^3 + (b_2c_2c_3c_4 - g_0b_4c_1c_4)s^2 + (b_1c_1c_2c_3c_4 - g_0b_3c_1c_3c_4 + g_0g_1b_5c_1c_3)s + b_0c_0c_1c_2c_3c_4$
$G(s)$	$\frac{1}{s(s^2 - g_0c_1)(s^2 - g_1c_3)}$
$H(s)$	$a_5s^5 + a_4c_4s^4 + (a_3c_3c_4 - g_0a_5c_1 - g_1a_5c_3)s^3 + (a_2c_2c_3c_4 - g_0a_4c_1c_4)s^2 + (a_1c_1c_2c_3c_4 - g_0a_3c_1c_3c_4 + g_0g_1a_5c_1c_3)s + a_0c_0c_1c_2c_3c_4$

Table 5.2 $F(s)$, $G(s)$ and $H(s)$ for G_mC implementations

2nd order CT $\Sigma\Delta M$	
$F(s)$	$b_2s^2 + b_1c_1s + b_0c_0c_1 - g_0b_2c_0c_1$
$G(s)$	$\frac{1}{s^2 - g_0c_0c_1}$
$H(s)$	$a_2s^2 + a_1c_1s + (a_0c_0c_1 - g_0a_2c_0c_1)$
3rd order CT $\Sigma\Delta M$	
$F(s)$	$b_3s^3 + b_2c_2s^2 + (b_1c_1c_2 - g_0b_3c_1c_2)s + b_0c_0c_1c_2$
$G(s)$	$\frac{1}{s(s^2 - g_0c_1c_2)}$
$H(s)$	$a_3s^3 + a_2c_2s^2 + (a_1c_1c_2 - g_0a_3c_1c_2)s + a_0c_0c_1c_2$
4th order CT $\Sigma\Delta M$	
$F(s)$	$b_4s^4 + b_3c_3s^3 + (b_2c_2c_3 - g_0b_4c_0c_1 - g_1b_4c_2c_3)s^2 + (b_1c_1c_2c_3 - g_0b_3c_0c_1c_3)s + (b_0c_0c_1c_2c_3 - g_0b_2c_0c_1c_2c_3 + g_0g_1b_4c_0c_1c_2c_3)$
$G(s)$	$\frac{1}{(s^2 - g_0c_0c_1)(s^2 - g_1c_2c_3)}$
$H(s)$	$a_4s^4 + a_3c_3s^3 + (a_2c_2c_3 - g_0a_4c_0c_1 - g_1a_4c_2c_3)s^2 + (a_1c_1c_2c_3 - g_0a_3c_0c_1c_3)s + (a_0c_0c_1c_2c_3 - g_0a_2c_0c_1c_2c_3 + g_0g_1a_4c_0c_1c_2c_3)$
5th order CT $\Sigma\Delta M$	
$F(s)$	$b_5s^5 + b_4c_4s^4 + (b_3c_3c_4 - g_0b_5c_1c_2 - g_1b_5c_3c_4)s^3 + (b_2c_2c_3c_4 - g_0b_4c_1c_2c_4)s^2 + (b_1c_1c_2c_3c_4 - g_0b_3c_1c_2c_3c_4 + g_0g_1b_5c_1c_2c_3c_4)s + b_0c_0c_1c_2c_3c_4$
$G(s)$	$\frac{1}{s(s^2 - g_0c_1c_2)(s^2 - g_1c_3c_4)}$
$H(s)$	$a_5s^5 + a_4c_4s^4 + (a_3c_3c_4 - g_0a_5c_1c_2 - g_1a_5c_3c_4)s^3 + (a_2c_2c_3c_4 - g_0a_4c_1c_2c_4)s^2 + (a_1c_1c_2c_3c_4 - g_0a_3c_1c_2c_3c_4 + g_0g_1a_5c_1c_2c_3c_4)s + a_0c_0c_1c_2c_3c_4$

Table 5.3 $\text{Re}\{D(s)\}$, $\text{Im}\{D(s)\}$, $\text{Re}\{N(s)\}$ and $\text{Im}\{N(s)\}$ for RC implementations

2nd order CT $\Sigma\Delta\text{M}$	
$\text{Re}\{D(s)\}$	$T \cdot (\sigma^3 - g_0 c_0 \sigma - 3\sigma \omega^2)$
$\text{Im}\{D(s)\}$	$T \cdot (-\omega^3 - g_0 c_0 \omega + 3\sigma^2 \omega)$
$\text{Re}\{N(s)\}$	$\left\{ a_2 \sigma^2 - a_2 \omega^2 + a_1 c_1 \sigma + (a_0 c_0 c_1 - g_0 a_2 c_0) \right\} \cdot \left\{ e^{-D\sigma} \cos(D\omega) - e^{-(T+D)\sigma} \cos((T+D)\omega) \right\}$ $- \left\{ 2a_2 \sigma \omega + a_1 c_1 \omega \right\} \cdot \left\{ -e^{-D\sigma} \sin(D\omega) + e^{-(T+D)\sigma} \sin((T+D)\omega) \right\}$
$\text{Im}\{N(s)\}$	$\left\{ a_2 \sigma^2 - a_2 \omega^2 + a_1 c_1 \sigma + (a_0 c_0 c_1 - g_0 a_2 c_0) \right\} \cdot \left\{ -e^{-D\sigma} \sin(D\omega) + e^{-(T+D)\sigma} \sin((T+D)\omega) \right\}$ $+ \left\{ 2a_2 \sigma \omega + a_1 c_1 \omega \right\} \cdot \left\{ e^{-D\sigma} \cos(D\omega) - e^{-(T+D)\sigma} \cos((T+D)\omega) \right\}$
3rd order CT $\Sigma\Delta\text{M}$	
$\text{Re}\{D(s)\}$	$T \cdot (\sigma^4 - g_0 c_1 \sigma^2 - 3\sigma^2 \omega^2 + \omega^4 + g_0 c_1 \omega^2 - 3\sigma^2 \omega^2)$
$\text{Im}\{D(s)\}$	$T \cdot (\sigma^3 \omega - g_0 c_1 \sigma \omega - 3\sigma \omega^3 - \sigma \omega^3 - g_0 c_1 \sigma \omega + 3\sigma^3 \omega)$
$\text{Re}\{N(s)\}$	$\left\{ a_3 \sigma^3 - 3a_3 \sigma \omega^2 + a_2 c_2 \sigma^2 - a_2 c_2 \omega^2 + (a_1 c_1 c_2 - g_0 a_3 c_1) \sigma + a_0 c_0 c_1 c_2 \right\}$ $\cdot \left\{ e^{-D\sigma} \cos(D\omega) - e^{-(T+D)\sigma} \cos((T+D)\omega) \right\}$ $- \left\{ 3a_3 \sigma^2 \omega - a_3 \omega^3 + 2a_2 c_2 \sigma \omega + (a_1 c_1 c_2 - g_0 a_3 c_1) \omega \right\}$ $\cdot \left\{ -e^{-D\sigma} \sin(D\omega) + e^{-(T+D)\sigma} \sin((T+D)\omega) \right\}$
$\text{Im}\{N(s)\}$	$\left\{ a_3 \sigma^3 - 3a_3 \sigma \omega^2 + a_2 c_2 \sigma^2 - a_2 c_2 \omega^2 + (a_1 c_1 c_2 - g_0 a_3 c_1) \sigma + a_0 c_0 c_1 c_2 \right\}$ $\cdot \left\{ -e^{-D\sigma} \sin(D\omega) + e^{-(T+D)\sigma} \sin((T+D)\omega) \right\}$ $+ \left\{ 3a_3 \sigma^2 \omega - a_3 \omega^3 + 2a_2 c_2 \sigma \omega + (a_1 c_1 c_2 - g_0 a_3 c_1) \omega \right\}$ $\cdot \left\{ e^{-D\sigma} \cos(D\omega) - e^{-(T+D)\sigma} \cos((T+D)\omega) \right\}$
4th order CT $\Sigma\Delta\text{M}$	
$\text{Re}\{D(s)\}$	$T \cdot \left\{ \sigma^5 - 10\sigma^3 \omega^2 + 5\sigma \omega^4 + (-g_0 c_1 - g_1 c_2) \cdot (\sigma^3 - 3\sigma \omega^2) + g_0 g_1 c_1 c_2 \sigma \right\}$
$\text{Im}\{D(s)\}$	$T \cdot \left\{ 5\sigma^4 \omega - 10\sigma^2 \omega^3 + \omega^5 + (-g_0 c_1 - g_1 c_2) \cdot (3\sigma^2 \omega - \omega^3) + g_0 g_1 c_1 c_2 \omega \right\}$
$\text{Re}\{N(s)\}$	$\left\{ a_4 (\sigma^4 - 6\sigma^2 \omega^2 + \omega^4) + a_3 c_3 (\sigma^3 - 3\sigma \omega^2) + (a_2 c_2 c_3 - g_0 a_4 c_0 - g_1 a_4 c_2) (\sigma^2 - \omega^2) \right\}$ $\left\{ + (a_1 c_1 c_2 c_3 - g_0 a_3 c_0 c_3) \sigma + (a_0 c_0 c_1 c_2 c_3 - g_0 a_2 c_0 c_2 c_3 + g_0 g_1 a_4 c_0 c_2) \right\}$ $\cdot \left\{ e^{-D\sigma} \cos(D\omega) - e^{-(T+D)\sigma} \cos((T+D)\omega) \right\}$ $- \left\{ a_4 (4\sigma^3 \omega - 4\sigma \omega^3) + a_3 c_3 (3\sigma^2 \omega - \omega^3) + 2(a_2 c_2 c_3 - g_0 a_4 c_0 - g_1 a_4 c_2) \sigma \omega \right\}$ $\left\{ + (a_1 c_1 c_2 c_3 - g_0 a_3 c_0 c_3) \omega \right\}$ $\cdot \left\{ -e^{-D\sigma} \sin(D\omega) + e^{-(T+D)\sigma} \sin((T+D)\omega) \right\}$

Table 5.3 (Continued) $\text{Re}\{D(s)\}$, $\text{Im}\{D(s)\}$, $\text{Re}\{N(s)\}$ and $\text{Im}\{N(s)\}$ for RC implementations

$\text{Im}\{N(s)\}$	$\left\{ \begin{aligned} & a_4(\sigma^4 - 6\sigma^2\omega^2 + \omega^4) + a_3c_3(\sigma^3 - 3\sigma\omega^2) + (a_2c_2c_3 - g_0a_4c_0 - g_1a_4c_2)(\sigma^2 - \omega^2) \\ & + (a_1c_1c_2c_3 - g_0a_3c_0c_3)\sigma + (a_0c_0c_1c_2c_3 - g_0a_2c_0c_2c_3 + g_0g_1a_4c_0c_2) \end{aligned} \right\}$ $\cdot \left\{ -e^{-D\sigma} \sin(D\omega) + e^{-(T+D)\sigma} \sin((T+D)\omega) \right\}$ $+ \left\{ \begin{aligned} & a_4(4\sigma^3\omega - 4\sigma\omega^3) + a_3c_3(3\sigma^2\omega - \omega^3) + 2(a_2c_2c_3 - g_0a_4c_0 - g_1a_4c_2)\sigma\omega \\ & + (a_1c_1c_2c_3 - g_0a_3c_0c_3)\omega \end{aligned} \right\}$ $\cdot \left\{ e^{-D\sigma} \cos(D\omega) - e^{-(T+D)\sigma} \cos((T+D)\omega) \right\}$
5th order CT $\Sigma\Delta\text{M}$	
$\text{Re}\{D(s)\}$	$T \cdot \left\{ \begin{aligned} & \sigma^6 - 15\sigma^4\omega^2 + 15\sigma^2\omega^4 - \omega^6 + (-g_0c_1 - g_1c_3) \cdot (\sigma^4 - 6\sigma^2\omega^2 + \omega^4) \\ & + g_0g_1c_1c_3(\sigma^2 - \omega^2) \end{aligned} \right\}$
$\text{Im}\{D(s)\}$	$T \cdot \left\{ 6\sigma^5\omega - 20\sigma^3\omega^3 + 6\sigma\omega^5 + (-g_0c_1 - g_1c_3) \cdot (4\sigma^3\omega - 4\sigma\omega^3) + 2g_0g_1c_1c_3\sigma\omega \right\}$
$\text{Re}\{N(s)\}$	$\left\{ \begin{aligned} & a_5(\sigma^5 - 10\sigma^3\omega^2 + 5\sigma\omega^4) + a_4c_4(\sigma^4 - 6\sigma^2\omega^2 + \omega^4) \\ & + (a_3c_3c_4 - g_0a_5c_1 - g_1a_5c_3)(\sigma^3 - 3\sigma\omega^2) \\ & + (a_2c_2c_3c_4 - g_0a_4c_1c_4)(\sigma^2 - \omega^2) + (a_1c_1c_2c_3c_4 - g_0a_3c_1c_3c_4 + g_0g_1a_5c_1c_3)\sigma \\ & + a_0c_0c_1c_2c_3c_4 \end{aligned} \right\}$ $\cdot \left\{ e^{-D\sigma} \cos(D\omega) - e^{-(T+D)\sigma} \cos((T+D)\omega) \right\}$ $- \left\{ \begin{aligned} & a_5(5\sigma^4\omega - 10\sigma^2\omega^3 + \omega^5) + a_4c_4(4\sigma^3\omega - 4\sigma\omega^3) \\ & + (a_3c_3c_4 - g_0a_5c_1 - g_1a_5c_3)(3\sigma^2\omega - \omega^3) \\ & + 2(a_2c_2c_3c_4 - g_0a_4c_1c_4)\sigma\omega + (a_1c_1c_2c_3c_4 - g_0a_3c_1c_3c_4 + g_0g_1a_5c_1c_3)\omega \end{aligned} \right\}$ $\cdot \left\{ -e^{-D\sigma} \sin(D\omega) + e^{-(T+D)\sigma} \sin((T+D)\omega) \right\}$
$\text{Im}\{N(s)\}$	$\left\{ \begin{aligned} & a_5(\sigma^5 - 10\sigma^3\omega^2 + 5\sigma\omega^4) + a_4c_4(\sigma^4 - 6\sigma^2\omega^2 + \omega^4) \\ & + (a_3c_3c_4 - g_0a_5c_1 - g_1a_5c_3)(\sigma^3 - 3\sigma\omega^2) \\ & + (a_2c_2c_3c_4 - g_0a_4c_1c_4)(\sigma^2 - \omega^2) + (a_1c_1c_2c_3c_4 - g_0a_3c_1c_3c_4 + g_0g_1a_5c_1c_3)\sigma \\ & + a_0c_0c_1c_2c_3c_4 \end{aligned} \right\}$ $\cdot \left\{ -e^{-D\sigma} \sin(D\omega) + e^{-(T+D)\sigma} \sin((T+D)\omega) \right\}$ $+ \left\{ \begin{aligned} & a_5(5\sigma^4\omega - 10\sigma^2\omega^3 + \omega^5) + a_4c_4(4\sigma^3\omega - 4\sigma\omega^3) \\ & + (a_3c_3c_4 - g_0a_5c_1 - g_1a_5c_3)(3\sigma^2\omega - \omega^3) \\ & + 2(a_2c_2c_3c_4 - g_0a_4c_1c_4)\sigma\omega + (a_1c_1c_2c_3c_4 - g_0a_3c_1c_3c_4 + g_0g_1a_5c_1c_3)\omega \end{aligned} \right\}$ $\cdot \left\{ e^{-D\sigma} \cos(D\omega) - e^{-(T+D)\sigma} \cos((T+D)\omega) \right\}$

Table 5.4 $\text{Re}\{D(s)\}$, $\text{Im}\{D(s)\}$, $\text{Re}\{N(s)\}$ and $\text{Im}\{N(s)\}$ for G_mC implementations

2nd order CT $\Sigma\Delta M$	
$\text{Re}\{D(s)\}$	$T \cdot (\sigma^3 - 3\sigma\omega^2 - g_0c_0c_1\sigma)$
$\text{Im}\{D(s)\}$	$T \cdot (3\sigma^2\omega - \omega^3 - g_0c_0c_1\omega)$
$\text{Re}\{N(s)\}$	$\{a_2\sigma^2 - a_2\omega^2 + a_1c_1\sigma + (a_0c_0c_1 - g_0a_2c_0c_1)\} \cdot \{e^{-D\sigma} \cos(D\omega) - e^{-(T+D)\sigma} \cos((T+D)\omega)\}$ $-\{2a_2\sigma\omega + a_1c_1\omega\} \cdot \{-e^{-D\sigma} \sin(D\omega) + e^{-(T+D)\sigma} \sin((T+D)\omega)\}$
$\text{Im}\{N(s)\}$	$\{a_2\sigma^2 - a_2\omega^2 + a_1c_1\sigma + (a_0c_0c_1 - g_0a_2c_0c_1)\} \cdot \{-e^{-D\sigma} \sin(D\omega) + e^{-(T+D)\sigma} \sin((T+D)\omega)\}$ $+\{2a_2\sigma\omega + a_1c_1\omega\} \cdot \{e^{-D\sigma} \cos(D\omega) - e^{-(T+D)\sigma} \cos((T+D)\omega)\}$
3rd order CT $\Sigma\Delta M$	
$\text{Re}\{D(s)\}$	$T \cdot (\sigma^4 - g_0c_1c_2\sigma^2 - 3\sigma^2\omega^2 + \omega^4 + g_0c_1c_2\omega^2 - 3\sigma^2\omega^2)$
$\text{Im}\{D(s)\}$	$T \cdot (\sigma^3\omega - g_0c_1c_2\sigma\omega - 3\sigma\omega^3 - \sigma\omega^3 - g_0c_1c_2\sigma\omega + 3\sigma^3\omega)$
$\text{Re}\{N(s)\}$	$\{a_3\sigma^3 - 3a_3\sigma\omega^2 + a_2c_2\sigma^2 - a_2c_2\omega^2 + (a_1c_1c_2 - g_0a_3c_1c_2)\sigma + a_0c_0c_1c_2\}$ $\cdot \{e^{-D\sigma} \cos(D\omega) - e^{-(T+D)\sigma} \cos((T+D)\omega)\}$ $-\{3a_3\sigma^2\omega - a_3\omega^3 + 2a_2c_2\sigma\omega + (a_1c_1c_2 - g_0a_3c_1c_2)\omega\}$ $\cdot \{-e^{-D\sigma} \sin(D\omega) + e^{-(T+D)\sigma} \sin((T+D)\omega)\}$
$\text{Im}\{N(s)\}$	$\{a_3\sigma^3 - 3a_3\sigma\omega^2 + a_2c_2\sigma^2 - a_2c_2\omega^2 + (a_1c_1c_2 - g_0a_3c_1c_2)\sigma + a_0c_0c_1c_2\}$ $\cdot \{-e^{-D\sigma} \sin(D\omega) + e^{-(T+D)\sigma} \sin((T+D)\omega)\}$ $+\{3a_3\sigma^2\omega - a_3\omega^3 + 2a_2c_2\sigma\omega + (a_1c_1c_2 - g_0a_3c_1c_2)\omega\}$ $\cdot \{e^{-D\sigma} \cos(D\omega) - e^{-(T+D)\sigma} \cos((T+D)\omega)\}$
4th order CT $\Sigma\Delta M$	
$\text{Re}\{D(s)\}$	$T \cdot \{\sigma^5 - 10\sigma^3\omega^2 + 5\sigma\omega^4 + (-g_0c_0c_1 - g_1c_2c_3) \cdot (\sigma^3 - 3\sigma\omega^2) + g_0g_1c_0c_1c_2c_3\sigma\}$
$\text{Im}\{D(s)\}$	$T \cdot \{5\sigma^4\omega - 10\sigma^2\omega^3 + \omega^5 + (-g_0c_0c_1 - g_1c_2c_3) \cdot (3\sigma^2\omega - \omega^3) + g_0g_1c_0c_1c_2c_3\omega\}$
$\text{Re}\{N(s)\}$	$\left\{ a_4(\sigma^4 - 6\sigma^2\omega^2 + \omega^4) + a_3c_3(\sigma^3 - 3\sigma\omega^2) + (a_2c_2c_3 - g_0a_4c_0c_1 - g_1a_4c_2c_3)(\sigma^2 - \omega^2) \right\}$ $\left\{ + (a_1c_1c_2c_3 - g_0a_3c_0c_1c_3)\sigma + (a_0c_0c_1c_2c_3 - g_0a_2c_0c_1c_2c_3 + g_0g_1a_4c_0c_1c_2c_3) \right\}$ $\cdot \{e^{-D\sigma} \cos(D\omega) - e^{-(T+D)\sigma} \cos((T+D)\omega)\}$ $-\left\{ a_4(4\sigma^3\omega - 4\sigma\omega^3) + a_3c_3(3\sigma^2\omega - \omega^3) + 2(a_2c_2c_3 - g_0a_4c_0c_1 - g_1a_4c_2c_3)\sigma\omega \right\}$ $\left\{ + (a_1c_1c_2c_3 - g_0a_3c_0c_1c_3)\omega \right\}$ $\cdot \{-e^{-D\sigma} \sin(D\omega) + e^{-(T+D)\sigma} \sin((T+D)\omega)\}$

Table 5.4 (Continued) $\text{Re}\{D(s)\}$, $\text{Im}\{D(s)\}$, $\text{Re}\{N(s)\}$ and $\text{Im}\{N(s)\}$ for G_mC implementations

$\text{Im}\{N(s)\}$	$\left\{ \begin{aligned} & a_4(\sigma^4 - 6\sigma^2\omega^2 + \omega^4) + a_3c_3(\sigma^3 - 3\sigma\omega^2) + (a_2c_2c_3 - g_0a_4c_0c_1 - g_1a_4c_2c_3)(\sigma^2 - \omega^2) \\ & + (a_1c_1c_2c_3 - g_0a_3c_0c_1c_3)\sigma + (a_0c_0c_1c_2c_3 - g_0a_2c_0c_1c_2c_3 + g_0g_1a_4c_0c_1c_2c_3) \end{aligned} \right\}$ $\cdot \left\{ -e^{-D\sigma} \sin(D\omega) + e^{-(T+D)\sigma} \sin((T+D)\omega) \right\}$ $+ \left\{ \begin{aligned} & a_4(4\sigma^3\omega - 4\sigma\omega^3) + a_3c_3(3\sigma^2\omega - \omega^3) + 2(a_2c_2c_3 - g_0a_4c_0c_1 - g_1a_4c_2c_3)\sigma\omega \\ & + (a_1c_1c_2c_3 - g_0a_3c_0c_1c_3)\omega \end{aligned} \right\}$ $\cdot \left\{ e^{-D\sigma} \cos(D\omega) - e^{-(T+D)\sigma} \cos((T+D)\omega) \right\}$
5th order CT $\Sigma\Delta M$	
$\text{Re}\{D(s)\}$	$T \cdot \left\{ \begin{aligned} & \sigma^6 - 15\sigma^4\omega^2 + 15\sigma^2\omega^4 - \omega^6 + (-g_0c_1c_2 - g_1c_3c_4) \cdot (\sigma^4 - 6\sigma^2\omega^2 + \omega^4) \\ & + g_0g_1c_1c_2c_3c_4(\sigma^2 - \omega^2) \end{aligned} \right\}$
$\text{Im}\{D(s)\}$	$T \cdot \left\{ 6\sigma^5\omega - 20\sigma^3\omega^3 + 6\sigma\omega^5 + (-g_0c_1c_2 - g_1c_3c_4) \cdot (4\sigma^3\omega - 4\sigma\omega^3) + 2g_0g_1c_1c_2c_3c_4\sigma\omega \right\}$
$\text{Re}\{N(s)\}$	$\left\{ \begin{aligned} & a_5(\sigma^5 - 10\sigma^3\omega^2 + 5\sigma\omega^4) + a_4c_4(\sigma^4 - 6\sigma^2\omega^2 + \omega^4) \\ & + (a_3c_3c_4 - g_0a_5c_1c_2 - g_1a_5c_3c_4)(\sigma^3 - 3\sigma\omega^2) \\ & + (a_2c_2c_3c_4 - g_0a_4c_1c_2c_4)(\sigma^2 - \omega^2) + (a_1c_1c_2c_3c_4 - g_0a_3c_1c_2c_3c_4 + g_0g_1a_5c_1c_2c_3c_4)\sigma \\ & + a_0c_0c_1c_2c_3c_4 \end{aligned} \right\}$ $\cdot \left\{ e^{-D\sigma} \cos(D\omega) - e^{-(T+D)\sigma} \cos((T+D)\omega) \right\}$ $- \left\{ \begin{aligned} & a_5(5\sigma^4\omega - 10\sigma^2\omega^3 + \omega^5) + a_4c_4(4\sigma^3\omega - 4\sigma\omega^3) \\ & + (a_3c_3c_4 - g_0a_5c_1c_2 - g_1a_5c_3c_4)(3\sigma^2\omega - \omega^3) \\ & + 2(a_2c_2c_3c_4 - g_0a_4c_1c_2c_4)\sigma\omega + (a_1c_1c_2c_3c_4 - g_0a_3c_1c_2c_3c_4 + g_0g_1a_5c_1c_2c_3c_4)\omega \end{aligned} \right\}$ $\cdot \left\{ -e^{-D\sigma} \sin(D\omega) + e^{-(T+D)\sigma} \sin((T+D)\omega) \right\}$
$\text{Im}\{N(s)\}$	$\left\{ \begin{aligned} & a_5(\sigma^5 - 10\sigma^3\omega^2 + 5\sigma\omega^4) + a_4c_4(\sigma^4 - 6\sigma^2\omega^2 + \omega^4) \\ & + (a_3c_3c_4 - g_0a_5c_1c_2 - g_1a_5c_3c_4)(\sigma^3 - 3\sigma\omega^2) \\ & + (a_2c_2c_3c_4 - g_0a_4c_1c_2c_4)(\sigma^2 - \omega^2) + (a_1c_1c_2c_3c_4 - g_0a_3c_1c_2c_3c_4 + g_0g_1a_5c_1c_2c_3c_4)\sigma \\ & + a_0c_0c_1c_2c_3c_4 \end{aligned} \right\}$ $\cdot \left\{ -e^{-D\sigma} \sin(D\omega) + e^{-(T+D)\sigma} \sin((T+D)\omega) \right\}$ $+ \left\{ \begin{aligned} & a_5(5\sigma^4\omega - 10\sigma^2\omega^3 + \omega^5) + a_4c_4(4\sigma^3\omega - 4\sigma\omega^3) \\ & + (a_3c_3c_4 - g_0a_5c_1c_2 - g_1a_5c_3c_4)(3\sigma^2\omega - \omega^3) \\ & + 2(a_2c_2c_3c_4 - g_0a_4c_1c_2c_4)\sigma\omega + (a_1c_1c_2c_3c_4 - g_0a_3c_1c_2c_3c_4 + g_0g_1a_5c_1c_2c_3c_4)\omega \end{aligned} \right\}$ $\cdot \left\{ e^{-D\sigma} \cos(D\omega) - e^{-(T+D)\sigma} \cos((T+D)\omega) \right\}$

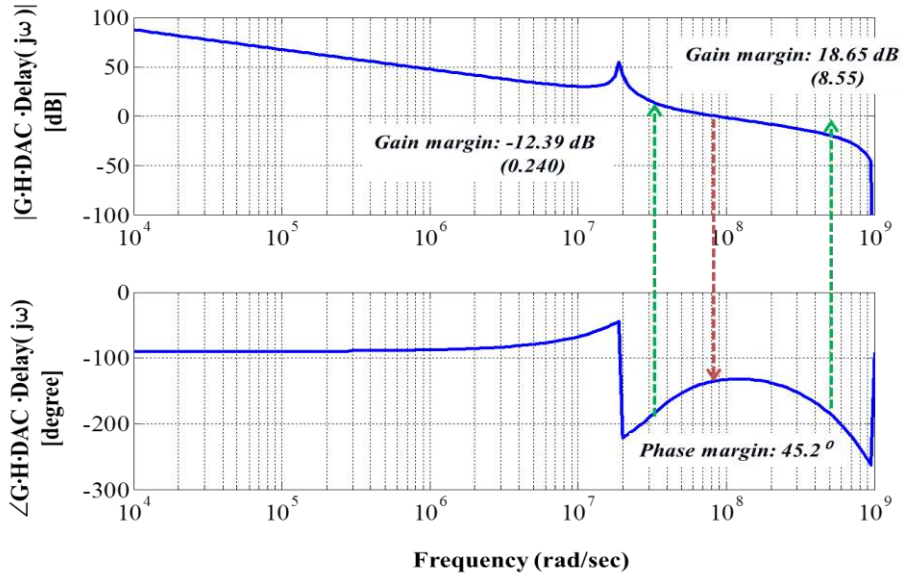


Figure 5.2 Bode plot for the 3rd order CT $\Sigma\Delta$ M shown in Fig 5.1 (a)

5.2 Stability Analysis for CT $\Sigma\Delta$ Ms that are not overloaded

Because the output of a $\Sigma\Delta$ M's quantizer has fixed quantization levels, its gain is a function of its input signal which is a function of the $\Sigma\Delta$ M's input signal. Therefore, the stability of a CT $\Sigma\Delta$ M depends upon the quantizer's input signal because a large enough input signal can generate a large signal at the quantizer's input which reduces the quantizer's gain and in turn can destabilize the modulator loop. In this section, a method for determining a $\Sigma\Delta$ M's maximum input signal power which keeps the $\Sigma\Delta$ M stable is developed.

To determine the maximum input signal power, $P_{\max S}$, that keeps a $\Sigma\Delta$ M stable, consider the STF and NTF models shown in Fig 5.3 (a) and (b) and assume that the quantizer's input, ψ , is a zero mean random process. Because ψ is a zero mean random process, the quantizer's input signal power, P_ψ , can be written as $P_\psi = \sigma_\psi^2$ where σ_ψ is the standard deviation of ψ . To keep a $\Sigma\Delta$ M stable, $\psi_{\max S} < 1/K_{\min S}$ where $\psi_{\max S}$ is the quantizer's maximum input amplitude that keeps the $\Sigma\Delta$ M stable. This condition is assumed to be true when $\mu \cdot \sigma_\psi < \psi_{\max S}$ or equivalently when

$$\sigma_{\psi}^2 < \left(\frac{\Psi_{\max S}}{\mu} \right)^2 = \left(\frac{1}{\mu \cdot K_{\min S}} \right)^2 \quad (5.20)$$

where μ is the standard deviation coefficient of σ_{ψ} as shown in Fig 5.4. Based on the empirical simulation results, μ is chosen as 3.6. Because the minimum quantizer gain that keeps a $\Sigma\Delta\text{M}$ stable is $K_{\min S}$, the quantizer's maximum input power, $P_{\psi_{\max S}}$, that keeps a $\Sigma\Delta\text{M}$ stable can be written as

$$P_{\psi_{\max S}} = \sigma_{\psi_{\max S}}^2 = \left(\frac{1}{\mu \cdot K_{\min S}} \right)^2. \quad (5.21)$$

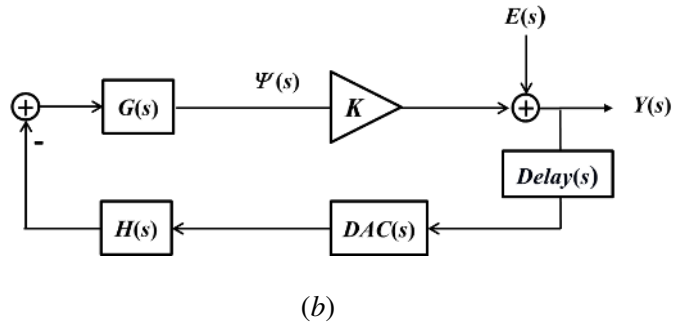
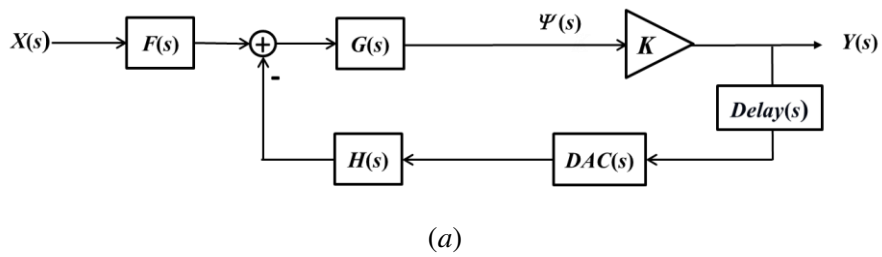


Figure 5.3 (a) Block diagram of a CT $\Sigma\Delta\text{M}$'s STF, (b) Block diagram of a CT $\Sigma\Delta\text{M}$'s NTF

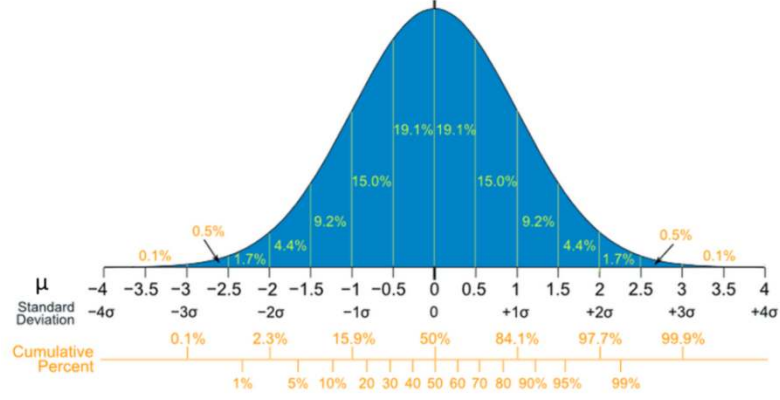


Figure 5.4 Bell curve of the standard normal distribution [22]

From the block diagrams shown in Fig 5.3, the quantizer's input power, σ_ψ^2 , can be written as

$$\sigma_\psi^2 = \frac{\sigma_x^2}{f_s} \cdot \frac{1}{K^2} \int_{-fs/2}^{fs/2} |STF(f)|_{K=K_{eff}}^2 df + \frac{\sigma_e^2}{f_s} \int_{-fs/2}^{fs/2} \left| \frac{G \cdot H \cdot DAC \cdot Delay}{1 + K \cdot G \cdot H \cdot DAC \cdot Delay}(f) \right|_{K=K_{eff}}^2 df. \quad (5.22)$$

where $K_{eff} = E[|\psi(n)|] / \sigma_\psi$. When $\sigma_\psi^2 = \sigma_{\psi_{maxS}}^2$, $K_{eff} = K_{des}$ where K_{des} is the value of K used to design the $\Sigma\Delta M$. Therefore, the quantizer's maximum input power, $\sigma_{\psi_{maxS}}^2$, that keeps a $\Sigma\Delta M$ stable can be written as

$$\sigma_{\psi_{maxS}}^2 = \frac{\sigma_{x_{maxS}}^2}{f_s} \cdot \frac{1}{K^2} \int_{-fs/2}^{fs/2} |STF(f)|_{K=K_{des}}^2 df + \frac{\sigma_{e_{maxS}}^2}{f_s} \int_{-fs/2}^{fs/2} \left| \frac{G \cdot H \cdot DAC \cdot Delay}{1 + K \cdot G \cdot H \cdot DAC \cdot Delay}(f) \right|_{K=K_{des}}^2 df \quad (5.23)$$

where $\sigma_{x_{maxS}}^2$ is the maximum input power that keeps the $\Sigma\Delta M$ stable and $\sigma_{e_{maxS}}^2$ is the quantization noise power when $\sigma_x^2 = \sigma_{x_{maxS}}^2$ and $\sigma_\psi^2 = \sigma_{\psi_{maxS}}^2$. Assuming that the $\Sigma\Delta M$'s input, output and quantization noise signals have means of zero, the $\Sigma\Delta M$'s output signal power, P_y , can be calculated as

$$P_y = E[y^2] = \sigma_y^2 = \frac{\sigma_x^2}{f_s} \int_{-fs/2}^{fs/2} |STF(f)|_{K=K_{eff}}^2 df + \frac{\sigma_e^2}{f_s} \int_{-fs/2}^{fs/2} |NTF(f)|_{K=K_{eff}}^2 df. \quad (5.24)$$

Therefore, at the maximum values of σ_x^2 and σ_e^2 that keep the $\Sigma\Delta\text{M}$ stable,

$$\sigma_y^2 = \frac{\sigma_{x_{\max S}}^2}{f_s} \int_{-fs/2}^{fs/2} |STF(f)|^2_{K=K_{des}} df + \frac{\sigma_{e_{\max S}}^2}{f_s} \int_{-fs/2}^{fs/2} |NTF(f)|^2_{K=K_{des}} df . \quad (5.25)$$

Subtracting (5.22) from (5.24) and solving the resulting equation for σ_e^2 , the quantization noise power, σ_e^2 , can be determined as

$$\sigma_e^2 = \frac{\sigma_y^2 - \sigma_\psi^2}{\frac{1}{f_s} \left[\int_{-fs/2}^{fs/2} |NTF(f)|^2_{K=K_{eff}} df - \int_{-fs/2}^{fs/2} \left| \frac{G \cdot H \cdot DAC \cdot Delay}{1 + K \cdot G \cdot H \cdot DAC \cdot Delay}(f) \right|^2_{K=K_{eff}} df \right]} . \quad (5.26)$$

Therefore, the maximum quantization noise power, $\sigma_{e_{\max S}}^2$, that keeps a $\Sigma\Delta\text{M}$ stable can be determined as

$$\sigma_{e_{\max S}}^2 = \frac{\sigma_y^2 - \sigma_{\psi_{\max S}}^2}{\frac{1}{f_s} \left[\int_{-fs/2}^{fs/2} |NTF(f)|^2_{K=K_{des}} df - \int_{-fs/2}^{fs/2} \left| \frac{G \cdot H \cdot DAC \cdot Delay}{1 + K \cdot G \cdot H \cdot DAC \cdot Delay}(f) \right|^2_{K=K_{des}} df \right]} . \quad (5.27)$$

Using (5.25), the maximum input power, $P_{x_{\max S}}$, that keeps a $\Sigma\Delta\text{M}$ stable can be determined as

$$P_{x_{\max S}} = \sigma_{x_{\max S}}^2 = \frac{\sigma_y^2 - \frac{\sigma_{e_{\max S}}^2}{f_s} \int_{-fs/2}^{fs/2} |NTF(f)|^2_{K=K_{des}} df}{\frac{1}{f_s} \int_{-fs/2}^{fs/2} |STF(f)|^2_{K=K_{des}} df} \quad (5.28)$$

where σ_y^2 is 1 for a single-bit quantizer and $\sigma_{e_{\max S}}^2$ is given in (5.27).

5.3 Stability Analysis Example of $\Sigma\Delta\text{Ms}$ that are not overloaded

To illustrate this method, consider two 4th order $\Sigma\Delta\text{Ms}$ where one of the $\Sigma\Delta\text{Ms}$ has a sampling frequency of 1GHz, a Chebyshev Type 2 NTF with 21dB of attenuation, an excess loop delay of $2T$ and the root loci shown in Fig 5.5 (a) and the other $\Sigma\Delta\text{M}$ has a sampling frequency of 1GHz, a Chebyshev Type 2 NTF with 18dB of attenuation, an excess loop delay of $2.5T$ and the root loci

shown in Fig 5.5 (b).

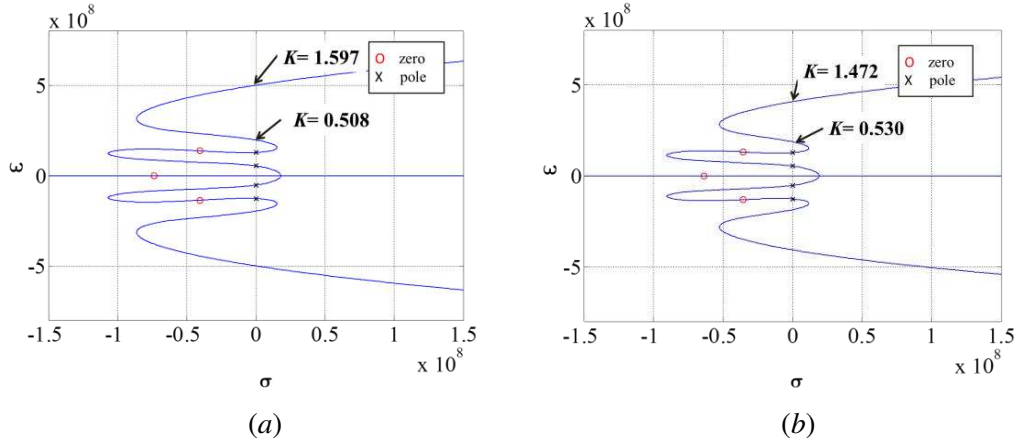


Figure 5.5 The root locus of 4th order CT $\Sigma\Delta$ Ms that uses Chebyshev Type 2 NTFs with a sampling frequency of 1GHz for (a) $D = 2T$, (b) $D = 2.5T$

From inspection of the plots, the 4th order CT $\Sigma\Delta$ Ms with $D = 2T$ and $D = 2.5T$ are stable when the minimum quantizer gains, $K_{\min S}$, are 0.508 and 0.530, respectively. Because these $K_{\min S}$ s are greater than $K_{\min O}$ (0.5), the CT $\Sigma\Delta$ M will not be overloaded before becoming unstable. Assuming a single bit quantizer with an output of ± 1 , the maximum quantizer inputs, $\psi_{\max S}$, that prevent the CT $\Sigma\Delta$ Ms from becoming unstable can be calculated as

$$\psi_{\max S} = \frac{1}{K_{\min S}} = \frac{1}{0.508} = 1.968 \quad (5.29)$$

and

$$\psi_{\max S} = \frac{1}{K_{\min S}} = \frac{1}{0.530} = 1.886. \quad (5.30)$$

Therefore, the CT $\Sigma\Delta$ Ms with $D = 2T$ and $D = 2.5T$ are unstable when $\psi_{\max S} > 1.968$ and $\psi_{\max S} > 1.886$, respectively. Using (5.21), quantizers' maximum input powers, $\sigma_{\psi_{\max S}}^2$, are

$$\sigma_{\psi_{\max S}}^2 = \left(\frac{1}{\mu \cdot K_{\min S}} \right)^2 = \left(\frac{1}{3.6 \cdot 0.508} \right)^2 = 0.299 \quad \text{for } D = 2T \quad (5.31)$$

and

$$\sigma_{\psi_{\max S}}^2 = \left(\frac{1}{\mu \cdot K_{\min S}} \right)^2 = \left(\frac{1}{3.6 \cdot 0.530} \right)^2 = 0.275 \quad \text{for } D = 2.5T. \quad (5.32)$$

Using (5.27), (5.31) and (5.32), the quantization noise powers, $\sigma_{e_{\max S}}^2$, that keeps the $\Sigma\Delta$ Ms stable can be determined as

$$\sigma_{e_{\max S}}^2 = \frac{1-0.299}{3.331-0.744} = 0.271 \quad \text{for } D = 2T \quad (5.33)$$

and

$$\sigma_{e_{\max S}}^2 = \frac{1-0.275}{3.416-0.789} = 0.276 \quad \text{for } D = 2.5T \quad (5.34)$$

where the term $\frac{1}{f_s} \int_{-fs/2}^{fs/2} |NTF(f)|_{K=K_{des}}^2 df$ and

the term $\frac{1}{f_s} \int_{-fs/2}^{fs/2} \left| \frac{G \cdot H \cdot DAC \cdot Delay}{1 + K \cdot G \cdot H \cdot DAC \cdot Delay} (f) \right|_{K=K_{des}}^2 df$ were calculated using the following

Matlab code and K_{des} was set to one in this example.

```
% The coefficients of transfer function F(s),G(s)and H(s)

% F(s)= F4*s^4+F3*s^3+F2*s^2+F1*s+F0;
% G(s)= 1/(s^4+G2*s^2+G0);
% H(s)= H3*s^3+H2*s^2+H1*s+H0;

%fs: Sampling frequency
%T=1/fs: Sampling period
%D:Excess loop delay

NTFsq=@(f) abs(((j.*2*pi.*f).^4+G2.*(j.*2*pi.*f).^2+G0).*((j.*2*pi.*f).*T)./
((j.*2*pi.*f).*T.*((j.*2*pi.*f).^4+G2.*(j.*2*pi.*f).^2+G0)+K.*(H3.*(j.*2*pi.*f).^3+H2.*(j.*2*pi.*f).^2+H1.*(j.*2*pi.*f)+H0).*(1-exp(-(j.*2*pi.*f).*T)).*exp(-(j.*2*pi.*f).*D))).^2;

NTF=integral(NTFsq,-fs/2,fs/2)/fs;

GHDACsq=@(f) abs(((H3.*(j.*2*pi.*f).^3+H2.*(j.*2*pi.*f).^2+H1.*(j.*2*pi.*f)+H0).*(1-exp(-(j.*2*pi.*f).*T)).*exp(-(j.*2*pi.*f).*D))./
((j.*2*pi.*f).*T.*((j.*2*pi.*f).^4+G2.*(j.*2*pi.*f).^2+G0)+(K.*(H3.*(j.*2*pi.*f).^3+H2.*(j.*2*pi.*f).^2+H1.*(j.*2*pi.*f)+H0).*(1-exp(-(j.*2*pi.*f).*T)).*exp(-(j.*2*pi.*f).*D))).^2;

GHDAC=integral(GHDACsq,-fs/2,fs/2)/fs;
```

Using (5.28), (5.33), and (5.34), the maximum input powers, $P_{x_{\max}}$, that keep the $\Sigma\Delta$ Ms stable are

$$P_{x_{\max}} = \sigma_{x_{\max}}^2 = 1 - 0.271 \cdot 3.331 = 0.097 \quad \text{for } D = 2T \quad (5.35)$$

and

$$P_{x_{\max}} = \sigma_{x_{\max}}^2 = 1 - 0.276 \cdot 3.416 = 0.057 \quad \text{for } D = 2.5T \quad (5.36)$$

where the term $\frac{1}{f_s} \int_{-fs/2}^{fs/2} |STF(f)|^2_{K=K_{des}} df$ was calculated using the following Matlab code.

```
% F(s) = F4*s^4+F3*s^3+F2*s^2+F1*s+F0;
% G(s) = 1/(s^4+G2*s^2+G0);
% H(s) = H3*s^3+H2*s^2+H1*s+H0;

STFsq=@(f) abs(((F4.*(j.*2*pi.*f).^4+F3.*(j.*2*pi.*f).^3+F2.*(j.*2*pi.*f).^2+F1.
*(j.*2*pi.*f)+F0.*(j.*2*pi.*f).*T)
./(((j.*2*pi.*f).^4+G2.*(j.*2*pi.*f).^2+G0).*(j.*2*pi.*f).*T+(H3.*(j.*2*pi.*f).
^3+H2.*(j.*2*pi.*f).^2+H1.*(j.*2*pi.*f)+H0).*(1-exp(-(j.*2*pi.*f).*T)).*exp(-
(j.*2*pi.*f).*D))).^2;

STF=integral(STFsq,-fs/2,fs/2)/fs;
```

Assuming a sinusoidal input signal, the maximum input signal power, $P_{x_{\max}}$, can be written as

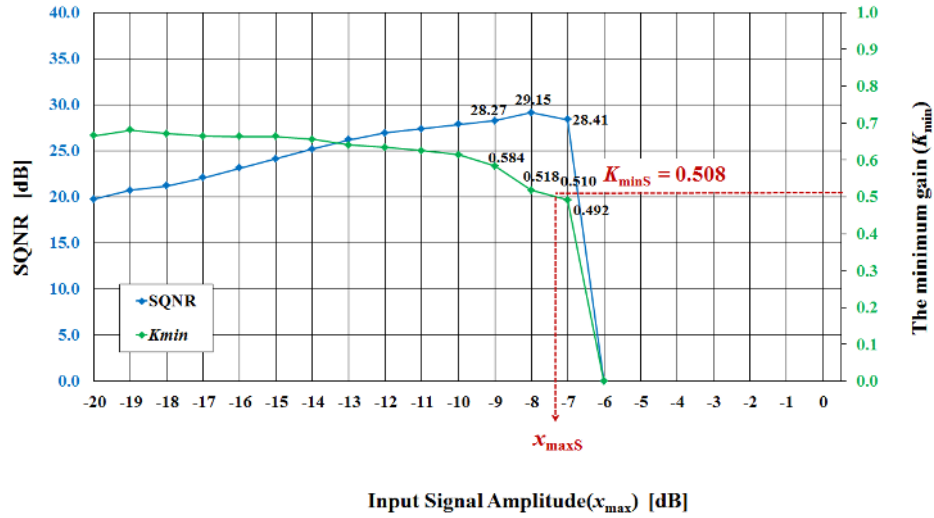
$$P_{x_{\max}} = \sigma_{x_{\max}}^2 = x_{\max}^2 / 2 \quad (5.37)$$

where x_{\max} is the $\Sigma\Delta$ M's maximum input amplitude that keeps a $\Sigma\Delta$ M stable. Using (5.35), (5.36), and (5.37), x_{\max} is estimated to be 0.441 (-7.1dB) for the 4th order CT $\Sigma\Delta$ Ms with $D = 2T$ and 0.339 (-9.4dB) for the 4th order CT $\Sigma\Delta$ Ms with $D = 2.5T$.

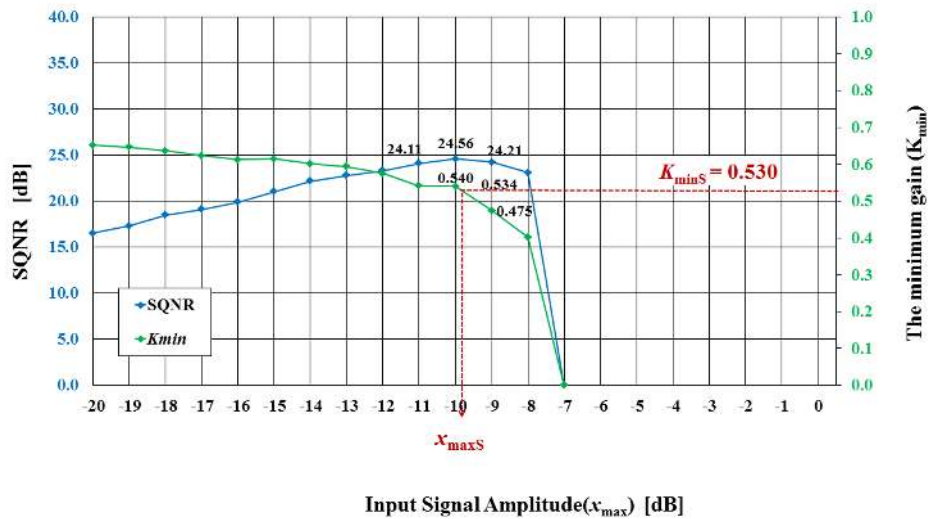
Fig 5.6 (a) shows the simulated SQNR and minimum quantizer gain for the 4th order CT $\Sigma\Delta$ M with $D = 2T$ in this example. The simulation results show that when $K=K_{\min} \cong 0.510$, the sinusoidal input signal has an amplitude of -7.4dB. The simulation results also show that the actual maximum sinusoidal input amplitude for the stability is -7.0dB which is close to the predicted maximum amplitude of -6.9dB.

Fig 5.6 (b) shows the simulated SQNR and minimum quantizer gain for the 4th order CT $\Sigma\Delta$ M with $D = 2.5T$ in this example. The simulation results show that when $K=K_{\min} \cong 0.534$, the

sinusoidal input signal has an amplitude of -9.8dB. The simulation results also show that the actual maximum sinusoidal input amplitude for the stability is -8.0dB which is close to the predicted maximum amplitude of -9.1dB.



(a)



(b)

Figure 5.6 Simulated SQNR and the minimum quantizer gain (K_{min}) using a sinusoidal input for the 4th order CT $\Sigma\Delta$ with (a) $D = 2T$, (b) $D = 2.5T$

5.4 Other Stability Simulation Results of CT $\Sigma\Delta$ Ms that are not overloaded

To illustrate this methodology's accuracy for predicting $x_{\max S}$, five 5th order CT $\Sigma\Delta$ Ms were also simulated. Table 5.5 shows the specification for the five 5th order as well as the two 4th order $\Sigma\Delta$ Ms discussed in Section 5.3. For each of the CT $\Sigma\Delta$ Ms, the predicted $x_{\max S}$ is compared to the simulated $x_{\max S}$.

Table 5.6 compares the theoretical minimum quantizer gain, $K_{\min S}$, obtained from the analytical root locus with the simulated minimum quantizer gain obtained when the simulated input signal is a sinusoidal that has an amplitude of $x_{\max S}$, the maximum predicted amplitude that keeps the $\Sigma\Delta$ M stable. Table 5.7 compares the predicted maximum input amplitude with the simulated maximum input amplitude that keeps the $\Sigma\Delta$ M stable. This table shows that all but one of the predictions are within 1dB of the simulation results.

Table 5.5 Specification for each CT $\Sigma\Delta$ M

(a) Common specification

Specification	
Sampling frequency	1GHz
Sinusoidal Input frequency	0.1MHz
Signal Bandwidth	20MHz

(b) NTF attenuation for each CT $\Sigma\Delta$ M

Excess loop delay (D)	NTF attenuation [dB]					
	0	$0.5T$	T	$1.5T$	$2T$	$2.5T$
2nd order CT $\Sigma\Delta$ Ms	-	-	-	-	-	-
3rd order CT $\Sigma\Delta$ Ms	-	-	-	-	-	-
4th order CT $\Sigma\Delta$ Ms	-	-	-	-	21	18
5th order CT $\Sigma\Delta$ Ms	-	46	35	27	22	17

Table 5.6 Comparison of the theoretical minimum quantizer gains and the simulated minimum quantizer gains at the predicted $x_{\max S}$

		Excess loop delay (D)	0	$0.5T$	T	$1.5T$	$2T$	$2.5T$
2nd order	Predicted $K_{\min S}$	-	-	-	-	-	-	-
	Simulated $K_{\min S}$	-	-	-	-	-	-	-
3rd order	Predicted $K_{\min S}$	-	-	-	-	-	-	-
	Simulated $K_{\min S}$	-	-	-	-	-	-	-
4th order	Predicted $K_{\min S}$	-	-	-	-	0.508	0.530	
	Simulated $K_{\min S}$	-	-	-	-	0.510	0.534	
5th order	Predicted $K_{\min S}$	-	0.518	0.528	0.534	0.548	0.550	
	Simulated $K_{\min S}$	-	0.529	0.536	0.546	0.552	0.556	

Table 5.7 Comparison of the predicted maximum sinusoidal input amplitude with the simulated maximum sinusoidal input amplitude that keeps the $\Sigma\Delta M$ stable

		Excess loop delay (D)	0	$0.5T$	T	$1.5T$	$2T$	$2.5T$	[dB]
2nd order	Predicted $x_{\max S}$	-	-	-	-	-	-	-	
	Simulated $x_{\max S}$	-	-	-	-	-	-	-	
3rd order	Predicted $x_{\max S}$	-	-	-	-	-	-	-	
	Simulated $x_{\max S}$	-	-	-	-	-	-	-	
4th order	Predicted $x_{\max S}$	-	-	-	-	-7.1	-9.4		
	Simulated $x_{\max S}$	-	-	-	-	-7.0	-8.0		
5th order	Predicted $x_{\max S}$	-	-10.8	-8.9	-7.7	-7.9	-6.1		
	Simulated $x_{\max S}$	-	-10.1	-8.5	-7.0	-7.0	-5.4		

5.5 Stability Analysis for overloaded CT $\Sigma\Delta$ Ms

When $K_{\min S} < K_{\min O}$, the CT $\Sigma\Delta$ M will be in overload before becoming unstable. When the CT $\Sigma\Delta$ M in Fig 5.3 is operating in overload, the linear models in Fig 5.3 are no longer valid and they need to be modified to reflect the effects of overload. When the $\Sigma\Delta$ M is overloaded, the output signal's amplitude is limited and the quantization error range increases.

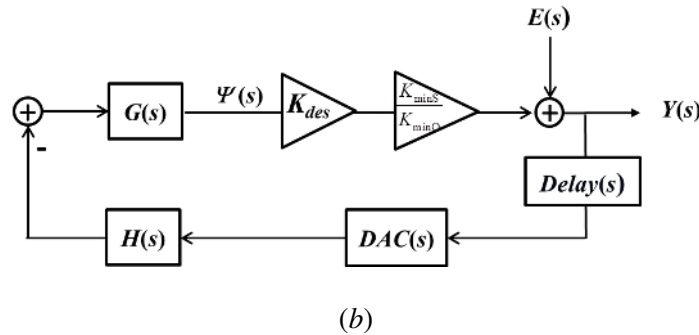
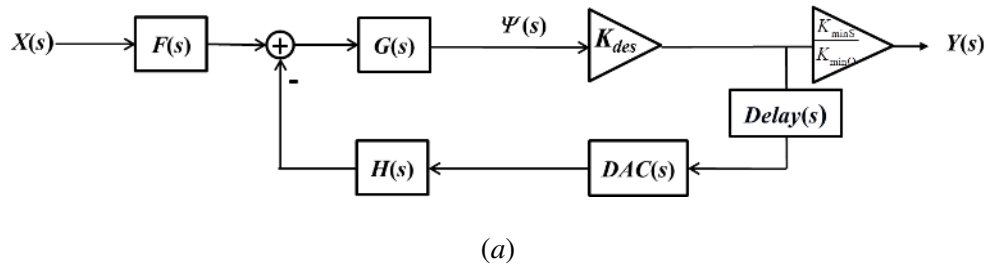


Figure 5.7 (a) A linear model for the CT $\Sigma\Delta$ M's STF in overload,
(b) A linear model for the CT $\Sigma\Delta$ M's NTF in overload

To model the $\Sigma\Delta$ M's output bitstream's inability to realize larger amplitudes, the gain, $K_{\min S}/K_{\min O}$, is added to the output of the STF block diagram in Fig 5.3 (a). Fig 5.7 (a) shows the resulting linear STF model for a CT $\Sigma\Delta$ M that is overloaded. To model the increased quantization noise range from $|e| < 1$ to $|e| < K_{\min O}/K_{\min S}$ that occurs when the $\Sigma\Delta$ M is overloaded, the quantization gain, $K_{\min S}/K_{\min O}$ is added to the NTF's loop filter. Fig 5.7 (b) shows the resulting linear NTF model for a CT $\Sigma\Delta$ M that is overloaded.

Therefore, to determine the input signal power that keep an overloaded $\Sigma\Delta$ stable, (5.23), (5.25), and (5.27) need to be modified to reflect overload model in Fig 5.7. From the block diagram of the CT $\Sigma\Delta$ in overload shown in Fig 5.7, the quantizer's input power, $\sigma_{\psi_{\max S}}^2$, that keeps an overloaded $\Sigma\Delta$ stable can be written as

$$\begin{aligned} \sigma_{\psi_{\max S}}^2 = & \frac{\sigma_{x_{\max S}}^2}{f_s} \cdot \frac{1}{K^2} \int_{-fs/2}^{fs/2} \left| \frac{K_{\min S}}{K_{\min O}} \cdot STF(f) \right|_{K=K_{des}}^2 df \\ & + \frac{\sigma_{e_{\max S}}^2}{f_s} \int_{-fs/2}^{fs/2} \left| \frac{G \cdot H \cdot DAC \cdot Delay}{1 + K \cdot \frac{K_{\min S}}{K_{\min O}} \cdot G \cdot H \cdot DAC \cdot Delay} (f) \right|_{K=K_{des}}^2 df \end{aligned} \quad (5.38)$$

where $\sigma_{x_{\max S}}^2$ is the maximum input power that keeps the overloaded $\Sigma\Delta$ stable and $\sigma_{e_{\max S}}^2$ is the maximum quantization noise power that keeps the overloaded $\Sigma\Delta$ stable. Assuming that the $\Sigma\Delta$'s input, output and quantization noise signals have means of zero, the $\Sigma\Delta$'s output signal power, σ_y^2 , can be calculated as

$$\begin{aligned} \sigma_y^2 = & \frac{\sigma_{x_{\max S}}^2}{f_s} \int_{-fs/2}^{fs/2} \left| \frac{K_{\min S}}{K_{\min O}} \cdot STF(f) \right|_{K=K_{des}}^2 df \\ & + \frac{\sigma_{e_{\max S}}^2}{f_s} \int_{-fs/2}^{fs/2} \left| \frac{1}{1 + K \cdot \frac{K_{\min S}}{K_{\min O}} \cdot G \cdot H \cdot DAC \cdot Delay} (f) \right|_{K=K_{des}}^2 df . \end{aligned} \quad (5.39)$$

Subtracting (5.38) from (5.39) and solving the resulting equation for $\sigma_{e_{\max S}}^2$, the maximum quantization noise power, $\sigma_{e_{\max S}}^2$, that keeps an overloaded $\Sigma\Delta$ stable can be determined as

$$\sigma_{e_{\max S}}^2 = \frac{\sigma_y^2 - \sigma_{\psi_{\max S}}^2}{\frac{1}{f_s} \left[\int_{-fs/2}^{fs/2} \left| \frac{1}{1 + K \cdot \frac{K_{\min S}}{K_{\min O}} \cdot G \cdot H \cdot DAC \cdot Delay} (f) \right|_{K=K_{des}}^2 df - \int_{-fs/2}^{fs/2} \left| \frac{G \cdot H \cdot DAC \cdot Delay}{1 + K \cdot \frac{K_{\min S}}{K_{\min O}} \cdot G \cdot H \cdot DAC \cdot Delay} (f) \right|_{K=K_{des}}^2 df \right]} \quad (5.40)$$

Using (5.39), the maximum input power, $P_{x_{\max S}}$, that keeps an overloaded $\Sigma\Delta M$ stable can be determined as

$$P_{x_{\max S}} = \sigma_{x_{\max S}}^2 = \frac{\sigma_y^2 - \frac{\sigma_{e_{\max S}}^2}{f_s} \int_{-fs/2}^{fs/2} \left| \frac{1}{1 + K \cdot \frac{K_{\min S}}{K_{\min O}} \cdot G \cdot H \cdot DAC \cdot Delay} (f) \right|^2 df}{\frac{1}{f_s} \int_{-fs/2}^{fs/2} \left| \frac{K_{\min S}}{K_{\min O}} \cdot STF(f) \right|^2 df} \quad (5.41)$$

where σ_y^2 is 1 for a single-bit quantizer and $\sigma_{e_{\max S}}^2$ is given in (5.40).

5.6 Stability Analysis Example of an overloaded $\Sigma\Delta M$

To illustrate this method, consider the root loci in Fig 5.8 (a), (b) and (c) which show the root loci for 3rd order $\Sigma\Delta M$ s with sampling frequencies of 1GHz, Chebyshev Type 2 NTFs with 47dB, 37dB, and 30dB attenuation in the stopband, respectively, and excess loop delay times, D , of 0, $0.5T$, and T , respectively. From inspection of the plots, the CT $\Sigma\Delta M$ s with $D = 0$, $D = 0.5T$, and $D = T$ are stable when the minimum quantizer gains, $K_{\min S}$, are 0.326, 0.359, and 0.376, respectively. Assuming a single bit quantizer with an output of ± 1 , the maximum quantizer input, $\psi_{\max S}$, that prevents the CT $\Sigma\Delta M$ s from becoming unstable is

$$\psi_{\max S} = \frac{1}{K_{\min S}}. \quad (5.42)$$

Therefore, the CT $\Sigma\Delta M$ s with $D = 0$, $D = 0.5T$, and $D = T$ are unstable when $\psi_{\max S} > 3.07$, $\psi_{\max S} > 2.78$, and $\psi_{\max S} > 2.66$, respectively.

Consider the 3rd order CT $\Sigma\Delta M$ that has an excess loop delay of $D = T$ of the root locus shown in Fig 5.8 (c). Because $K_{\min S} < K_{\min O}$, this $\Sigma\Delta M$ will be overloaded when it becomes unstable. To predict the maximum input signal power that keeps the $\Sigma\Delta M$ stable, (5.21) can be used to determine

$$\sigma_{\psi_{\max S}}^2 = \left(\frac{1}{\mu \cdot K_{\min S}} \right)^2 = \left(\frac{1}{3.6 \cdot 0.376} \right)^2 = 0.546 \quad (5.43)$$

where $K_{\min S} = 0.376$ and $\mu = 3.6$.

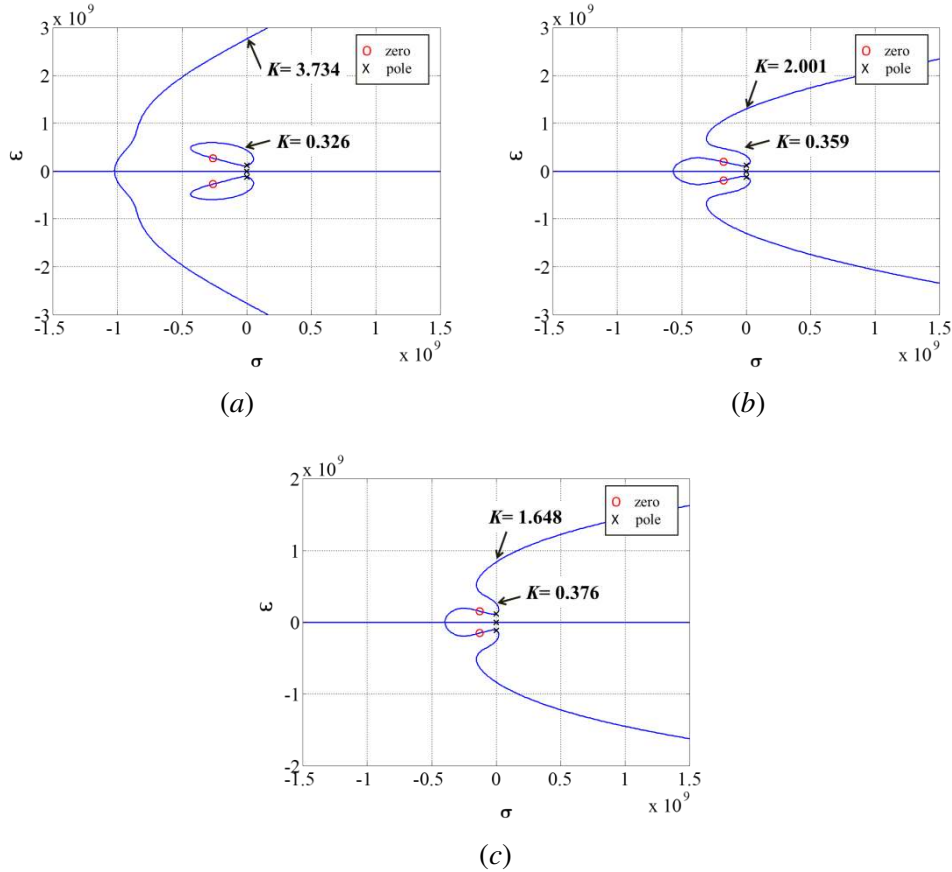


Figure 5.8 The root locus of 3rd order CT $\Sigma\Delta$ Ms that uses Chebyshev Type 2 NTFs with a sampling frequency of 1GHz for (a) $D = 0$, (b) $D = 0.5T$, (c) $D = T$

Using (5.40) and (5.43), the quantization noise power, $\sigma_{e_{\max S}}^2$, that keeps this $\Sigma\Delta$ M stable when overloaded can be determined as

$$\sigma_{e_{\max S}}^2 = \frac{1 - 0.546}{3.329 - 1.763} = 0.290 \quad (5.44)$$

where the term $\frac{1}{f_s} \int_{-fs/2}^{fs/2} \left| \frac{1}{1 + K \cdot \frac{K_{\min S}}{K_{\min O}} \cdot G \cdot H \cdot DAC \cdot Delay} (f) \right|_{K=K_{des}}^2 df$ and the term

$\frac{1}{f_s} \int_{-fs/2}^{fs/2} \left| \frac{G \cdot H \cdot DAC \cdot Delay}{1 + K \cdot \frac{K_{\min S}}{K_{\min O}} \cdot G \cdot H \cdot DAC \cdot Delay} (f) \right|_{K=K_{des}}^2 df$ were calculated using the following Matlab

code and K_{des} was set to one in this example.

```
% The coefficients of transfer function F(s),G(s)and H(s)

% F(s)= F3*s^3+F2*s^2+F1*s+F0
% G(s)= 1/(s^3+G1*s)
% H(s)= H3*s^3+H2*s^2+H1*s+H0

%fs: Sampling frequency
%T=1/fs Sampling period
%D:Excess loop delay

%kminS:The maximum quantizer gain that keeps a ΣΔM stable
%kminO:The maximum quantizer gain that prevents a ΣΔM from overloading

NTFsq=@(f) abs(((j.*2*pi.*f).^3+G1.*j.*2*pi.*f).*(j.*2*pi.*f.*T))...
./(((j.*2*pi.*f).^3+a.*j.*2*pi.*f).*(j.*2*pi.*f.*T)+K.*(kminS/kminO).*(
(H2.*(j.*2*pi.*f).^2+H1.*(j.*2*pi.*f)+H0).*(1-exp(-j.*2*pi.*f.*T)).*exp(-
j.*2*pi.*f.*D))).^2;

NTF=integral(NTFsq,-fs/2,fs/2)/fs;

GHDACsq=@(f) (abs((H2.*(j.*2*pi.*f).^2+H1.*(j.*2*pi.*f)+H0).*(1-exp(-
j.*2*pi.*f.*T)).*exp(-j.*2*pi.*f.*D))./(((j.*2*pi.*f).^3+G1.*j.*2*pi.*f).
*(j.*2*pi.*f.*T)+K.*(kminS/kminO).*(H2.*(j.*2*pi.*f).^2+H1.*(j.*2*pi.*f)+H0).*(
1-exp(-j.*2*pi.*f.*T)).*exp(-j.*2*pi.*f.*D))))).^2;

GHDAC=integral(GHDACsq,-fs/2,fs/2)/fs;
```

Using (5.41) and (5.44), the maximum input power, $P_{x_{\max S}}$, that keeps this $\Sigma\Delta M$ stable when overloaded is

$$P_{x_{\max S}} = \sigma_{x_{\max S}}^2 = \frac{1 - 0.290 \cdot 3.329}{\left(\frac{0.376}{0.5}\right)^2} = 0.061. \quad (5.45)$$

where the term $\frac{1}{f_s} \int_{-fs/2}^{fs/2} \left| \frac{K_{\min S}}{K_{\min O}} \cdot STF(f) \right|_{K=K_{des}}^2 df$ was calculated using the following Matlab code.

```

% F(s) = F3*s^3+F2*s^2+F1*s+F0
% G(s) : 1/(s^3+G1*s)
% H(s) = H3*s^3+H2*s^2+H1*s+H0

STFsq=@(f) abs.*((kminS/kmin0).*(F3.*(j.*2*pi.*f).^3+F2.*(j.*2*pi.*f).^2+F1.*(j
.*2*pi.*f)+F0)).*(j.*2*pi.*f).*T)...
./(((j.*2*pi.*f).^3+a.*j.*2*pi.*f).*(j.*2*pi.*f.*T)+(H2.*(j.*2*pi.*f).^2+H1.*(j
.*2*pi.*f)+H0).*(1-exp(-j.*2*pi.*f.*T)).*exp(-j.*2*pi.*f.*D))).^2;

STF=integral(STFsq,-fs/2,fs/2)/fs;

```

Assuming a sinusoidal input signal,

$$P_{x_{\max S}} = \sigma_{x_{\max S}}^2 = x_{\max S}^2 / 2 \quad (5.46)$$

where $x_{\max S}$ is the $\Sigma\Delta M$'s maximum input amplitude that keep the $\Sigma\Delta M$ stable in overload. Using (5.45) and (5.46), $x_{\max S}$ is estimated to be 0.349 (-9.1dB).

Fig 5.9 shows the simulated SQNR and minimum quantizer gain for the 3rd order CT $\Sigma\Delta M$ with $D = T$ in this example. The simulation results show that the sinusoidal input amplitude is -8.5dB when K_{\min} is 0.387. The results also show that the $\Sigma\Delta M$ becomes unstable when the maximum sinusoidal input is greater than -7.0dB and K_{\min} is 0.306.

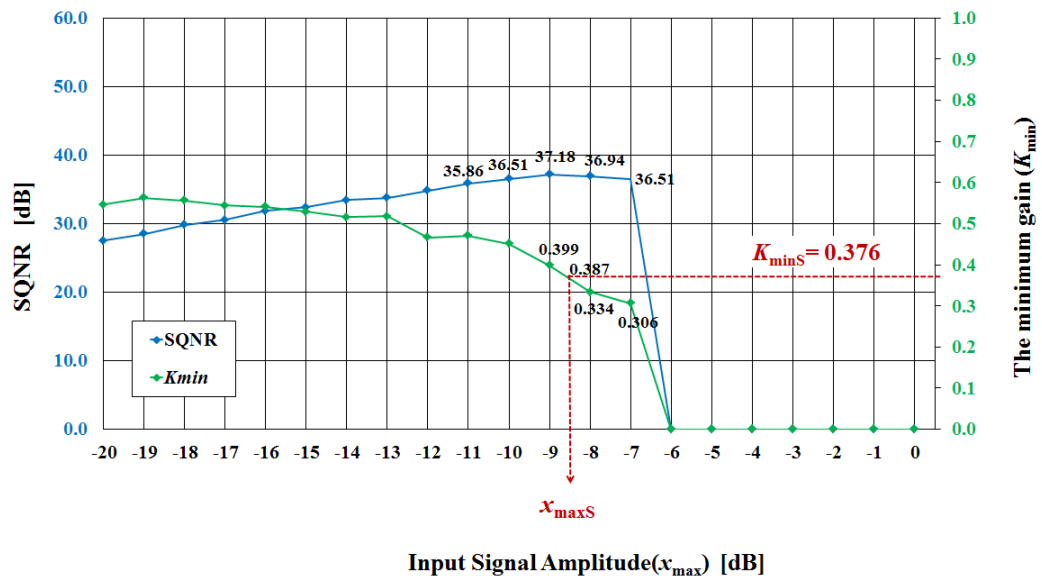
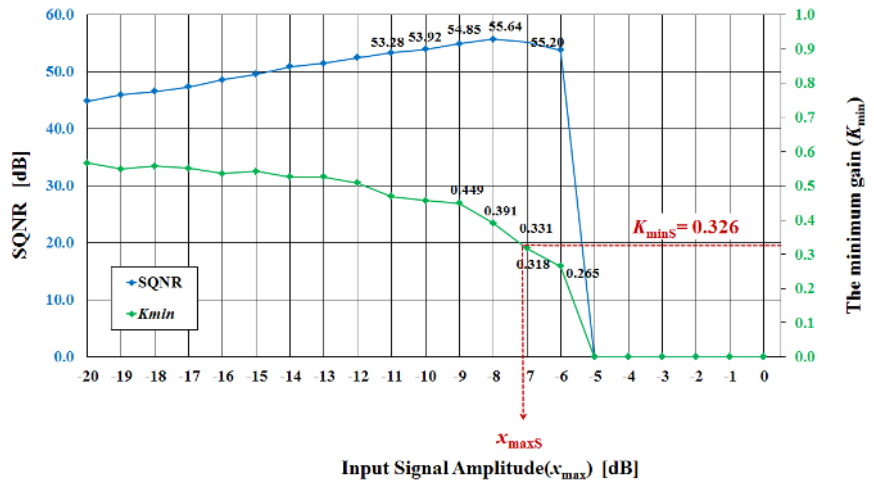
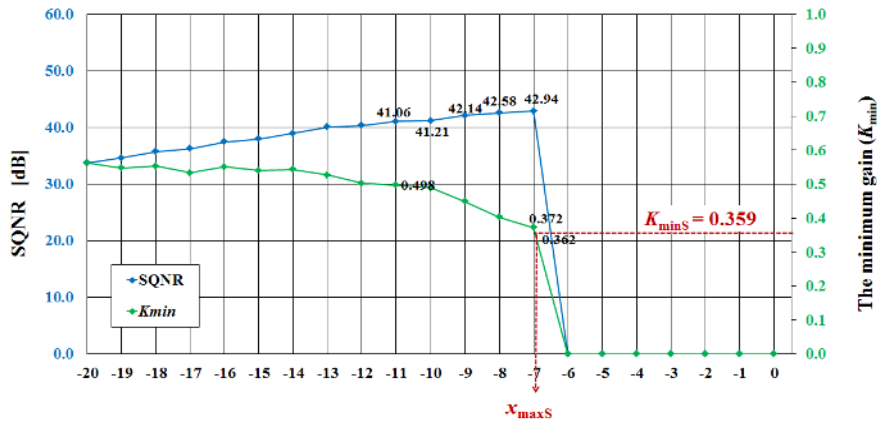


Figure 5.9 Simulated SQNR and the minimum quantizer gain (K_{\min}) using a sinusoidal input for the 3rd order CT $\Sigma\Delta M$ with $D = T$ in example

The maximum sinusoidal input amplitudes, $x_{\max S}$ were also predicted for the other 3rd order CT $\Sigma\Delta$ Ms that have the root loci shown in Fig 5.8 (a) and (b). Their $x_{\max S}$ values were predicted to be 0.457 (-6.8dB) and 0.484 (-6.3dB) for the CT $\Sigma\Delta$ Ms that have the root loci shown in Fig. 5.8 (a) and (b), respectively. These $\Sigma\Delta$ Ms were also simulated using a sinusoidal input with a frequency of 0.1MHz.



(a)



(b)

Figure 5.10 Simulated SQNR and the quantizer's minimum gain (K_{\min}) for the 3rd order CT $\Sigma\Delta$ M for (a) $D=0$ (b) $D=0.5T$

Fig 5.10 (a) shows the SQNRs and the quantizer's minimum gain, K_{\min} , as a function of input signal's amplitude for the $\Sigma\Delta\text{M}$ with $D = 0$. As shown in the Fig 5.10 (a), the $\Sigma\Delta\text{M}$'s SQNR increases linearly until the input signal's amplitude is approximately -12 dB, and $K_{\min} = 0.508$. As the input signal's amplitude is increased above -12 dB, the SQNR increases nonlinearly as a function of input signal's amplitude because the $\Sigma\Delta\text{M}$ is overloaded. As the input signal's amplitude is increased above -6 dB, the $\Sigma\Delta\text{M}$'s SQNR degrades dramatically and the $\Sigma\Delta\text{M}$'s SQNR cannot be restored to its previous values even when the $\Sigma\Delta\text{M}$'s input is decreased to its previous amplitudes. As mentioned earlier, the maximum sinusoidal input amplitude was predicted to be -6.8dB when $K_{\min\text{S}}$ is 0.326. The simulation results show that the sinusoidal input amplitude is -7.2dB when K_{\min} is 0.331 and that the $\Sigma\Delta\text{M}$ becomes unstable when the sinusoidal input amplitude is greater than -6dB and K_{\min} is 0.265.

Fig 5.10 (b) shows the SQNR and the minimum gain, K_{\min} , as a function of input signal amplitude for the $\Sigma\Delta\text{M}$ that has the root locus shown in Fig 5.8 (b) and an excess loop delay of $0.5T$. The simulation results show that when the input signal's amplitude is increased above -7 dB, or K_{\min} is less than 0.359, the $\Sigma\Delta\text{M}$ becomes unstable. For this $\Sigma\Delta\text{M}$, the maximum sinusoidal input amplitude was predicted to be -6.3dB when $K_{\min\text{S}}$ is 0.359. The simulation results show that when the sinusoidal input amplitude is -6.9dB and K_{\min} is 0.362, the $\Sigma\Delta\text{M}$ becomes unstable.

5.7 Other Simulation Results of overloaded $\Sigma\Delta\text{M}$ s

To illustrate this methodology's accuracy for predicting the stability in overload, six 3rd order, four 4th order, and one 5th order CT were simulated and these stability points are compared to their predicted stability points. Table 5.8 (a) compares the predicted minimum stable quantizer gain, $K_{\min\text{S}}$, with the simulated minimum quantizer gain, K_{\min} , when the sinusoidal input has the maximum predicted stable input amplitude for the 3rd through 5th order CT $\Sigma\Delta\text{M}$ s. The examples were selected because the $\Sigma\Delta\text{M}$ s satisfied the condition, $K_{\min\text{S}} < K_{\min\text{O}}$ which implies that the $\Sigma\Delta\text{M}$ will be overloaded before becoming unstable. Each $\Sigma\Delta\text{M}$ had a sinusoidal input with an input

frequency of 0.1MHz and a sampling frequency of 1GHz. For each order $\Sigma\Delta\text{M}$, the excess loop delay was chosen as $0, 0.5T, T, 1.5T, 2T$ and $2.5T$. The results show that little difference exists between the predicted $K_{\min\text{S}}$ and the simulated K_{\min} for each of the $\Sigma\Delta\text{Ms}$. Table 5.8 (b) compares the predicted maximum input amplitude, $x_{\max\text{S}}$, with the simulated input amplitude, x_{\max} , at predicted minimum stable quantizer gain, $K_{\min\text{S}}$, for the 3rd through 5th order CT $\Sigma\Delta\text{Ms}$. The results show that little difference exists between the predicted $x_{\max\text{S}}$ and the simulated x_{\max} at predicted $K_{\min\text{S}}$, for each of the $\Sigma\Delta\text{Ms}$. Table 5.8 (c) compares the predicted maximum input amplitude, $x_{\max\text{S}}$, and the simulated maximum input amplitude, x_{\max} .

Table 5.8 Comparison of the prediction and the simulation

(a) Predicted minimum stable quantizer gain and simulated quantizer gain for sinusoidal input with predicted maximum amplitude

Excess loop delay (D)	Predicted Min. stable quantizer gain ($K_{\min\text{S}}$)						Simulated quantizer gain (K_{\min}) for sinusoidal input with predicted Max. input amplitude					
	0	$0.5T$	T	$1.5T$	$2T$	$2.5T$	0	$0.5T$	T	$1.5T$	$2T$	$2.5T$
3rd order CT $\Sigma\Delta\text{Ms}$	0.326	0.359	0.376	0.389	0.396	0.410	0.331	0.362	0.387	0.401	0.399	0.438
4th order CT $\Sigma\Delta\text{Ms}$	0.459	0.481	0.491	0.503	0.508	0.530	0.475	0.502	0.503	0.521	-	-
5th order CT $\Sigma\Delta\text{Ms}$	0.501	0.518	0.528	0.535	0.548	0.550	0.508	-	-	-	-	-

(b) Predicted maximum input amplitude and simulated input amplitude at predicted $K_{\min\text{S}}$

Excess loop delay (D)	Predicted Max. input amplitude ($x_{\max\text{S}}$)						Simulated input amplitude (x_{\max}) at predicted $K_{\min\text{S}}$					
	0	$0.5T$	T	$1.5T$	$2T$	$2.5T$	0	$0.5T$	T	$1.5T$	$2T$	$2.5T$
3rd order CT $\Sigma\Delta\text{Ms}$	-6.8	-6.3	-9.1	-9.7	-11.3	-36.1	-6.8	-6.9	-8.5	-9.5	-11.0	-35.8
4th order CT $\Sigma\Delta\text{Ms}$	-7.6	-8.7	-8.4	-8.1	-	-	-8.0	-8.4	-7.9	-8.0	-	-
5th order CT $\Sigma\Delta\text{Ms}$	-9.6	-	-	-	-	-	-9.5	-	-	-	-	-

(c) Predicted maximum input amplitude and simulated maximum input amplitude

Excess loop delay (D)	Predicted Max. input amplitude ($x_{\max\text{S}}$)						Simulated Max. input amplitude (x_{\max})					
	0	$0.5T$	T	$1.5T$	$2T$	$2.5T$	0	$0.5T$	T	$1.5T$	$2T$	$2.5T$
3rd order CT $\Sigma\Delta\text{Ms}$	-6.8	-6.3	-9.1	-9.7	-11.3	-36.1	-6.0	-6.9	-7.1	-9.4	-9.4	-35.6
4th order CT $\Sigma\Delta\text{Ms}$	-7.6	-8.7	-8.4	-8.1	-	-	-7.8	-8.2	-7.7	-7.6	-	-
5th order CT $\Sigma\Delta\text{Ms}$	-9.6	-	-	-	-	-	-9.0	-	-	-	-	-

5.8 Conclusion

Table 5.9 (a), (b), and (c) summarize the stability analysis for both overloaded CT $\Sigma\Delta$ M's and CT $\Sigma\Delta$ M's that are not overloaded which were used in Section 5.4 and 5.7. The overloaded $\Sigma\Delta$ M's which satisfies the condition, $K_{\min S} < K_{\min O}$, are colored in orange and the $\Sigma\Delta$ M's that are not overloaded which satisfies the condition, $K_{\min S} > K_{\min O}$, are colored in blue. Table 5.9 (d) shows that all but one of the predictions are within 1.2dB of the simulation results. Because $\Sigma\Delta$ M's SQNR depends on the input frequency, the maximum input signal amplitudes vary for different frequencies of the input signal [32, 33]. This is especially true for low input frequencies close to DC where a $\Sigma\Delta$ M's SQNR can degrade at smaller input amplitudes. It may therefore be possible that the discrepancies between the predicted $x_{\max S}$ and the simulated $x_{\max S}$ might be a result of the chosen input frequency.

Table 5.9 Summary of the stability analysis
for both overloaded CT $\Sigma\Delta$ M and CT $\Sigma\Delta$ M that are not overloaded

Overloaded $\Sigma\Delta$ M ($K_{\min S} < K_{\min O}$) $\Sigma\Delta$ M that is not overloaded ($K_{\min S} > K_{\min O}$)

(a) Predicted minimum stable quantizer gain and simulated quantizer gain
for sinusoidal input with predicted maximum amplitude

Excess loop delay (D)	Predicted Min. stable quantizer gain ($K_{\min S}$)						Simulated quantizer gain (K_{\min}) for sinusoidal input with predicted Max. input amplitude					
	0	$0.5T$	T	$1.5T$	$2T$	$2.5T$	0	$0.5T$	T	$1.5T$	$2T$	$2.5T$
3rd order CT $\Sigma\Delta$ M	0.326	0.359	0.376	0.389	0.396	0.410	0.331	0.362	0.387	0.401	0.399	0.438
4th order CT $\Sigma\Delta$ M	0.459	0.481	0.491	0.503	0.508	0.530	0.475	0.502	0.503	0.521	0.510	0.534
5th order CT $\Sigma\Delta$ M	0.501	0.518	0.528	0.535	0.548	0.550	0.508	0.529	0.536	0.546	0.552	0.556

(b) Predicted maximum input amplitude and simulated input amplitude at predicted $K_{\min S}$

Excess loop delay (D)	Predicted Max. input amplitude ($x_{\max S}$)						Simulated input amplitude (x_{\max}) at predicted $K_{\min S}$					
	0	$0.5T$	T	$1.5T$	$2T$	$2.5T$	0	$0.5T$	T	$1.5T$	$2T$	$2.5T$
3rd order CT $\Sigma\Delta$ M	-6.8	-6.3	-9.1	-9.7	-11.3	-36.1	-6.8	-6.9	-8.5	-9.5	-11.0	-35.8
4th order CT $\Sigma\Delta$ M	-7.6	-8.7	-8.4	-8.1	-7.1	-9.4	-8.0	-8.4	-7.9	-8.0	-7.4	-9.8
5th order CT $\Sigma\Delta$ M	-9.6	-10.8	-8.9	-7.7	-8.2	-6.1	-9.5	-10.3	-8.7	-7.4	-7.6	-5.7

(c) Predicted maximum input amplitude and simulated maximum input amplitude

Excess loop delay (D)	Predicted Max. input amplitude ($x_{\max S}$)						Simulated Max. input amplitude (x_{\max})					
	0	$0.5T$	T	$1.5T$	$2T$	$2.5T$	0	$0.5T$	T	$1.5T$	$2T$	$2.5T$
3rd order CT $\Sigma\Delta$ M	-6.8	-6.3	-9.1	-9.7	-11.3	-36.1	-6.0	-6.9	-7.1	-9.4	-9.4	-35.6
4th order CT $\Sigma\Delta$ M	-7.6	-8.7	-8.4	-8.1	-7.1	-9.4	-7.8	-8.2	-7.7	-7.6	-7.0	-8.0
5th order CT $\Sigma\Delta$ M	-9.6	-10.8	-8.9	-7.7	-8.2	-6.1	-9.0	-10.1	-8.5	-7.0	-7.0	-5.4

(d) The difference between predicted maximum input amplitude and
simulated maximum input amplitude

Excess loop delay (D)	The difference between predicted Max. input amplitude ($x_{\max S}$) and simulated Max. input amplitude (x_{\max})						
	0	$0.5T$	T	$1.5T$	$2T$	$2.5T$	
3rd order CT $\Sigma\Delta$ M	-0.8	0.6	-2.0	-0.3	-1.9	-0.5	
4th order CT $\Sigma\Delta$ M	0.2	-0.5	-0.7	-0.5	-0.1	-1.4	
5th order CT $\Sigma\Delta$ M	-0.6	-0.7	-0.4	-0.7	-1.2	-0.7	

CHAPTER 6

CONCLUSIONS

This dissertation introduced a $\Sigma\Delta$ simulation method that uses the delta transform to determine difference equations that model CT $\Sigma\Delta$ s. This method is compared with conventional simulation methods in terms of simplicity, speed, and accuracy in Chapter 3. This new method proved to be a simple method that provided results as accurate as SPICE simulations and could be performed within reasonable times.

This dissertation also introduced an overload and stability analyses for single-loop, single-bit CT $\Sigma\Delta$ s. In Chapter 4's overload analysis, the minimum quantizer gain, $K_{\min O}$, that prevents a $\Sigma\Delta$ from overloading is determined and a method that uses the minimum quantizer gain, $K_{\min O}$, to determine the maximum input power that prevents overloading was developed. $\Sigma\Delta$ simulations performed using the delta transform were used to compare the predicted maximum input power and the simulated maximum input power that prevents overloading. The results of the simulated and predicted overload condition were very similar. In Chapter 4, a set of linear models were also developed for CT $\Sigma\Delta$ operating in overload. Using these models, the SQNR for a $\Sigma\Delta$ in overload could be estimated. CT $\Sigma\Delta$ simulations were performed using the delta transform and their results were compared with estimations generated with the linear models. For each of the CT $\Sigma\Delta$ s, the simulated SQNRs at low input frequency coincided with the estimated SQNRs.

In Chapter 5, an analytical root locus method developed in [48, 49] was used to determine the stability criteria for CT $\Sigma\Delta$ s that include exponential functions in their characteristic equations. From the analytical root locus, the minimum quantizer gain, $K_{\min S}$, that keeps a CT $\Sigma\Delta$ stable could be determined. In Chapter 5's stability analysis, the minimum quantizer gain, $K_{\min S}$, that keeps a $\Sigma\Delta$ stable is determined and a method that uses the minimum quantizer gain, $K_{\min S}$, to

determine the maximum input power that keeps the $\Sigma\Delta\text{M}$ stable was developed. The maximum input power that guarantees stability for both a $\Sigma\Delta\text{M}$ in overload and $\Sigma\Delta\text{M}$ that is not overloaded could be estimated. $\Sigma\Delta\text{M}$ simulations performed using the delta transform were used to compare the predicted maximum input power and the simulated maximum input power that keeps the $\Sigma\Delta\text{M}$ stable. The results of the simulated and predicted stability condition were very similar.

In conclusion, a circuit designer can take measures to prevent the CT $\Sigma\Delta\text{Ms}$ from becoming unstable and overloading using $K_{\min\text{S}}$ and $K_{\min\text{O}}$, and further predict the SQNR.

REFERENCES

- [1] B. Razavi, *Data Conversion System Design*. Piscataway, NJ: IEEE Press, 1995.
- [2] James A.Cherry and W.Martin Snelgrove, *Continuous-time delta sigma modulators for high-speed A/D conversion*, Norwell, MA: Kluwer, 2000.
- [3] Newman, M.J and Holmes, D.G, “Delta operator digital filters for high performance inverter applications”, *Power Electronics specialist conference*, vol. 3, pp. 1407-1412, 2002.
- [4] Yves Geerts, Michiel Steyaert, Willy Sansen, *Design of multi-bit delta-sigma A/D converters*, 2002.
- [5] J.M, de la Rosa, “Sigma-Delta Modulators: Tutorial Overview, Design Guide, and State-of-the Art Survey”, *IEEE Transactions on Circuits and Systems I: Regular papers*, vol. 58, pp. 1-21, anuary 2011.
- [6] Pervez M.Aziz, Henrik V. Sorenses, Jan van der Spiegel, “An Overview of Sigma-Delta Converters”, *IEEE Signal Processing Magazine*, 1/1996-vol.13, pp.61-84; ISSN 1053-5888
- [7] Alan V. Oppenheim, R.W.Schafer, *Discrete time signal processing*, prentice Hall, 2009
- [8] R. Schreier and G. C. Temes, *Understanding Delta-Sigma Data Converters*. New York: Wiley-Interscience, 2005.
- [9] F. Henkel, U. Langmann, A. Hanke, S. Heinen, and E Wagner. “A 1-MHz-bandwidth second-order continuous-time quadrature bandpass sigma-delta modulator for low-IF radio receivers”. *Solid-State Circuits, IEEE Journal of*, 37(12), 1628–1635, December 2002.
- [10] T.C. Caldwell and D.A. Johns. “A time-interleaved continuous-time $\Sigma\Delta$ modulator with 20-MHz signal bandwidth”. *Solid-State Circuits, IEEE Journal of*, 41(7), 1578–1588, July 2006.
- [11] A. Gharbiya, D. A. Jones, “On the implementation of Input-Feedforward Delta-Sigma modulators”, *IEEE transactions on circuits and systems*, vol. 53, no. 6, 2006.
- [12] J.Silva, U.Moon, J.Steensgaard, and G.Temes, “Wideband low distortion delta-sigma ADC topology”, *Electron. Lett*, vol. 37, no.12, pp. 737-738, Jun. 2001.
- [13] A. Leuciuc, “ On the nonlinearity of integrators in continuous time delta sigma modulators”, *Circuits and Systems*, 2001. MWSCAS 2001. Proceedings of the 44th IEEE 2001 Midwest Symposium on, pp. 862-865, vol. 2, 2001.
- [14] J. A. Cherry and W. M. Snelgrove, *Continuous-Time Delta-Sigma Modulators for High Speed A/D Conversion Theory, Practice and Fundamental Performance Limits: Kluwer Academic*, New York, NY, USA, 2002.
- [15] Hung-Yuan Chu, Chun-Hung Yang, Chi-Wai Leng, Chien-Hung Tsai, “A top-down, mixed-level design methodology for CT BP $\Delta\Sigma$ modulator using verilog-A”, *Circuits and Systems*, 2008, pp.1390-1393, 2008.
- [16] G.Ushaw, S.McLaughlin, “On the stability and configuration of sigma delta modulators”, *Circuits and Systems*,1994. vol. 5, pp. 349-352, 1994.
- [17] J.A. Cherry and W.M. Snelgrove, “Approaches to simulating continuous-time delta sigma modulators”, *Circuits and Systems*, vol.1, pp.587-590, 1998.
- [18] Ajoy Opal, “Sampled data simulation of linear and nonlinear circuits”, *Computer-aided design of integrated circuits and systems, IEEE*, vol.15, pp.295-307, 1996.
- [19] J.A. Cherry and W.M. Snelgrove, “Excess loop delay in continuous time delta sigma modulators”, *Circuits and Systems*, vol.46, pp.376-389, 1999.
- [20] Paulo Aguirre, Vinicius Camargo, “Behavioral modeling of continuous time modulators in Matlab/Simulink”, *Circuits and Systems (LASCAS), IEEE Fourth Latin American Symposium*, 2013.
- [21] R. Schaumann, Mac Van Valkenburg, *Design of analog Filters: Valkenburg*, Oxford, 2009
- [22] R.H. Middleton and G.C. Goodwin, *Digital Control and Estimation: A Unified Approach*, ser. Prentice-Hall Information and Systems Sciences Series, T. Kailath, Ed. Engelwood Cliffs, NJ: Prentice-Hall, 1990.

- [23] M. W. Hauser and R. W. Brodersen, "Circuit and technology consideration for MOS delta-sigma A/D converters", IEEE Int. Symp. Circuit and Systems, pp. 1310-1315, 1986.
- [24] R. Schreier, "An empirical study of high-order single-bit delta-sigma modulators", IEEE Trans. Circ, Syst. II, pp. 461-466, 1993.
- [25] R. Schreier, G.C. Temes, Understanding delta-sigma data converters, IEEE press, 2005.
- [26] M. Kozak, I. Kale, Oversampled delta sigma modulators, Kluwer academic, 2003.
- [27] R. Schreier, "An empirical study of high-order single-bit delta sigma modulators," IEEE Transactions on Circuits and Systems II, vol. 40, no. 8, pp. 461-466, 1993.
- [28] H. Tang, "Symbolic statistical analysis of SNR variation for delta-sigma modulators," IEEE Transactions on Circuits and Systems II, vol. 54, no. 8, pp. 720-724, 2007.
- [29] M. A. Al-Alaoui and R. Ferzli, "An enhanced first-order sigma delta modulator with a controllable signal-to-noise ratio," IEEE Transactions on Circuits and Systems I, vol. 53, no. 3, pp. 634-643, 2006.
- [30] Y. Geerts, M. Steyaert, and W. M. C. Sansen, Design of Multi-Bit Delta-Sigma A/D Converters, Kluwer Academic Publishers, Boston, Mass, USA, 2002.
- [31] P.M. Aziz, H. V. Sorensen, and J. Van der Spiegel, "An overview of sigma-delta converters," IEEE Signal Processing Magazine, vol. 13, no. 1, pp. 61-84, 1996.
- [32] Michal pavlik, Martin Magat, Lukas Fucik and Jiri Haze, "Matlab-Modeling, Programming and Simulation", ISBN 978-953-307-125-1, 2010.
- [33] Søren Hein, Avideh Zakhor, "Sigma Delta Modulators: Nonlinear Decoding Algorithms and Stability Analysis", ISBN 978-079-239-309-2, 1993.
- [34] J. A. Cherry and W. M. Snelgrove.: Continuous-Time Delta-Sigma Modulators for High Speed A/D Conversion Theory, Practice and Fundamental Performance Limits: Kluwer Academic, New York, NY, USA, 2002.
- [35] S. H. Ardalan, and J.J. Paulos.: An analysis of non-linear behaviour in Σ - Δ modulators. In: IEEE Trans. on Circuits and Syst., vol. CAS-34, no. 6, pp.1157-1162, 1987.
- [36] N. Wong, and N.G. Tung-Sang.: DC stability analysis of higher-order, lowpass sigma-delta modulators with distinct unit circle NTF zeroes. In: IEEE Trans. on Circuits & Syst.-II, vol. 50, issue 1, pp. 12-30, 2003
- [37] J. Zhang, P.V. Brennan, D. Juang, D. E. Vinogradova, and P.D. Smith.: Stable analysis of a sigma-delta modulator. In: Proc. IEEE Int. Symp. Circuits Syst., vol.1, pp.1-961-1-964, 2003.
- [38] P. Steiner, and W. Yang.: Stability analysis of the second-order sigma-delta modulator. In: Proc. IEEE Int. Symp. Circuits Syst., vol. 5, pp. 365-368, 1994.
- [39] J. Zhang, P.V. Brennan, D. Juang, E. Vinogradova, and P.D. Smith.: Stable boundaries of a 2nd-order sigma-delta modulator. In: Proc. South. Symp.Mixed Signal Design, 2003.
- [40] N. A. Fraser, and B. Nowrouzian.: A novel technique to estimate the statistical properties of sigma-delta A/D converters for the investigation of DC stability. In: Proc. IEEE Int. Symp. Circuits Syst., vol.3, pp.111-289-111-292, 2002.
- [41] D. Reefman, J.D. Reiss, E. Janssen, and M.B. Sandler.: Description of limit cycles in sigma-delta modulators. In: IEEE Trans. on Circuits and Syst-I., vol. 52, issue 6, pp.1211 - 1223, 2005.
- [42] S. Hein, and A. Zakhor.: On the stability of sigma-delta modulators. In: IEEE Trans. on Signal Processing, vol. 41, no.7, pp. 2322-2348, 1993.
- [43] R. Schreier and W. M. Snelgrove.: Bandpass Sigma-Delta modulator. In: Electronics letters, vol. 25, no. 23, pp. 1560-1561, 1989.
- [44] Lars Risbo.: FPGA Based 32 Times Oversampling 8th-order Sigma-Delta Audio DAC. In: Proc. 96th AES Convention, Preprint # 3808, 1994.
- [45] W. L. Lee and C. G. Sodini.: A topology for higher interpolative coders. In: Proceedings of ISCAS, pp. 459-462, 1987.
- [46] R. Schreier and G.C. Temes.: Understanding delta sigma data converters: Wiley-IEEE express, 2004.

- [47] John, B.: Essentials of control techniques and theory, CRC pressInc, 2009.
- [48] Bendrukov,G.A, Teodorchik,K,F: The analytic theory of constructing root loci. In: automation and remote control, vol. 20, pp. 340-344, 1959.
- [49] Cogan,B.:Use of the analytic method and computer algebra to plot root loci. In: International journal of electrical engineering education. vol. 35, pp. 350-356, 1998.
- [50] D'azzo, J.J, Houpis, C.H.: Linear control system analysis and design conventional and modern, Mc Graw Hill, New York, 1988.
- [51] Ogata, K.: Modern control engineering, Prentice Hall, 2002.
- [52] Palm,W.J.:Control system engineering, John Wiley & Sons, 1986.
- [53] Cogan.B, Paor.A.M.: Analytic root locus and LAMBERT W function in control of a process with time delay. In: Journal of electrical engineering, vol. 62, pp. 327-334, 2011
- [54] K.Kang, P.Stubberud: A comparison of continuous time sigma delta modulator simulation methods. In: IEEE International Midwest Symposium on Circuits and Systems, pp. 495-498, 2014.
- [55] <http://www.mathsisfun.com/data/standard-normal-distribution.html>
- [56] Michal pavlik, Martin Magat, Lukas Fucik and Jiri Haze, "Matlab-Modeling, Programming and Simulation", ISBN 978-953-307-125-1, 2010.
- [57] Søren Hein, Avidesh Zakhor, "Sigma Delta Modulators: Nonlinear Decoding Algorithms and Stability Analysis", ISBN 978-079-239-309-2, 1993.
- [58] Josh Reiss: Towards a procedure for stability analysis of high order sigma delta modulators. In: 119th audio engineering society convention, 2005.
- [59] Sakkarapani Balagopal, Vishal Saxen: A Low-Power Single-bit continuous time sigma delta converter with 92.5dB Dynamic range for biomedical application. In: Journal of Low power electronics and applications, vol.2, pp.197-209, 2012.

CURRICULUM VITAE

Graduate College
University of Nevada, Las Vegas

Kyung Kang

Degrees:

Bachelor of Engineering in Electrical and Electronics Engineering, 2001
Korea University, South Korea

Master of Engineering in Electrical and Electronics Engineering, 2003
Korea University, South Korea

Special Honors and Awards:

The Outstanding Teaching Award, Dept. of Electrical & Computer Eng., UNLV, 2012.
Graduate Assistant Scholarship, Dept. of Electrical & Computer Eng., UNLV, 2009-2014.
Best Employee Prize, LCD R&D Team, Samsung Electronics, 2004.
The New Employee of the Year, LCD R&D Team, Samsung Electronics, 2003.
Grantee of Industry-Academic Cooperation, Samsung Electronics, 2001-2002.
Brain Korea (BK 21) Scholarship, Korea University, 2001-2002.
Graduate All-expense Award Scholarship, Korea University, 2001-2002.
2nd Prize in the Electronic Circuit Design Exhibition, Korea University, 2000.

Professional Experiences:

Senior Engineer, LCD R&D Team, Samsung Electronics, South Korea, 2003-2008.
Research Assistant, Dept. of Electrical & Electronics Eng., Korea University, 2001-2003.

Patents:

Hybrid COG structure, Samsung Electronics, 2007.
Input Connector Pin with W-WAN Noise Improvement, Samsung Electronics, 2006.
Logic Structure for Reduction of Output voltage variation in Source IC, Samsung Electronics, 2006.
Input Connector including HVS functionality, Samsung Electronics, 2004.
LED FPC through the Source PCB, Samsung Electronics, 2003.

Publications:

1. K. Kang, P. Stubberud, "A Comparison of Continuous Time Sigma Delta Modulator Simulation Methods", IEEE 57th International Midwest Symposium on, pp. 495-498, Texas, USA, August 2014.
2. K. Kang, P. Stubberud, "Stability Analysis of Continuous Time Sigma Delta Modulators", 23rd International Conference on Systems Engineering, Las Vegas, USA, August 2014.
3. K. Kang, Y. S. Park, "A Study on the Optimized Design of PLL to Accelerated Lock Using FLL", The Korean Institute of Electrical and Electronic Material Engineers, 2002
4. Y. S., Woo, K. Kang, Y. M. Jang, et al., "The Design of Charge Pump PLL with two PFD", The Korean Institute of Electrical Engineers, 2001

Dissertation Title:

Simulation, and Overload and Stability Analysis of Continuous Time Sigma Delta Modulator

Dissertation Examination Committee:

Committee Chair, Peter Stubberud, Ph.D.

Committee Member, Sahjendra Singh, Ph.D.

Committee Member, Ebrahim Saberinia, Ph.D.

Committee Member, R. Jacob Baker, Ph.D.

Graduate Faculty Representative, Laxmi Gewali, Ph.D.